# DEVELOPMENT OF ALGORITHMS FOR FAULT DETECTION IN DISTRIBUTION SYSTEMS

MOUSTAFA ERSOI

DECEMBER 2003

# DEVELOPMENT OF ALGORITHMS FOR FAULT DETECTION IN DISTRIBUTION SYSTEMS

**A THESIS SUBMITTED TO**
**THE GRADUATE SCHOOL OF NATURAL AND APPLIED SCIENCES**
**OF**
**THE MIDDLE EAST TECHNICAL UNIVERSITY**

**BY**

**MOUSTAFA ERSOI**

**IN PARTIAL FULFILMENT OF THE REQUIREMENTS FOR THE DEGREE OF**
**MASTER OF SCIENCE**
**IN**
**THE DEPARTMENT OF ELECTRICAL AND ELECTRONIC ENGINEERING**

**DECEMBER 2003**

Approval of the Graduate School of Natural and Applied Science

_____ _____

Prof. Dr. Canan Özgen
Director

I certify that this thesis satisfies all the requirements as a thesis for the degree of Master of Science.

_____ _____
Prof. Dr. Mübeccel DEMİREKLER
Head of Department

This is to certify that we have read this thesis and that in our opinion it is fully adequate, in scope and quality, as a thesis for the degree of Master of Science.

_____ _____
Prof. Dr. Nevzat Özay
Supervisor

Examining Committee Members

Prof. Dr. Ahmet RUMELİ _____

Prof. Dr. Nevzat ÖZAY _____

Prof. Dr. Arif ERTAŞ _____

Prof. Dr. Mirzahan HIZAL _____

Osman Bülent TÖR _____

## ABSTRACT

### DEVELOPMENT OF ALGORITHMS FOR FAULT DETECTION IN DISTRIBUTION SYSTEMS

MOUSTAFA, Ersoi

M.S., Department of Electrical and Electronics Engineering

Supervisor: Prof.Dr. Nevzat Özay

December 2003, 101 pages

In this thesis, the possibility of detection of fault location in the cable distribution systems by using traveling waves due to fault and circuit breaker operations is investigated. Waveforms originated from both actions and fault steady state are separately analyzed.

During such switching actions, high frequency variations which are absent in the steady state conditions, take place. In order to simulate high frequency changes properly, system elements are modeled accordingly. In other words, frequency dependent models are introduced, and they are used in Electro-Magnetic Transients Program (EMTP).

Since the characteristics of waveforms are different for separately analyzed portions, different fault locating algorithms with their limitations are introduced.



Keywords: Traveling Waves, Fault Locating in Distribution Systems, High Frequency Transformer Model, Cable Model, Bus-bar Model, EMTP

# ÖZ

## DAĞITIM SİSTEMLERİNDE HATA YERİNİN BELİRLENMESİ İÇİN ALGORİTMALAR GELİŞTİRMEK

MOUSTAFA, Ersoi
Y.L., Elektrik ve Elektronik Mühendisliği Bölümü
Danışman: Prof.Dr. Nevzat Özay
Aralık 2003, 101 sayfa

Bu tezde, hata ve kesici çalışmasından kaynaklanan yürüyen dalgaların kullanımı ile kablo dağıtım sistemlerinde hata yerinin tespiti olasılığı araştırılmıştır. Geçiçi ve kararlı rejimlerden oluşan dalga şekilleri ayrı ayrı analiz edilmiştir.

Bu şekilde ki anahtarlama işlemlerinde, kararlı rejimlerde bulunmayan yüksek frekans varyasyonları oluşmaktadır. Yüksek frekans değişimlerini düzgün simule edebilmek için, sistem elemanları gerekli şekilde modellenmiştir. Bir başka deyişle frekansa bağımlı modeller tanımlanmış ve Elektro-Manyetik Geçiçi Rejim Programında (EMTP) kullanılmıştır.

Dalga karakteristikleri değişik kısımlarda farklı özellikler gösterdiğinden değişik hata tespit algoritmaları getirdikleri kısıtlamalarla birlikte sunulmuştur.

Anahtar Kelimeler: Yürüyen Dalgalar, Dağıtım Sistemlerinde Hata Yeri Tespiti, Yüksek Frekans Trafo Modeli, Kablo Modeli, Bara Modeli, EMTP

To my wife and son

**ACKNOWLEDGEMENTS**

I would like to thank my supervisor Prof. Dr. Nevzat ÖZAY for his guidance, patience, and encouragements not only for this thesis but also for my entire engineering career.

I would also like to thank Prof. Dr. Ahmet RUMELİ, Prof. DR. Arif ERTAŞ, and Prof. Dr. Mirzahan HIZAL for their valuable advices and encouragements throughout my studies.

Special thanks to Ulaş KARAAĞAÇ and Osman Bülent TÖR for their technical advices.

Finally, I would like to express my appreciation to my father, mother, and brother for their support, patience and encouragements.

**TABLE OF CONTENTS**

ABSTRACT ..... i ....
ÖZ ..... ii .....
ACKNOWLEDGMENTS ..... iii ...
TABLE OF CONTENTS ..... iv ...
LIST OF FIGURES ..... vii ...
LIST OF TABLES ..... x ...
CHAPTER
**1. INTRODUCTION ..... 1**
1.1 Fault Location Problem..... 1 ...
1.2 The purpose and scope of the thesis..... 5 ..
2. **MODELING OF DISTRIBUTION SYSTEM ELEMENTS..... 6**
2.1 Introduction..... 6 ...
2.2 Derivation of models..... 6 ...
2.1.1 Derivation of **c**able model..... 6 .
2.2.1.1 Series impedance matrix ..... 8 ..
2.2.1.2 Shunt admitance matrix ..... 11 ..
2.2.1.3 Cables in transmission system..... 13
2.2.2 Derivation of bus-bar model..... 14
2.2.3 Derivation of High Frequency Transformer Model…….…… 16
2.2.3.1 Ideal two winding transformer and general differential equation..... 16 ...
2.2.3.2 Transient ocsillations in the primary winding..... 21 .
2.2.3.3 The initial and the final distributions..... 22

2.2.3.4 Complete solution for grounded and isolated neutral ……24
2.2.3.5 Terminal transients and reaction at the line terminal.....25 .
2.2.4 Stub line model.....31 ..
2.2.5 Earth model .....34 .

2.3 EMTP models.....35 ..
2.3.1 Cable model .....36 ..
2.3.2 Bus-bar model .....36 .
2.3.3 High frequency transformer model .....38
2.3.4 Source, main transformer, and switch models……..……40
2.3.5 Earth model .....41 .

**3. ANALYSES OF TRAVELLING WAVES DUE TO FAULTS .....43**
3.1 Introduction .....43 ..
3.2 Verification of simulation results by calculation.....43 .
3.3 Effects of modeling of the elements of distribution system .....50
3.4 Analyses with cable shield included .....52 .
3.4.1 Single feeder systems.....54 .
3.4.2 Single observation point and system with several braches..... 64
3.4.3 Single phase multi-branch systems……..…66
3.5 Analyses on 3-phase systems……..…… 67

**4. ANALYSIS OF TRAVELLING WAVES DUE TO CIRCUIT BREAKER OPERATION……..76**

4.1 Introduction……76
4.2 Wave characteristics……76
4.3 Analyses of the systems……79
4.3.1 Three-phase single branch systems……..……80
4.3.2 Single observation point and system with three braches.....….88

**5. CONCLUSIONS ……....92**

**REFERENCES ……. 97**

## LIST OF FIGURES

**FIGURE**

1.1 Classical Distribution System ……1
1.2 The System Designed by TUBITAK-BILTEN ……...…3
1.3 Oscillations during Fault and CB Operation ……4
1.4 Multi-feeder Distribution System ……..4
2.1 Coaxial Loops Defined for Derivation of Cable Model……..…... 7
2.2 Relative Positions of Cables ……..……...……10
2.3 Positions of the Cables in the Metallic Pipe ……..……15
2.4 Complete Idealized Circuit of a Two Winding Transformer ….……...…18
2.5 Ideal Complete Equivalent Circuit for a Primary Winding …….…… 20
2.6 Transformer Model for Complete Terminal Transients ……..……26
2.7 Simplified Model for Complete Terminal Transients ……...…29
2.8 LC Equivalent of Transformer for Terminal Transients ……30
2.9 Initial / Final Equivalents of Transformer for Terminal Transients……...…31
2.10 Capacitive Stub-line ……..……...32
2.11 Inductive Stub-line ……... 33
2.12 Calculated LC Response ……...34
2.15 Position of Bus-bars in the Metallic Conductor ……... 38
2.16 Single Phase High Frequency Transformer ……... 39
2.17 Three-phase High Frequency Transformer ……..……..…40
3.1 Simple Circuit That Contains All System Elements ……...44
3.2 Reflection Coefficient at Point A ……..…44
3.3 Reflection Coefficients at Point B ……..……45
3.4 Reflection Coefficients at Point C and E ……..…….45

3.5 Reflection Coefficient at Point C ……46
3.6 Reflection Coefficients of Entire System ……46
3.7 Simplification Process for Manual Calculations ……47
3.7a A practical feeder branch
3.7b Transformer replaced by its LC equivalent
3.7c L and C represented as stub lines
3.8 Lattice Diagram of First Few Reflections ……48
3.9 Comparison of Simulation and Calculation Results ……49
3.10 Waveform for the Fault at Point B ……50
3.11 Waveform for the Fault at Point C ……51
3.12 Waveform for the Fault at Point D ……51
3.13 Distribution Systems ……53
3.13a Single-feeder System
3.13b Single-feeder two Branch System
3.13c Multi-feeder System
3.14 Waveform for the Fault before Bus 1 …… 54
3.15 Waveform for the Fault at Bus 1 ……55
3.16 Waveform for the Fault after Bus 1 ……55
3.17 Comparison of Single-mode and Two-mode Waveforms ……56
3.18 Waveform for the Fault before Bus 2……56
3.19 Waveform for the Fault after Bus 2 ……57
3.20 Waveform for the Fault before Bus 4 ……57
3.21 Waveform for the Fault after Bus 4……58
3.22 Waveform for the Fault before and after Bus 7 ……59
3.23 Waveform for the Fault before Bus 2 ……61
3.24 Waveform for the Fault after Bus 2 ……61
3.25 Waveform for the Fault before and after Bus 4 ……62
3.26 Waveform for the Fault before and after Bus 7 ……62
3.27 Waveform for the Fault after Bus 4 and Bus 5 ……65
3.28 Waveform for the Fault after Bus 4 ……65
3.29 Waveform for the Fault after Bus 4 ……66
3.30 Waveform for the Fault at Bus 4 ……67

3.31 Three-phase Multi-feeder System ……68
3.32 Waveform for the Fault before Bus 1……69
3.33 Waveform for the Fault after Bus 1 ……..69
3.34 Waveform for the Fault before and after Bus 4 ……70
3.35 Current in the Faulted-phase at the Fault Instant ……71
3.36 Current in the Healthy-phase at the Fault Instant ……..71
3.37 Voltage in the Healthy-phase at the Fault Instant ……..72
3.38 Waveforms for Different Types of Faults ……..74
4.1 Waveform for the Fault before Bus 1 ……77
4.2 Waveform for the Fault at Bus 1 ……78
4.3 Waveform for the Fault at Bus 1……. 78
4.4 Waveform for the Fault after Bus 1……..…79
4.5 Three-phase Single-feeder System …….. 80
4.6 Waveform for the Fault after Bus 7……..81
4.7 Reflection coefficient configuration …….. ……83
4.8 Comparison of Waveforms for the faults at different DTC's……84
4.9 Single-feeder Three-branch System ……89
4.10 Comparison of faults at Bus 3 and Bus 5 ……90
4.11 Comparison of faults at Bus 3, Bus 4, and Bus 5…… 90
4.12 Waveform for the fault at Bus 4……91
5.1 Waveforms for Fault Initiation for Different Fault Resistance ……...94
5.2 Waveforms for Fault Initiation for Different Fault Resistance …… 96

## LIST OF TABLES

**TABLES**

3.1 Fault Distance that are Calculated from the Time Delay between Successive Reflections ..... 60
3.2 Fault Distance that are Calculated from the Sinusoidal Period of Related Waveforms..... 63
3.3 Corrected Values for the Faults at Bus 1 and Bus 2..... 64
3.4 Error due to Increase in Feeder Number. ..... 67
3.5 Fault Distance that are Calculated from the Sinusoidal Period of Related Waveforms..... 70
3.6 Calculated Fault Distances for Different Fault Types..... 73
3.7 Corrected Fault Distances for Different Fault Types..... 75
4.1 Measured Traveling Time (msec) (from CB Operation to Slope Change)..... 81
4.2 Phase to Ground Fault (for “3x1ph" Cable System)..... 82
4.3 Phase to Ground Fault (for "1x3ph" Cable System)..... 82
4.4 Velocities Found from Direct Travel Time Measurements Corresponding to Slope Change..... 85
4.5 Calculations from Slope Change Assuming Average Multiplicand ..... 86
4.6 Calculations from Slope Change Assuming Nearest Two Busses to the Fault as Reference..... 87
4.7 Calculation from First Peak..... 87
4.8 Calculation from the Sinusoidal Period..... 88

5.1 Calculation From Steady-state Current and Voltage
Values Assuming Homogeneous Earth and solid Fault…….....93
5.2 Comparison of Calculated Fault Distance For
Different Fault Impedances…….…… …..93

# CHAPTER 1

# INTRODUCTION

## 1.1 Fault Location Problem

Larger distribution systems become necessary as service area and demand to the electricity increase. Classical system design, which employs circuit breaker (CB) selectivity as a protection and fault location scheme, cannot be used for such large systems, since the time needed to provide selectivity increase beyond the permissible short circuit limits of the system elements. For example, such a distribution system that includes 11 distribution transformer centers (DTC) as shown in Fig. 1.1, and assuming the necessary time for selectivity is 0.3 sec, operation time of the main CB is 7.0 sec which is too large considering the permissible short circuit time for such systems is 1.0 or 1.5 sec at most [9].

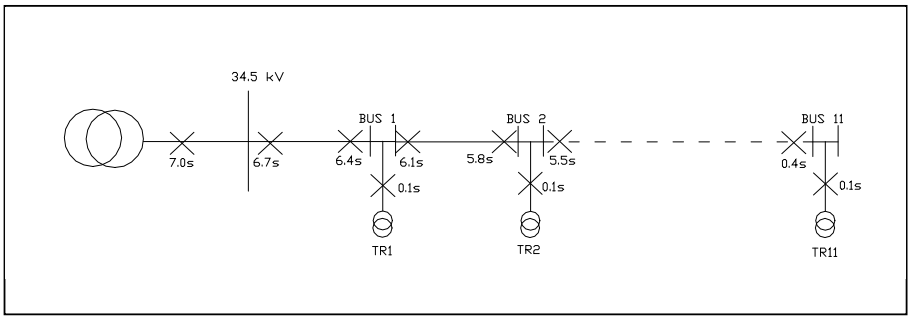


Fig. 1.1 Classical Distribution System

In practice, CB's are not used in all DTC's because selectivity cannot be embedded as given above. Even if there are CB's in the substation, they are not equipped with proper relays and the CB's can merely be used for switching operations.
If the permissible short circuit duration of the system equipment is one second, under these circumstances there can be only 3 properly equipped CB's in cascade; one for the power transformer, one for the feeder, and finally one for the DTC transformer. In case of a fault on the cable system in between, the feeder breaker operates, and the each cable section has to be separately tested one by one so that the location of the fault can be determined. This obviously takes very long time (roughly 2 hours if there are 10 DTC on the feeder) which is quite unacceptable in today's requirements for electrical power.

It is clear that, classical system design cannot meet the required criterion anymore. A new design introduced by TUBITAK-BILTEN (Fig. 1.2) eliminates this limitation. This distribution system is a loop designed and radially operated system. It employs only two cascaded CB's per a main substation one of which is the backup for the other. In this system, CB operates at the fault instant and isolates the all the DTC's instantaneously. The fault location is determined by using the data collected from each DTC via fiber optic cable. These data indicate that whether or not short circuit or fault current has already passed from the related DTC. At the end, fault location is determined to be between the last DTC that the current is observed and the last DTC that no fault current has gone, and the line is re-energized after isolating faulty section. Alternatively, data can be transmitted via telephone lines or radio frequencies but the idea remains still the same.

This system can be expanded freely without any consideration about fault clearing time. On the other hand, it needs expensive investment, because of installation of fault detection equipment on the each DTC. Alternative method could be the detection of the fault location by using traveling waves originated due to fault and CB operation. If this can be achieved, the same system can be realized with lower price and less effort since only one fault detection equipment per feeder will be placed to the main substation.

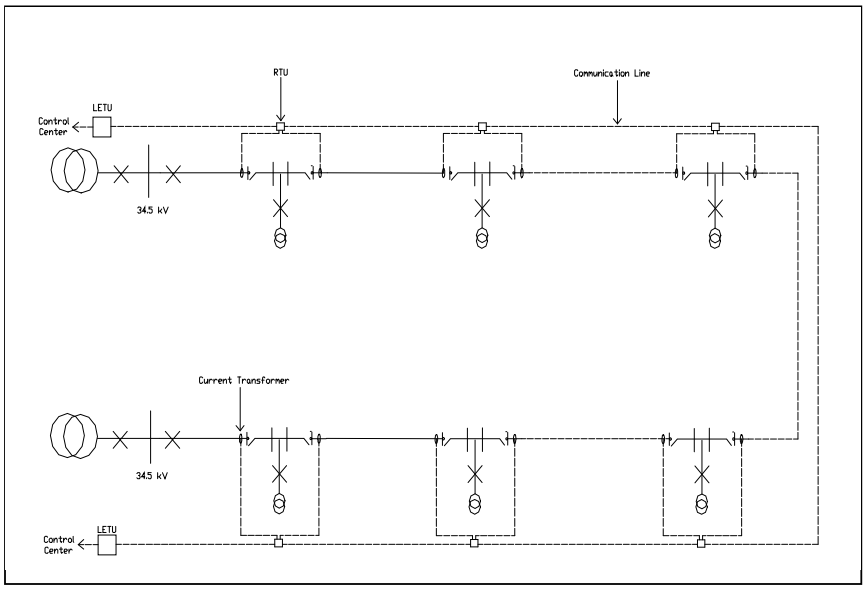


Fig.1.2 The System Designed by TUBITAK-BILTEN

Considering the distribution systems with cables that also contain shield wires, system under investigation becomes relatively independent from ground or grounding conditions.

Sample of traveling waves that arise due to fault and fault clearing actions are in Fig. 1.3. Between these two events there is also steady state during the fault. Thus, complete event can be examined as three separate parts as already indicated.

The main idea is finding unique characteristics of such waveforms related to the fault distance. For example, at the fault instant relatively large oscillations take place. For different fault locations waveform changes according to traveling distance, system layout and system elements between fault and observation point. If the change in waveform can uniquely be related with the fault distance to the observation point, this phenomenon can be used to detect the fault location.

Similarly, reflections due to fault clearing can be examined for further information. Actually fault clearing waveform will be simpler than the previous waveform when multi-feeder substation is under investigation. For such a system (Fig. 1.4) the

traveling waves due to fault travel entire system while originated waves due to fault clearing remains only in the corresponding branch due to isolation with CB operation.

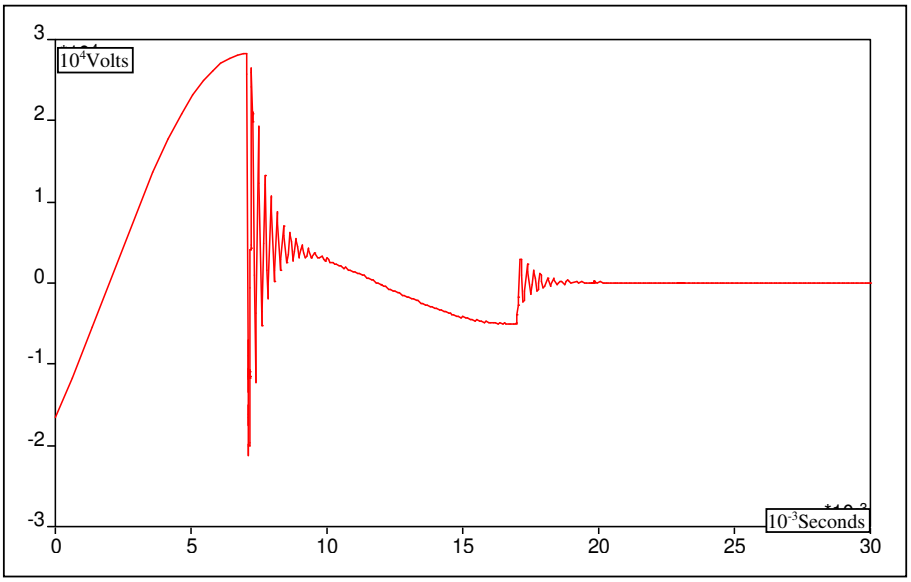


Fig. 1.3 Oscillations during Fault and CB Operation

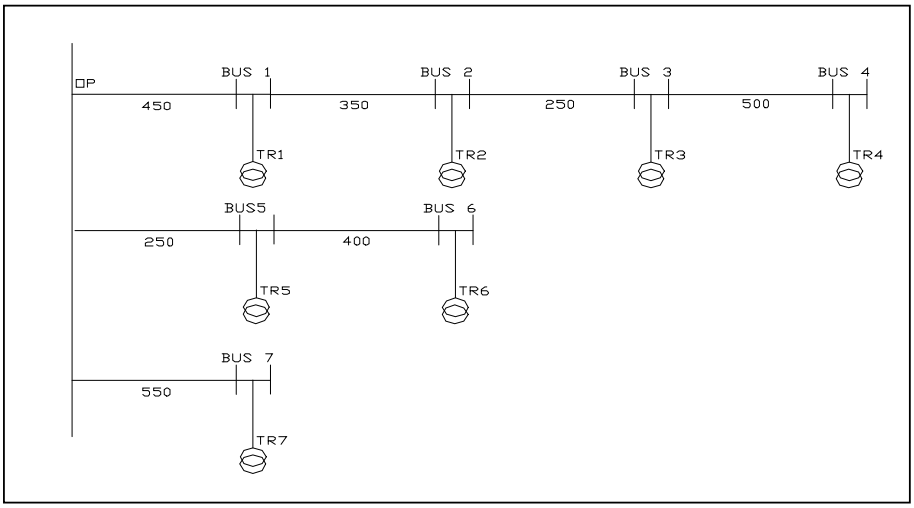


Fig. 1.4 Multi-feeder Distribution System

Finally, fault location can be deduced from the fault impedance by analyzing voltage and current waveforms during the fault steady state. This impedance composed of impedances of cables, bus bars, shield wires and spark gap. Except for

the spark gap impedance, all impedances are well defined. The spark gap impedance changes according to conditions at the fault region, and it must be analyzed for different conditions.

### 1.2 The Purpose and Scope of the Thesis

The aim of this thesis is to analyze the system behavior during the times of fault and fault clearing with the operation of CB by modeling the high frequency characteristics of system elements.

In Chapter 2, high frequency mathematical models of system elements (cable, transformer, and bus-bar) are derived, and the usage of these models in computer simulations is explained with necessary assumptions and modifications.

In Chapter 3, reflection coefficients in the system are discussed and basic characteristics of system elements obtained in Chapter 2 are analyzed on a simple system. Then traveling waves due to fault are analyzed for different distribution system layouts (single- feeder, multi-feeder, multi-branch, etc.), first on single-phase single-mode systems, then on single-phase two-mode systems, and eventually on three-phase systems. Also different fault types (phase to ground, 2-phase to ground, etc.) for the three-phase systems are discussed. Fault location algorithm by using fault transient is introduced.

In Chapter 4, the characteristic of waveform due to fault clearing is explained, and traveling waves are analyzed in a similar manner as in Chapter 3. Different fault location algorithms related to various characteristics of these kind of waveforms are introduced and discussed in the in the view point of simplicity and accuracy.

Finally Chapter 5 includes, concluding remarks and comparison of introduced algorithms with present method that is based on the determination of the fault location by calculating fault impedance from steady-state voltage and current values during fault.

# CHAPTER 2

# MODELING OF DISTRIBUTION SYSTEM ELEMENTS

## 2.1 Introduction

Distribution system, under investigation, mainly consists of circuit breakers, cables, bus-bars, and transformers. Each element should be modeled appropriately to simulate transient and steady state responses of system during fault and fault clearing instants. In addition appropriate earth model should be introduced by considering practical situations.

Modeling of each element, assumptions and necessary theories will be explained throughout this chapter.

## 2.2 Derivations of Models

### 2.2.1 Derivation of Cable Model [1] [2]

The derivation of cable model is mainly based on general matrix equations that define system.

$$\frac{dV}{dx} = -Z.I$$
$$\frac{dI}{dx} = -Y.V \qquad \text{Eqn. (2.1)}$$

Every cable can have core, sheath, and armor. For that reason, cables can be assumed as a minor multi-conductor system itself. Mathematical model can be constructed under following assumptions:

- The system is homogeneous along longitude axis, and all conductors in system are assumed mutually parallel and they are parallel to the earth surface.
- Attenuation in current and voltage is negligible along a length of cable comparable with its side dimensions.
- Since the charge introduced into soil will be displaced quickly enough (order of $10^{-8}$ s at $\rho = 1000\ \Omega m$), the electric charges in the system maybe assumed to be surface charges, so that time varying lateral electric field has the same form as the electrostatic field.
- Additional to the (n) conductor system, earth is (n+1)th conductor.

In addition to these assumptions three coaxial loops are defined for the cable that have core, sheath, and armor as in Fig. 2.1. Note that, loop 1 is formed by the core conductor and metallic sheath as return, loop 2 is formed by metallic sheath and metallic armor as return, finally loop 3 is formed by metallic armor and earth as return.

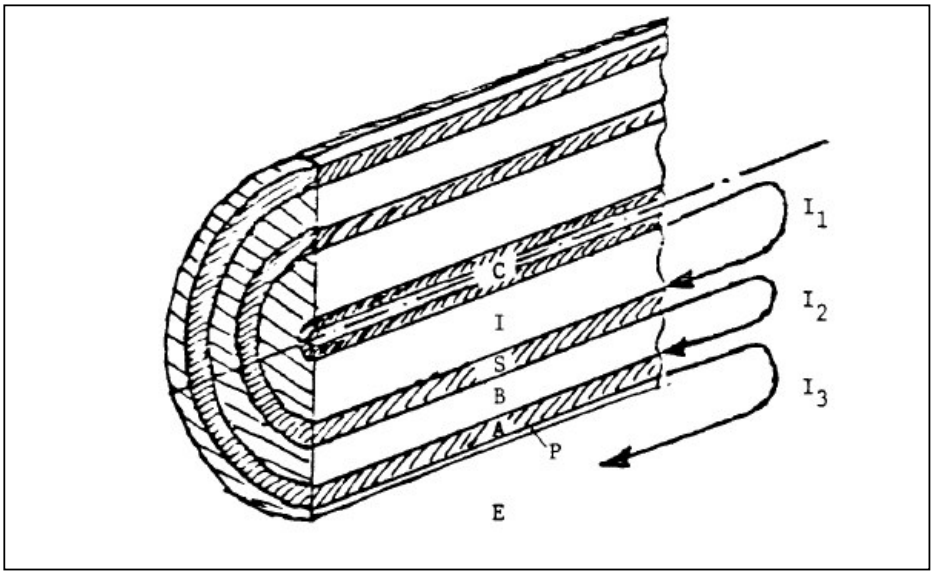


Fig. 2.1 Coaxial Loops Defined for Derivation of Cable Model

#### 2.2.1.1. Series Impedance Matrix [2]

For such a three conductor cable, general form of loop equations is as follows:

$$-\begin{bmatrix} \frac{dV_1}{dx} \\ \frac{dV_2}{dx} \\ \frac{dV_3}{dx} \end{bmatrix} = \begin{bmatrix} Z_{11} & Z_{12} & Z_{13} \\ Z_{21} & Z_{22} & Z_{23} \\ Z_{31} & Z_{32} & Z_{33} \end{bmatrix} \begin{bmatrix} I_1 \\ I_2 \\ I_3 \end{bmatrix} \qquad \text{Eqn. 2.2}$$

More specifically,

$$\begin{aligned} Z_{11} &= Z_{c/o} + Z_{c\_s} + Z_{s/i} \\ Z_{22} &= Z_{s/o} + Z_{s\_a} + Z_{a/i} \\ Z_{33} &= Z_{a/o} + Z_{a\_e} + Z_e \end{aligned} \qquad \text{Eqn. 2.3}$$

Note that, all impedances are given for unit length, and defined as follows

$Z_{c/o}$: Internal impedance of tubular core with return path outside the tube (in this case through the sheath),

$Z_{c\_s}$: Impedance of insulation between core and sheath,

$Z_{s/i}$: Internal impedance of tubular sheath with return path inside the tube (in this case through core conductor),

$Z_{s/o}$: Internal impedance of tubular sheath with return path outside (in this case through the armor),

$Z_{s\_a}$: Impedance of insulation between sheath and armor,

$Z_{a/i}$: Internal impedance of tubular armor with return path inside (in this case through the sheath),

$Z_{a/o}$: Internal impedance of tubular armor with return path outside (in this case through the earth),

$Z_{a\_e}$: Impedance of insulation between armor and earth,

$Z_e$ : Earth impedance with return path metallic armor.

Having opposite directions with respect to the defined loops, the coupling impedances $Z_{12} = Z_{21}$, and $Z_{23} = Z_{32}$ are negative.

$Z_{12} = Z_{21} = -Z_{s\text{-}m}$ = mutual impedance of tubular sheath between the inside loop 1 and outside loop 2.

$Z_{23} = Z_{32} = -Z_{a\text{-}m}$ = mutual impedance of tubular armor between the inside loop 2 and outside loop 3.

$Z_{13} = Z_{31} = 0$ since loop 1 and loop 3 have no common branch.

Although the insulation impedances can be calculated easily, calculating the internal impedance and mutual impedance of tubular conductor is rather complicated.

$$Z_{insulation} = j\omega \frac{\mu_i}{2\pi} \ln \frac{r}{q} \qquad \text{Eqn. 2.4}$$

where $\mu_i$= permeability of insulation

r = outside radius of insulation

q = inside radius of insulation

The internal impedance and mutual impedance of a tubular conductor are found with modified Bessel functions (r and q are outside and inside radius respectively).

$$Z_{tube\_in} = \frac{\rho m}{2\pi qD}\{I_0(mq)K_1(mr) + K_0(mq)I_1(mr)\} \qquad \text{Eqn. 2.5}$$

$$Z_{tube\_out} = \frac{\rho m}{2\pi rD}\{I_0(mr)K_1(mq) + K_0(mr)I_1(mq)\} \qquad \text{Eqn. 2.6}$$

$$Z_{tube\_mutual} = \frac{\rho}{2\pi qrD} \qquad \text{Eqn. 2.7}$$

where, $D = I_1(mr)K_1(mq) - I_1(mq)K_1(mr)$, Eqn. 2.8

and $m = \sqrt{\frac{j\omega\mu}{\rho}}$ Eqn. 2.9

Finally $Z_{earth}$ can be found by using Pallaczek formula, for self earth-return impedance

$$Z_{earth} = \frac{\rho m^2}{2\pi}\left\{K_0(md) - K_0(mD) + \int_{-\infty}^{\infty} \frac{\exp(-h+H)\sqrt{\alpha^2+m^2}}{|\alpha|+\sqrt{\alpha^2+m^2}} \exp(j\alpha R)\, d\alpha\right\} \quad \text{Eqn. 2.10}$$

Then the mutual earth return impedance for cables system,

$$Z_{mutual} = \frac{\rho m^2}{2\pi}\left\{K_0(md) - K_0(mD) + \int_{-\infty}^{\infty} \frac{\exp(-h+y)\sqrt{\alpha^2+m^2}}{|\alpha|+\sqrt{\alpha^2+m^2}} \exp(j\alpha x)\, d\alpha\right\}$$

Eqn. 2.11

From the Fig. 2.2,

$d = \sqrt{x^2 + (h-y)^2}$ = direct distance between cables i & k

$D = \sqrt{x^2 + (h+y)^2}$ = distance between cable i and image of cable k in the air, and

$\alpha$ = integration constant

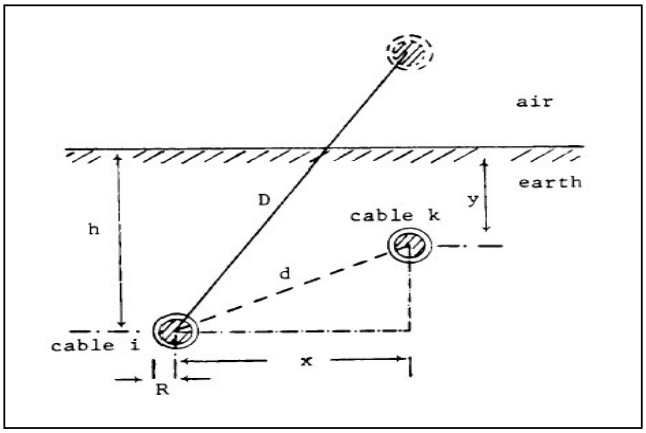


Fig.2.2 Relative Positions of Cables

Note that, if cable has solid core then $Z_{c/i} = 0$, and also if there is no insulation around armor $Z_{ins} = 0$.

At the end, loop voltages and currents must be converted into phase (core, sheath, and armor) voltages and currents by using following terminal conditions:

$$\begin{aligned} V_1 &= V_{core} - V_{sheath} \\ V_2 &= V_{sheath} - V_{armor} \\ V_3 &= V_{armor} \end{aligned} \quad \text{and} \quad \begin{aligned} I_1 &= I_{core} \\ I_2 &= I_{sheath} + I_{core} \\ I_3 &= I_{armor} + I_{sheath} + I_{core} \end{aligned} \qquad \text{Eqn. 2.12}$$

Where, $V_{core}$ = voltage from core to ground
$V_{sheath}$ = voltage from sheath to ground
$V_{armor}$ = voltage from armor to ground

Finally,

$$\begin{bmatrix} dV_{core}/dx \\ dV_{sheath}/dx \\ dV_{armor}/dx \end{bmatrix} = \begin{bmatrix} Z_{cc} & Z_{cs} & Z_{ca} \\ Z_{sc} & Z_{ss} & Z_{sa} \\ Z_{ac} & Z_{as} & Z_{aa} \end{bmatrix} \begin{bmatrix} I_{core} \\ I_{sheath} \\ I_{armor} \end{bmatrix} \qquad \text{Eqn. 2.13}$$

$$\text{with} \quad \begin{aligned} Z_{cc} &= Z_{11} + 2Z_{12} + Z_{22} + 2Z_{23} + Z_{33} \\ Z_{cs} &= Z_{sc} = Z_{12} + Z_{22} + 2Z_{23} + Z_{33} \\ Z_{ca} &= Z_{ac} = Z_{sa} = Z_{as} = 2Z_{23} + Z_{33} \\ Z_{ss} &= Z_{22} + 2Z_{23} + Z_{33} \\ Z_{aa} &= Z \end{aligned} \qquad \text{Eqn. 2.14}$$

### 2.2.1.2. Shunt Admittance Matrix [2]

Defined equations for the loops in Fig. 2.1 are uncoupled for the current changes along cable. This fact greatly simplifies the derivation of shunt admittance matrix compared to series impedance matrix as follows:

$$-\frac{dI_i}{dx} = Y\,V \qquad \text{Eqn. 2.15}$$

$$-\begin{bmatrix} dI_1/dx \\ dI_2/dx \\ dI_3/dx \end{bmatrix} = \begin{bmatrix} G_1 + j\omega C_1 & 0 & 0 \\ 0 & G_2 + j\omega C_2 & 0 \\ 0 & 0 & G_3 + j\omega C_3 \end{bmatrix} \begin{bmatrix} V_1 \\ V_2 \\ V_3 \end{bmatrix}$$

$G_i$ and $C_i$ are the shunt conductance and capacitance (per unit length) respectively, for each insulation level. Absence of insulation level introduces ($V_i$ = 0) to the related equation. For most cases, shunt conductance is negligible. $C_i$ can easily be calculated as:

$$C = \frac{2\pi\varepsilon_0\varepsilon_r}{\ln\frac{r}{q}}, \qquad \text{Eqn. 2.16}$$

where q and r are inside radius and outside radius respectively.

Once necessary parameters are found, Eqn. 2.15 should be converted into core, sheath, and armor values as follows.

$$-\begin{bmatrix} dI_c/dx \\ dI_s/dx \\ dI_a/dx \end{bmatrix} = \begin{bmatrix} Y_1 & -Y_1 & 0 \\ -Y_1 & Y_1 + Y_2 & -Y_2 \\ 0 & -Y_2 & Y_2 + Y_3 \end{bmatrix} \begin{bmatrix} V_{core} \\ V_{sheath} \\ V_{armor} \end{bmatrix} \qquad \text{Eqn. 2.17}$$

where $Y_i = G_i + j\omega C_i$

### 2.2.1.3 Cables in the Transmission System [2]

Usually cables are laid so close that coupling between phases also should be accounted. It is obvious that, the magnetic field at the outside of cable due to loop 1 and loop 2 in Fig. 2.1 is zero, since vector sum of current $I_1$ passing through the core and sheath is zero. Similarly current $I_2$ passing through sheath and armor is also summed up to zero. On the other hand, return path of loop 3 is earth. Therefore, the first two expressions in Eqn. 2.2 remain the same while the third one should be modified to include coupling effect. Resultant loop impedance matrix is as follows.

$$[Z_{loop}]=\begin{bmatrix} \begin{bmatrix} Z_{11a} & Z_{12a} & 0 \\ Z_{21a} & Z_{22a} & Z_{23a} \\ 0 & Z_{32a} & Z_{33a} \end{bmatrix} & \begin{bmatrix} 0 & 0 & 0 \\ 0 & 0 & 0 \\ 0 & 0 & Z_{ab} \end{bmatrix} & \begin{bmatrix} 0 & 0 & 0 \\ 0 & 0 & 0 \\ 0 & 0 & Z_{ac} \end{bmatrix} \\ & \begin{bmatrix} Z_{11b} & Z_{12b} & 0 \\ Z_{21b} & Z_{22b} & Z_{23b} \\ 0 & Z_{32b} & Z_{33b} \end{bmatrix} & \begin{bmatrix} 0 & 0 & 0 \\ 0 & 0 & 0 \\ 0 & 0 & Z_{bc} \end{bmatrix} \\ \textit{symmetric} & & \begin{bmatrix} Z_{11c} & Z_{12c} & 0 \\ Z_{21c} & Z_{22c} & Z_{23c} \\ 0 & Z_{32c} & Z_{33c} \end{bmatrix} \end{bmatrix} \quad \text{Eqn. 2.18}$$

where, $Z_{ab}$, $Z_{ac,}$ $Z_{bc}$ are mutual outer loop equations. By using terminal conditions, loop matrix can be transformed into phase matrix.

$$[Z_{phase}]=\begin{bmatrix} [Z_{self-a}] & [Z_{mutual-ab}] & [Z_{mutual-ac}] \\ & [Z_{self-b}] & [Z_{mutual-bc}] \\ \textit{symmetric} & & [Z_{self-c}] \end{bmatrix} \quad \text{Eqn. 2.19}$$

Here the self impedance matrices are identical to impedance matrix in Eqn 2.13, and mutual impedance matrices, having identical elements, are:

$$[Z_{mutual}]=\begin{bmatrix} Z_{ab} & Z_{ab} & Z_{ab} \\ Z_{ab} & Z_{ab} & Z_{ab} \\ Z_{ab} & Z_{ab} & Z_{ab} \end{bmatrix} \qquad \text{Eqn. 2.20}$$

It is clear that, absence of one tubular conductor i.e. armor, reduces the dimension of matrices but the idea is still the same.

Since there is no coupling among the three phases in the shunt admittances, resulted shunt admittance is rather simple.

$$[Y_{phase}]=\begin{bmatrix} [Y_a] & 0 & 0 \\ 0 & [Y_b] & 0 \\ 0 & 0 & [Y_c] \end{bmatrix} \qquad \text{Eqn. 2.21}$$

Sub-admittance matrices are in the same form with the admittance matrix in Eqn. 2.17.

### 2.2.2 Derivation of bus-bar model [2]

Bus-bar will be modeled as cable through metallic pipe [3]. Since metallic pipe is conductive, it introduces an additional conductor to the system. Furthermore, system becomes more complicated, because cables and metallic pipe are not concentric, and pipe material is magnetic in which there is a current flow depending on saturations effects. On the other hand, penetration depth into the pipe is less than the pipe thickness, so it can be assumed that whole current returns through the pipe not through the earth, which greatly simplifies the calculations. Simply, earth return in the previous calculations replaces with pipe return especially for transient cases.

From the view point of primal assumptions made previously, only the return path of loop 3 in Fig 2.1 is changed as the pipe. Thus, for the three parallel cable system discussed for former case, $Z_{33a}$, $Z_{33b}$, $Z_{33c}$ should be expressed by using the loop

formed by armor and pipe. Also, mutual impedances $Z_{ab}$, $Z_{bc}$, $Z_{ca}$ are to be expressed by using two such loops. Modified formulas are as follows…

$$Z_{insulation} = j\omega\frac{\mu_0}{2\pi}\ln\left\{\frac{q}{r_i}\left[1-\left(\frac{d_i}{q}\right)^2\right]\right\} \qquad \text{Eqn. 2.22}$$

where q, $R_i$, and $d_i$ are defined in Fig. 2.3

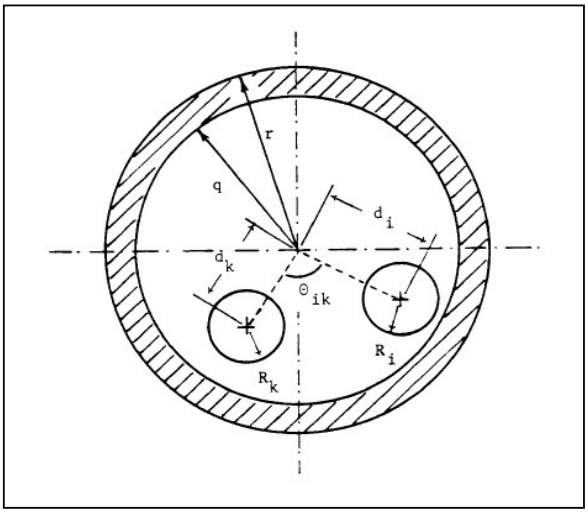


Fig. 2.3 Positions of the Cables in the Metallic Pipe

The impedances $Z_{33a}$, $Z_{33b}$, $Z_{33c}$ need to be calculated by substituting $Z_{pipe\text{-}in}$ instead of $Z_{earth}$ since new return path is through the pipe.

$$Z_{pipe-in} = j\omega\frac{\mu}{2\pi}\left\{\frac{K_0(mq)}{mqK_1(mq)}+2\sum_{n=1}^{\infty}\left(\frac{d_i}{q}\right)^{2n}\frac{K_n(mq)}{n\mu_r K_n(mq)-mqK_n'(mq)}\right\} \qquad \text{Eqn. 2.23}$$

$\mu$ = permeability of pipe,

$K_i$ = modified Bessel function of the second kind order of i, and

$K'_i$ = derivative of $K_i$ .

Note that, for concentric case $Z_{pipe\text{-}in} = Z_{earth}$.

Finally, mutual impedances $Z_{ab}$, $Z_{bc}$, $Z_{ca}$ can be found as,

$$Z_{mutual} = j\omega\frac{\mu_0}{2\pi}\left\{\ln\frac{q}{\sqrt{d_i^2 + d_k^2 - 2d_i d_k\cos\theta_{ik}}} + \mu_r\frac{K_0(mq)}{mqK_1(mq)}\right\}$$

$$+\sum_{n=1}^{\infty}\left(\frac{d_i d_k}{q^2}\right)^n\cos(n\theta_{ik})\left(2\mu r\frac{K_n(mq)}{n\mu_r K_n(mq) - mqK_n'(mq)} - \frac{1}{n}\right) \qquad \text{Eqn. 2.24}$$

### 2.2.3 Derivation of High Frequency Transformer Model [4]

It is known that, the transformer model for 50 Hz cannot be used to determine transient reflections, since transient frequency is much higher than 50 Hz. Note that, transients can mainly be classified as "Internal Transients" and "Terminal Transients". Although both of them are parts of complete solution, the former one is not related with the topic of thesis, so internal reflections will not be questioned. Further classification can be done as "Primary Reflections" and "Secondary Reflections". Latter one will not be examined, because only former one is under consideration. Thus, primary terminal reflections can be calculated by using simple equivalent circuit, which is derived from the most general transformer model.

#### 2.2.3.1 Ideal two winding transformer general differential equation

**Capacitance and Flux Linkages:**

Although capacitance network of a transformer is very complicated, it can be simplified by permissible approximations i.e. distributed nature of the circuit constants of subsidiary elements of the winding could be disregarded, and small capacitances can be neglected. As a result, all capacitances can be summed up as follows:

$K_1$ = Total capacitance from turns to adjacent turns,

$C_1$ = Average capacitance to the tank, and

$C_3$ = Capacitance from winding to winding.

The effective inductance of windings mainly consists of three parts.

- The interlinkages due to flux which is common all turns of winding,
- The partial interlinkages,
- Interlinkages due to other winding.

Actually the situation is more complicated, since during transients, current is different in different parts of the same winding and it changes continuously. Therefore, equations introduced to calculate the flux linkages must be not only enough to be handled in complicated equations but also they must be sufficiently complete to describe adequately the essential characteristics of the transients. For that reason, flux linkages cannot be accounted for by a uniformly distributed self inductance as in transmission line theory since the mutual inductances between parts of the same winding plays an important role. On the other hand, assumption of linearly graded mutual inductance between the parts of the winding provides simple mathematical expression by yielding the essential characteristics to the transients. Finally all these assumption and approximations lead following flux equations.

$$\phi_1 = \frac{0.4\pi(mlt)}{2h}(n_1 i_1 + \sigma n_2 i_2)\left[al + x(l-x)\right] \qquad \text{Eqn. 2.25a}$$

$$\phi_2 = \frac{0.4\pi(mlt)}{2h}(\sigma n_1 i_1 + n_2 i_2)\left[al + x(l-x)\right] \qquad \text{Eqn. 2.25b}$$

Note that, also there are series resistance and leakage conductance between coils and ground. These loss factors are negligible and elimination of them greatly simplifies the problem. Resulted circuit diagram for high frequency model of transformer is shown in Fig. 2.4.

Following relations can be derived from Fig. 2.4.

$$i_{k1} = K_1 \frac{\partial^2 e_1}{\partial x \partial t} \qquad \text{Eqn. 2.26}$$

$$i_{k2} = K_2 \frac{\partial^2 e_2}{\partial x \partial t} \qquad \text{Eqn. 2.27}$$

$$i_{C1} = C_1 \frac{\partial e_1}{\partial t} = \frac{\partial i_{k1}}{\partial x} + \frac{\partial i_{L1}}{\partial x} - i_{C3} \qquad \text{Eqn. 2.28}$$

$$i_{C2} = C_2 \frac{\partial e_2}{\partial t} = \frac{\partial i_{k2}}{\partial x} + \frac{\partial i_{L2}}{\partial x} + i_{C3} \qquad \text{Eqn. 2.29}$$

$$i_{C3} = C_3 \frac{\partial}{\partial t}(e_1 - e_2) \qquad \text{Eqn. 2.30}$$

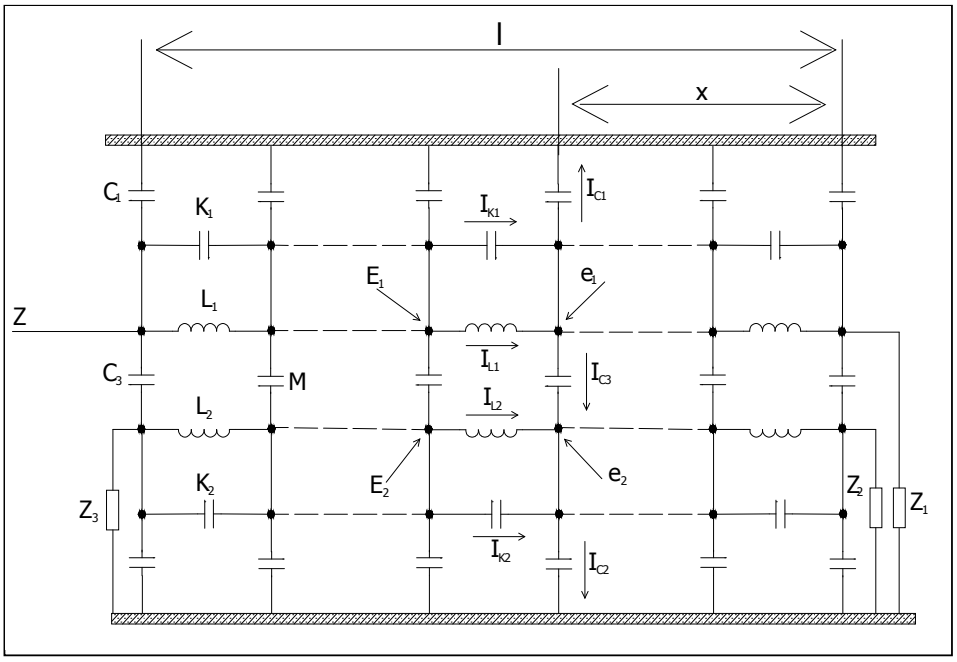


Fig. 2.4 Complete Idealized Circuit of a Two Winding Transformer

By differentiating the flux equations three times,

$$\frac{\partial^4 e_1}{\partial x^4} = -\frac{\partial^2}{\partial t \partial x}\left(L_1 i_{L1} + M i_{L2}\right) \qquad \text{Eqn. 2.31}$$

$$\frac{\partial^4 e_2}{\partial x^4} = -\frac{\partial^2}{\partial t \partial x}\left(M i_{L1} + L_2 i_{L2}\right) \qquad \text{Eqn. 2.32}$$

Note that,

$$L_1 = \frac{0.4\pi n_1^2 (mlt)}{10^8 h} \text{ H/Unit Axial Length (ual)}$$

$$L_2 = \frac{0.4\pi n_2^2 (mlt)}{10^8 h} \text{ H/ual} \qquad \text{Eqn. 2.33}$$

$$M = \frac{0.4\pi n_1 n_2 \sigma (mlt)}{10^8 h} \text{ H/ual}$$

where mlt = mean length of turn

By combining equations (2.26) (2.27), (2.28), (2.29), and (2.30)

$$\frac{\partial^2}{\partial t \partial x} i_{L1} = (C_1 + C_3)\frac{\partial^2 e_1}{\partial t^2} - C_3 \frac{\partial^2 e_2}{\partial t^2} - K_1 \frac{\partial^4 e_1}{\partial x^2 \partial t^2} \qquad \text{Eqn. 2.34}$$

$$\frac{\partial^2}{\partial t \partial x} i_{L2} = (C_2 + C_3)\frac{\partial^2 e_2}{\partial t^2} - C_3 \frac{\partial^2 e_1}{\partial t^2} - K_2 \frac{\partial^4 e_2}{\partial x^2 \partial t^2} \qquad \text{Eqn. 2.35}$$

Substitute (2.34) and (2.35) into (2.31) and (2.32) respectively

$$\frac{\partial^4 e_1}{\partial x^4} - L_1 K_1 \frac{\partial^4 e_1}{\partial x^2 \partial t^2} - MK_2 \frac{\partial^4 e_2}{\partial x^2 \partial t^2} + (L_1 C_1 + L_1 C_3 - MC_3)\frac{\partial^2 e_1}{\partial t^2} + (MC_2 + MC_3 - L_1 C_3)\frac{\partial^2 e_2}{\partial t^2} = 0 \qquad \text{Eqn. 2.36}$$

$$\frac{\partial^4 e_2}{\partial x^4} - L_2 K_2 \frac{\partial^4 e_2}{\partial x^2 \partial t^2} - MK_1 \frac{\partial^4 e_1}{\partial x^2 \partial t^2} + (L_2 C_2 + L_2 C_3 - MC_3)\frac{\partial^2 e_2}{\partial t^2} + (MC_1 + MC_3 - L_2 C_3)\frac{\partial^2 e_1}{\partial t^2} = 0 \qquad \text{Eqn. 2.37}$$

Most general equation for either e = $e_1$ or e = $e_2$

$$\frac{\partial^8 e}{\partial x^8} - (L_1 K_1 + L_2 K_2)\frac{\partial^8 e}{\partial x^6 \partial t^2} + K_1 K_2 (L_1 L_2 - M^2)\frac{\partial^8 e}{\partial x^4 \partial t^4} + [L_1 C_1 + L_2 C_2 + (L_1 + L_2 - 2M)]\frac{\partial^6 e}{\partial x^4 \partial t^2} - (L_1 L_2 - M^2)(K_1 C_2 + K_1 C_3 + K_2 C_1 + K_2 C_3)\frac{\partial^6 e}{\partial x^2 \partial t^4} + (L_1 L_2 - M^2)(C_1 C_2 + C_2 C_3 + C_1 C_3)\frac{\partial^4 e}{\partial t^4} = 0 \qquad \text{Eqn. 2.38}$$

### 2.2.3.2. Transient Oscillations in the Primary Winding

Secondary winding has almost no effect on primary oscillations. Therefore two winding system can be replaced by single winding system without destroying essential characteristics of oscillations. Then simplified equation can be handled relatively easier. On the other hand, circuit constants especially inductance coefficient must be corrected for accuracy. Another drawback of simplification is absence of minor frequency set. According to Fig. 2.5 fundamental relations are:

$$i_1 = K\frac{\partial^2 e}{\partial x \partial t} \qquad \text{Eqn. 2.39}$$

$$i_3 = g\frac{\partial e}{\partial x} \qquad \text{Eqn. 2.40}$$

$$i_4 = \left(G + C\frac{\partial}{\partial t}\right)e = \frac{\partial}{\partial x}\left(i_1 + i_2 + i_3\right) \qquad \text{Eqn. 2.41}$$

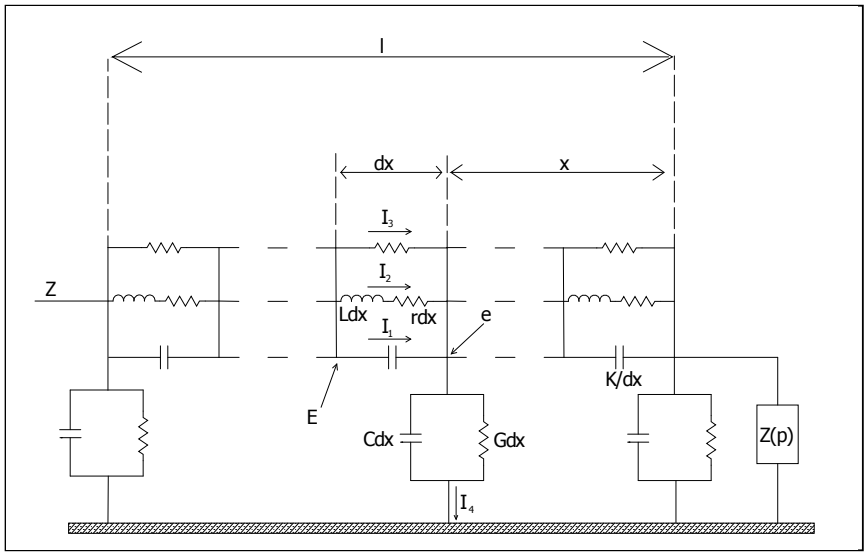


Fig. 2.5 Ideal Complete Equivalent Circuit for a Primary Winding

$$\frac{\partial e}{\partial x} = ri_2 + \frac{n}{10^8}\frac{\partial \phi}{\partial t} \qquad \text{Eqn.2.42a}$$

$$= ri_2 + \frac{\partial}{\partial t}\int_0^l M(x,y)i_2(y)dy \qquad \text{Eqn. 2.42b}$$

$$= ri_2 + \frac{\partial}{\partial t}\{L'i_2(x) + \int_0^l M(x,y)[i_2(y) - i_2(x)]dy \qquad \text{Eqn. 2.42c}$$

where $L' = \int_0^l M(x,y)dy$ = self inductance

$$\phi = \phi_m + \phi_l = \phi_m + \frac{0.4\pi(mlt)n}{2h}\int_0^x\int_x^l i_2 dy\,dx \qquad \text{Eqn. 2.43}$$

where $\phi_m$ = flux mutual to entire winding, and

$\phi_l$ = flux due to partial interlinkages.

From (2.42a) and (2.43)

$$\frac{\partial^4 e}{\partial x^4} = r\frac{\partial^3 i_2}{\partial x^3} - \frac{0.4\pi(mlt)n^2}{h10^8}\frac{\partial^2 i_2}{\partial x \partial t}$$
$$= r\frac{\partial^3 i_2}{\partial x^3} - L\frac{\partial^2 i_2}{\partial x \partial t} \qquad \text{Eqn. 2.44}$$

$L = \frac{0.4\pi(mlt)n^2}{h10^8}$ = inductance per unit axial length of winding

From equations (2.39), (2.40), and (2.41)

$$L\frac{\partial^2 i_2}{\partial x \partial t} = L\left(G + C\frac{\partial}{\partial t}\right)\frac{\partial e}{\partial t}e - L\frac{\partial^2 i_1}{\partial x \partial t} - L\frac{\partial^2 i_3}{\partial x \partial t}$$
$$= LG\frac{\partial e}{\partial t} + LC\frac{\partial^2 e}{\partial t^2} - LK\frac{\partial^4 e}{\partial x^2 \partial t^2} - gL\frac{\partial^3 e}{\partial x^2 \partial t} \qquad \text{Eqn. 2.45}$$

and

$$r\frac{\partial^3 i_2}{\partial x^3} = rG\frac{\partial^2 e}{\partial x^2} + rC\frac{\partial^3 e}{\partial x^2} + rC\frac{\partial^3 e}{\partial x^2 \partial t} - rK\frac{\partial^5 e}{\partial x^4 \partial t} - gr\frac{\partial^4 e}{\partial x^4} \qquad \text{Eqn. 2.46}$$

Substituting equations (2.45) and (2.46) in (2.41)

$$rK\frac{\partial^5 e}{\partial x^4 \partial t} + (1+gr)\frac{\partial^4 e}{\partial x^4} - LK\frac{\partial^4 e}{\partial x^2 \partial t^2} - (rC + gL)\frac{\partial^3 e}{\partial x^2 \partial t}$$
$$- rG\frac{\partial^2 e}{\partial x^2} + LC\frac{\partial^2 e}{\partial t^2} + LG\frac{\partial e}{\partial t} = 0 \qquad \text{Eqn.2.47}$$

Neglecting losses Eqn 2.32 reduces to

$$\frac{\partial^4 e}{\partial x^4} - LK\frac{\partial^4 e}{\partial x^2 \partial t^2} + LC\frac{\partial^2 e}{\partial t^2} = 0 \qquad \text{Eqn. 2.48}$$

the total current from (3)

$$i_1 + i_2 + i_3 = \left(G + C\frac{\partial}{\partial t}\right)\int e dx \qquad \text{Eqn. 2.49}$$

The solution of these equations must satisfy:

- The differential equation
- The terminal condition at x = 0 and x = l
- The initial distribution at t = 0
- The final distribution at t = ∞

**2.2.3.3. The initial and the final distributions**

At the first instant current through capacitances are infinite, while current in inductive winding is zero, and in the resistances the currents are finite. So the initial distribution of potential depends upon the capacitances. As a result only capacitive circuit will be considered. Combination of equations (2.25a) and (2.26) gives:

$$\frac{\partial^2 e}{\partial x^2} - \frac{C}{K}e = \frac{\partial^2 e}{\partial x^2} - \alpha^2 e = 0 \qquad \text{where } \alpha = \sqrt{C/K} \qquad \text{Eqn. 2.50}$$

Therefore solution for initial distribution

$$e = E\frac{Z(p)p\sqrt{CK}\cosh\alpha x + \sinh\alpha x}{Z(p)p\sqrt{CK}\cosh\alpha l + \sinh\alpha l}\Bigg]_{p=\infty}$$

for grounded neutral $Z(p) = 0 \Rightarrow e = \dfrac{\sinh\alpha x}{\sinh\alpha l}E$ Eqn. 2.51

for isolated neutral $Z(p) = \infty \Rightarrow e = \dfrac{\cosh\alpha x}{\cosh\alpha l}E$ Eqn. 2.52

For an infinite rectangular wave, after transient period (theoretically $t=\infty$) the capacitances act as an open circuit and inductances act as a short circuit. Then distributions are determined by the resistances.

From equations (2.25b), (2.26) and (2.27)

$$\frac{\partial^2 e}{x^2} - RGe = \frac{\partial^2 e}{\partial x^2} - \beta^2 e = 0 \qquad \text{Eqn. 2.53}$$

*where* $R = \dfrac{r}{1+gr}$ = Resistance of parallel r and g, $\beta^2 = RG$

The solution is

$$e = E \left. \frac{Z(p)\sqrt{\dfrac{G}{R}}\cosh \beta x + \sinh \beta x}{Z(p)\sqrt{\dfrac{G}{R}}\cosh \beta l + \sinh \beta l} \right]_{p=0} \qquad \text{Eqn. 2.54}$$

For a grounded or inductance in neutral $Z(p)=0 \Rightarrow e = \dfrac{\sinh \beta x}{\sinh \beta l} E$ Eqn. 2.55

For an isolated or capacitance in the neutral

$$Z(p)=\infty \Rightarrow e = \frac{\cosh \beta x}{\cosh \beta l} E \qquad \text{Eqn. 2.56}$$

For resistance $R_0$ in the neutral

$$e = E \left. \frac{R_0\sqrt{G/R}\cosh \beta x + \sinh \beta x}{R_0\sqrt{G/R}\cosh \beta l + \sinh \beta l} \right]_{p=0} \qquad \text{Eqn. 2.57}$$

Note that forms of general equations for initial and final distribution are the same.

### 2.2.3.4 Complete solution for grounded and isolated neutral

Complete solution for grounded network is…

$$e = E\frac{\sinh \beta x}{\sinh \beta l} + E\sum_{1}^{\infty} \frac{2(-1)^s s\pi\left(\alpha^2 - \beta^2\right)l^2}{\left(\alpha^2 l^2 + s^2\pi^2\right)\left(\beta^2 l^2 + s^2\pi^2\right)} e^{-\gamma_s t}\left(\cos \omega_s t + \frac{\tau_s}{\omega_s}\sin \omega_s t\right)\sin\frac{s\pi x}{l} \qquad \text{Eqn.2.58}$$

$$\cong E\frac{\sinh \beta x}{\sinh \beta l} + E\sum_{1}^{\infty} A_s e^{-\gamma_s t}\cos \omega_s t \sin\frac{s\pi x}{l}$$

where $A_s = \dfrac{2(\cos s\pi)s\pi\left(\alpha^2 - \beta^2\right)l^2}{\left(\alpha^2 l^2 + s^2\pi^2\right)\left(\beta^2 l^2 + s^2\pi^2\right)}$

If losses neglected $\beta = 0$ for (r = g = G = 0), then

$$e = E\frac{x}{l} + E\sum_{1}^{\infty}\frac{2\cos s\pi}{s\pi}\left(\frac{\alpha^2 l^2}{\left(\alpha^2 l^2 + s^2\pi^2\right)}\right)\sin\frac{s\pi x}{l}\cos\frac{s^2\pi^2 t}{l^2\sqrt{L\left(C + K\dfrac{s^2\pi^2}{l^2}\right)}}$$

Eqn. 2.59

Effects of losses can be observed by comparing equations (2.58) and (2.59) such that:

- Oscillations die out by exponential decrement factors.
- Amplitude of oscillations is decreased.
- Frequency of oscillations is decreased.
- The final distribution or axis of oscillations is shifted.

The solution for no losses and infinite rectangular applied wave is:

$$e = E + E\sum_{1}^{\infty} B_s \cos\frac{s\pi x}{2\ell}\cos\Omega_s t \qquad \text{Eqn. 2.60}$$

where $B_s = \dfrac{-16\alpha^2\ell^2 \sin\dfrac{s\pi}{2}}{s\pi\left(s^2\pi^2 + 4\alpha^2\ell^2\right)}$, and $\Omega_s = \dfrac{\dfrac{s^2\pi^2}{4\ell^2}}{\sqrt{L\left(C + Ks^2\pi^2/4\ell^2\right)}}$

#### 2.2.3.5 Terminal transients and reaction at the line terminal

It must be noted that, the most general equation found before can be applied only the two extreme cases namely either the terminals are grounded or open circuited. Moreover, even the calculation for these cases is very time consuming, and it cannot directly be applied to the computer simulations. Therefore simpler appropriate equivalent circuit that can be applied to such simulation is necessary.

Equivalent circuit can be applied by understanding which factors are major, and which are minor or subsidiary importance. These factors can be driven by examining Fig. 2.6. Paths connecting terminals to ground can be summed up as follows:

- From primary line terminal to primary neutral through the inductance of the primary winding. Mutual winding is also effective when there is current in secondary winding.
- From secondary line terminal to secondary neutral through the inductance of the secondary winding, and influenced by mutual inductance.
- Through turn to turn series capacitance. Note that total series capacitances $K_1$ and $K_2$ are not entirely replaceable by lumped capacitances.
- Through effective capacitances between terminal to ground.
- Through effective capacitances between primary and secondary winding.
- Composite paths, partly through capacitances and partly through inductances, giving rise to natural oscillations.

All these requirements can be satisfied by the model shown in Fig. 2.6. This model has the necessary degrees of freedom to conform the above terminal effects. Moreover, model can be further simplified for special cases. For example, as it is

pointed before, at the impact instant distributions are determined by capacitive network, and terminal impedances. Therefore resultant model for this case is in Fig 2.6. Note that, switches $Z_1$, $Z_2$, and $Z_3$ are infinite when related terminals open circuited, and they equal to zero when these terminals grounded. Effective capacitance of transformer with respect to terminal line can be calculated as:

$$C_0 \cong \sqrt{CK} \qquad \text{Eqn. 2.61a}$$

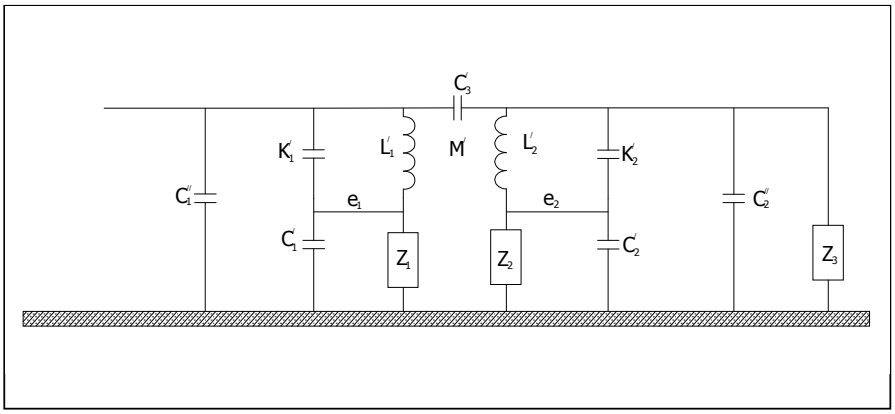


Fig. 2.6 Transformer Model for Complete Terminal Transients

$C_0$ must be equal to the effective capacitance of the equivalent circuit in Fig. 2.6, with the neutrals grounded, that is:

$$C_{01} = C_1'' + K_1' + C_3' \qquad \text{Eqn. 2.61b}$$

$$C_{02} = C_2'' + K_2' + C_3' \qquad \text{Eqn. 2.61c}$$

Note that, if $Z_1 = Z_2 = \infty$, for an applied abrupt voltage $E_1$:

$$\frac{e_1}{E_1} = \frac{K_1'}{K_1' + C_1'} \quad at \quad t = 0$$

$$\frac{e_2}{E_2} = \frac{K_2'}{K_2' + C_2'} \quad at \quad t = 0 \qquad \text{Eqn. 2.62}$$

It is known that, whether the neutral is grounded or not, the initial distributions are practically zero at the neutral. So, the expressions $e_1/E_1$ *and* $e_2/E_2$ are small. Accordingly $K_1'$ *and* $K_2'$ are small compared to $C_1'$ *and* $C_2'$ respectively.

If secondary neutral is grounded and secondary line terminal is open circuited i.e. $(Z_2 = 0 \text{ and } Z_3 = \infty)$ for an applied abrupt voltage to primary line terminal, the corresponding secondary line terminal voltage can be calculated as:

$$\frac{E_2}{E_1} = \frac{C_3'}{C_3' + K_2' + C_2''} \qquad \text{Eqn. 2.63}$$

If primary neutral is opened $(Z_1 = \infty)$ while secondary terminals are grounded $(Z_2 = Z_3 = 0)$ natural oscillations can be calculated from general equations in section 2.3.3.1. In that case effective inductance of primary becomes the leakage inductance.

$$L_1'' = L_1' - \left(\frac{M'^2}{L_2'}\right), \qquad \text{Eqn. 2.64}$$

and the neutral voltage is:

$$\begin{aligned} e_1 &= E_1\left\{1 - \frac{C_1'}{C_1' + K_1'}\cos\left(\frac{t}{\sqrt{L_1''(C_1' + K_1')}}\right)\right\} \\ &\cong E_1\left[1 - \cos\left(\frac{t}{\sqrt{L_1''C_1'}}\right)\right] \end{aligned} \qquad \text{Eqn. 2.65}$$

As a result, oscillation frequency of neutral voltage is twice of the line frequency as in practical case. Note that neutral voltage frequency is $1/\left(2\pi\sqrt{L_1''C_1'}\right)$. This is the same as the natural frequency of oscillation of an isolated neutral if:

$$C_1' = \frac{1}{(2\pi f_1)^2 L_1''} \text{ Farad,} \qquad \text{Eqn. 2.66}$$

$$C_2' = \frac{1}{(2\pi f_2)^2 L_2''} \text{Farad,} \qquad \text{Eqn. 2.67}$$

by Eqn 2.62

$$K_1' = \frac{1}{(2\pi f_1)^2 L_1''}\left(\frac{e_1}{E_1 - e_1}\right) \qquad \text{Eqn. 2.68a}$$

$$K_2' = \frac{1}{(2\pi f_2)^2 L_2''}\left(\frac{e_2}{E_2 - e_2}\right) \qquad \text{Eqn. 2.68b}$$

From equations (2.61) and (2.63);

$$C_3' = \frac{E_2}{E_1} C_{02} \qquad \text{Eqn. 2.69}$$

and by Eqn. 2.61

$$\begin{aligned} C_1'' &= C_{01} - (K_1' + C_3') \\ &= C_{01} - \frac{E_2}{E_1} C_{02} - \frac{1}{(2\pi f_1)^2 L_1''}\left(\frac{e_1}{E_1 - e_1}\right) \end{aligned} \qquad \text{Eqn. 2.70}$$

$$C_2'' = C_{02} - \frac{E_2}{E_1} C_{02} - \frac{1}{(2\pi f_2)^2 L_2''}\left(\frac{e_2}{E_2 - e_2}\right) \qquad \text{Eqn. 2.71}$$

Then, rational values to all the constants of the general equivalent circuit can be assigned.

Model can be further simplified by deleting $K_1'$ *and* $K_2'$. Although they yield small initial voltages at neutral, they do not affect either the frequency or amplitude of the neutral oscillations. Furthermore, neutral oscillations are outside the scope of this thesis.

$C_3'$ accounts for the initial voltage at the secondary line terminal. If secondary is grounded, $C_3'$ can be deleted, provided that $C_1''$ *and* $C_2''$ are correspondingly increased to satisfy Eqn.2.61. On the other hand, this is not the case if the line terminal is connected to surge impedance. When the equation Eqn. 2.38 is solved for that case and processed it yields:

$$\frac{E_2}{E_1} = 0.193\varepsilon^{-10.8t} \qquad \text{Eqn. 2.72}$$

Therefore $C_3'$ can be ignored for all practical cases i.e. transformer is connected to an underground cable overhead line, or generator. Then equivalent circuit becomes as in Fig. 2.7, so that effective capacitance of transformer appears lumped between line and ground.

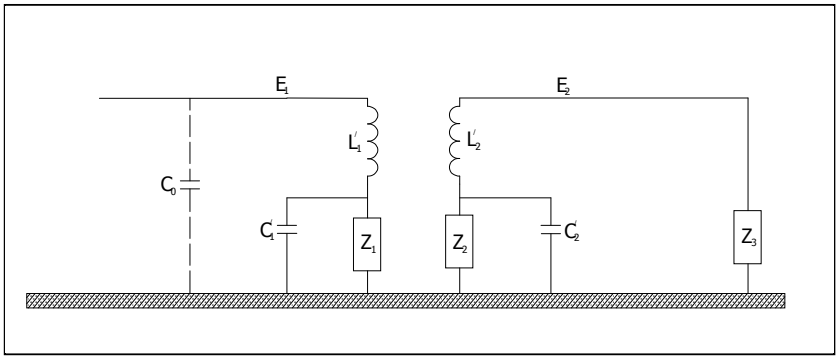


Fig. 2.7 Simplified Model for Complete Terminal Transients

Line terminal distribution of potential is needed to analyze the fault location and distinguish the faults that occur before or after the transformer. As just pointed, the effective capacitance of a transformer appears between line and ground. This capacitance, which is quite small i.e. 0.0002μF to 0.001μF for ordinary transformers, controls the initial stage of reflections from the line terminal, but it becomes quickly charged and transformer (if grounded neutral) acts as a pure inductance. Thus, model is simplified as in Fig. 2.8. The switch (S) is open for isolated neutral and closed for grounded neutral.

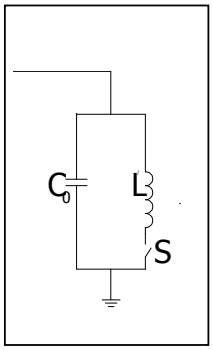


Fig. 2.8 LC Equivalent of Transformer for Terminal Transients

If this model is connected to the end of line having characteristic impedance Z, the solution is…

$$e = \frac{2E}{ZC}\frac{1}{n-m}\left(\varepsilon^{-mt} - \varepsilon^{-nt}\right) \qquad \text{Eqn. 2.73}$$

where $m = \frac{1}{2ZC} - \sqrt{\frac{1}{(2ZC)^2} - \frac{1}{LC}} \cong \frac{Z}{L}$

$$n = \frac{1}{2ZC} + \sqrt{\frac{1}{(2ZC)^2} - \frac{1}{LC}} \cong \frac{1}{ZC}$$

hence approximately

$$e = 2E\left(\varepsilon^{-tZ/L} - \varepsilon^{-t/ZC}\right) \qquad \text{Eqn. 2.74}$$

As an example, if C = $0.001 \times 10^{-6}$ F, L = 0.05H, and Z = 500 Ω

$$e = 2E\left(\varepsilon^{-0.01t} - \varepsilon^{-2t}\right)$$

It can be seen that, the transient consists of a steep front determined by Z and C, and a long tail determined by Z and L. Accordingly model can be further simplified as pure capacitance for the initial stage and pure inductance for the final stage as in Fig. 2.9.

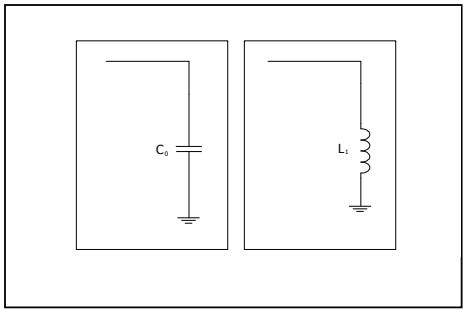


Fig. 2.9 Initial and Final Equivalents of Transformer for Terminal Transients

### 2.2.4 Stub line model

As far as reflections are concerned, inductances and capacitances can be represented as stub lines. This application greatly simplifies the calculations while making easier to understand reflection characteristics of related elements. According to stub line theory the capacitances will be represented by the open circuited stub lines and the inductances by short circuited stub lines. Lengths and other parameters of such lines can be found as follows.

**Stub line for capacitance**

Before starting any derivation it will be useful to define necessary parameters. $Z_0$ and $Z_s$ in Fig. 2.10 are the surge impedance of main line and stub line respectively. Other necessary parameters are as follows.

$T_s$ = travel time of wave through stub line

$\ell_s$ = length of step line

$C_s$ = unit capacitor ($C_2 = \ell_s C_s$ = total capacitance of stub line)

$L_s$ = unit inductance

$\tau = Z_0C_2$ = time constant of system

V = propagation velocity of wave

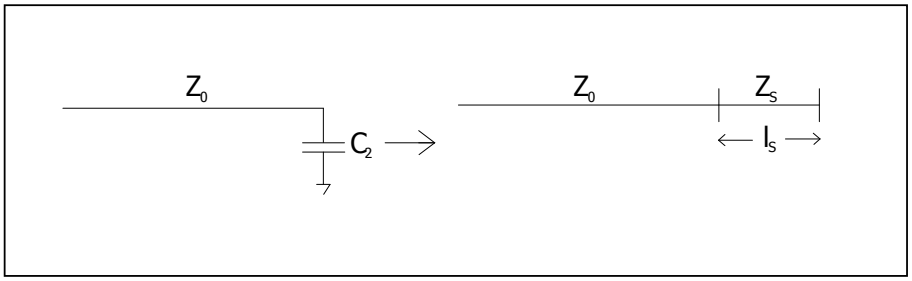


Fig. 2.10 Capacitive Stub-line

According to theory $T_s << Z_0 C_2$ is needed. Therefore assume $T_s \leq 0.1 Z_0 C_2$

$$T_s = \frac{\ell_s}{V} = \frac{\ell_s}{\frac{1}{\sqrt{L_s C_s}}} = \ell_s \sqrt{L_s C_s} \qquad \text{Eqn. 2.75}$$

$$Z_s = \sqrt{\frac{L_s}{C_s}} \Rightarrow \sqrt{L_s} = Z_s \sqrt{C_s} \qquad \text{Eqn. 2.76}$$

$$T_s = \ell_s \sqrt{L_s C_s} = \ell_s C_s Z_s = Z_s C_2 \qquad \text{Eqn. 2.77}$$

$$\text{let } T_s = Z_s C_2 = 0.1 Z_0 C_2 \Rightarrow Z_s = 0.1 Z_0 \qquad \text{Eqn. 2.78}$$

As a result, letting the parameters as specified above enables to represent capacitor as stub line. Stub line will be left open circuited as in Fig. 2.10.

**Stub line for inductor**

Newly introduced and modified variables are as follows.

$\tau = \frac{L_2}{Z_0} =$ time constant of system, where $L_2 = \ell_s L_s =$ total inductance

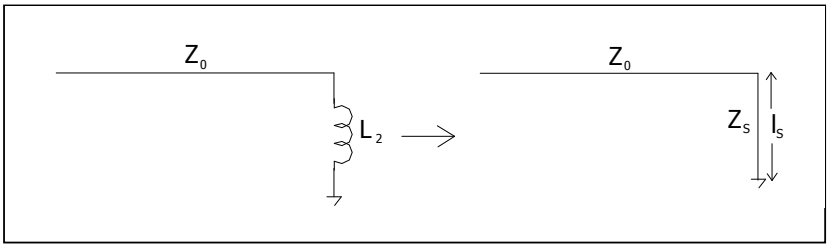


Fig. 2.11 Inductive Stub-line

Similarly $T_s << \frac{L_2}{Z_0}$, and let $T_s \le 0.1\frac{L_2}{Z_0}$

Then, by Eqn. 2.75 $T_s = \frac{\ell_s}{V} = \frac{\ell_s}{\frac{1}{\sqrt{L_s C_s}}} = \ell_s \sqrt{L_s C_s}$

$$Z_s = \sqrt{\frac{L_s}{C_s}} \Rightarrow \sqrt{C_s} = \frac{\sqrt{L_s}}{Z_s} \qquad \text{Eqn. 2.79}$$

Let $T_s = \frac{L_2}{Z_s} = 0.1\frac{L_2}{Z_0} \Rightarrow Z_s = \frac{Z_0}{0.1} = 10Z_0$

Once the all parameters of stub line are specified as found, it will be short circuited as in Fig. 2.11.

As a result, LC equivalent circuit of transformer can be represented as a stub line, and response can be calculated by accounting series of reflections instead of solving differential equations. Both methods give the same result as in Fig. 2.12.

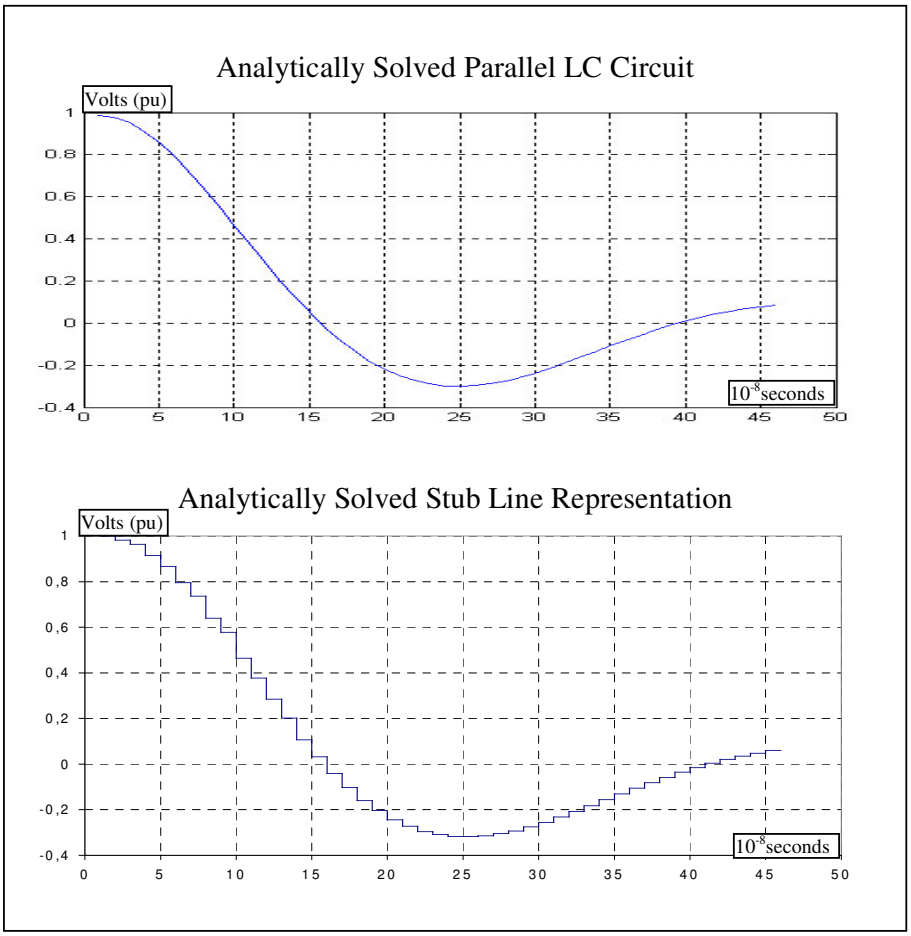


Fig. 2.12 Calculated LC Response

### 2.2.5 Earth Model [2]

Although the formulas related with earth impedances were given in previous sections, it will be useful to further investigate this concept. Because given formulas should slightly be modified according to environmental properties of cable location. For example, cable can directly be located to the soil or it can be located into cable ducts or pipes. These differences can be accounted by adjusting outermost radius of the related cable.

Mainly there are two earth models, semi-infinite earth model and infinite earth model. Related model are to be chosen according to the penetration depth for given frequency and the depth of cable location. Depth of penetration is given as…

$$d_{penetration} = \frac{\sqrt{2}}{|m|} = 503\sqrt{\frac{\rho_{earth(\Omega m)}}{f_{(Hz)}}} \qquad \text{Eqn. 2.80}$$

When penetration depth exceeds the burying depth it is assumed semi-infinite earth, otherwise it will be infinite earth. For the former cases formulas given in the eqn. 2.10 & eqn. 2.11 are valid. On the other hand, formulas should be modified as follows for latter case.

$$Z_{earth} = \frac{\rho m K_0(mr)}{2\pi r K(mR)} \qquad \text{Eqn. 2.81}$$

$$Z_{mutual} = \frac{\rho K_0(md)}{2\pi r R_i R_k K_1(mR_i) K_1(mR_k)} \qquad \text{Eqn. 2.82}$$

note that, these formulas derived from tubular conductor formula by letting…
q = R, (inside radius of tubular conductor = outside radius of the cable)
$r \to \infty$, (outer radius of tubular conductor goes infinity)

**2.3 EMTP Models [5]**

An EMTP (Electro-Magnetic Transients Program) is going to be used for the solution of the transients involved in the distribution system which is composed of the elements modeled in the previous sections. The ability of the build in functions available in EMTP to cope with the desired models will be examined in the following sections.

### 2.3.1 Cable Model

Necessary parameters to model the cable can be obtained either by calculation or from its data-sheet provided by manufacturer. In fact, manufacturer data is sufficient for many applications, especially in steady state, but it cannot cover all practical applications when detailed simulations are considered. In addition, precise value of R, L and C becomes more important when high frequency applications are considered. Build in EMTP function “Cable Constants” routine can easily handle any possible practical situation.

Frequency dependence is another important subject. Because of transient events, i.e. reflections, resonance, etc, there will be number of changes in different frequencies. Cable model should also be capable of responding appropriately to the different frequencies. In other words, the cable model should be frequency dependent. Fortunately, frequency dependence can easily be satisfied by using another EMTP routine, named “Semlyen Setup”. Semlyen setup calculates frequency dependent parameters of cable and punches the resultant parameters as a separate file which can directly be embedded into EMTP code as a conductor between defined nodes.

### 2.3.2 Bus-bar Model [3]

Being one of the discontinuity points in the system, bus-bars must be modeled and their effects should be examined for the sake of analyses. Unfortunately there is no build in function in EMTP to directly model the bus-bars which enclosed by metal cell. For that reason, bus-bars will be modeled approximately by using present EMTP facilities.

Before starting to model such bus-bars, certain criteria should be established. By being surrounded by grounded metallic cell which affect capacitance of system considerably, bus-bars are different from aerial lines. By the absence of insulation, sheath, and armor around the core conductor, also, they are different from cables,

too. Furthermore, phases placed apart from each other to prevent flashovers. Thus bus-bars cannot be classified as aerial line or cable. Under these circumstances bus-bars can be modeled by EMTP as follows.

- **Metal Cell That Surrounds the Bus-bar:** Using "cable constants" metal cell can be modeled as a pipe that surrounds a conductor. Furthermore, pipe can separately be grounded just like the metal cell done in reality. Approximation is introduced in the shape of enclosure. Although the metal cell is rectangular, the pipe can only be defined in cylindrical shape. Thus, unlike the rectangular metal cell the pipe uniformly surrounds the conductor.
- **Cross-section:** Desired cross-section can easily be achieved by simply editing conductor radius accordingly in the "cable constants" routine.

- **Frequency Dependence:** As it pointed above, bus-bar model should be frequency dependent like the rest of circuit elements. "Cable constants" routine can be imbedded into "Semlyen Setup" routine to produce frequency dependent model.

Since all specification cannot be satisfied at the time, resultant bus-bar model will be an approximate model with acceptable simplifications for this study. As a result, bus-bar will be modeled as bare conductor passing through metal pipe as shown in Fig. 2.15. Bus-bar is going to be constituted by using (2 x 3m 240mm$^2$) bare solid core conductor enclosed by pipe. This can be achieved by assigning cable that has only core conductor, its first insulating layer is nothing but air, and finally it is surrounded by circular metallic pipe.

Once parameters are found frequency dependence will be satisfied by using "Semlyen setup" routine as described in the previous section.

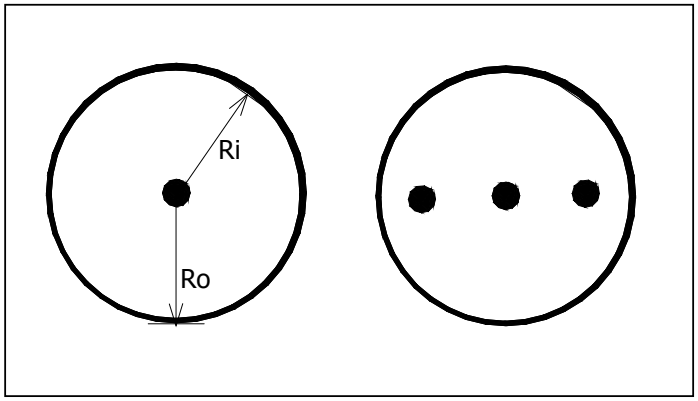


Fig. 2.15 Position of Bus-bars in the Metallic Conductor

### 2.3.3 High Frequency Transformer Model [6]

Transient phenomena in transformer can basically be explained as follows…

a) When surge hits to the transformer, current starts to flow first in the dielectric structure then in the winding by charging winding capacitances. Up to 1 μs flux cannot penetrate in the ferromagnetic core, so that core losses of inductance can be neglected while losses in conductors and dielectrics are important.
b) After 1 μs flux starts to penetrate in the core. As a result, inductance characteristics shift from air core to iron core between 1 μs to 10 μs period. Although current primarily flows through the capacitances, it also begins to flow in conductors.
c) Finally the transformer becomes stable after 10 μs. The conductor losses include skin effect and proximity effects, and the core losses include the eddy current effect. Also there are dielectric and transformer tank losses.

There is no built in EMTP capability for these kinds of transients. However appropriate model can be introduced to achieve required goals. Note that, transformer characteristics will be linear, since saturation cannot penetrate the iron core. For single phase systems proposed "EMTP High Frequency Transformer Model" is given in Fig. 2.16. This transformer will be called as "EMTP Transformer" throughout rest of this thesis. Output characteristics of EMTP transformer and the transformer in Fig. 2.6 are almost the same except for minor differences. Single phase EMTP transformer can be extended into three phase EMTP transformer by adding necessary capacitances namely inter-phase capacitances and connecting three single phase transformers as Δ–Y. Resulted model is in Fig. 2.17 [7].

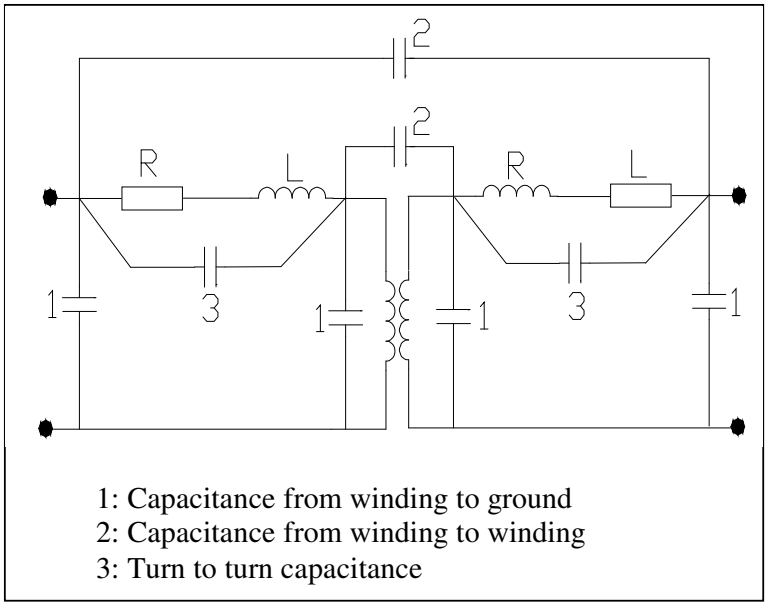


Fig. 2.16 Single Phase High Frequency Transformer

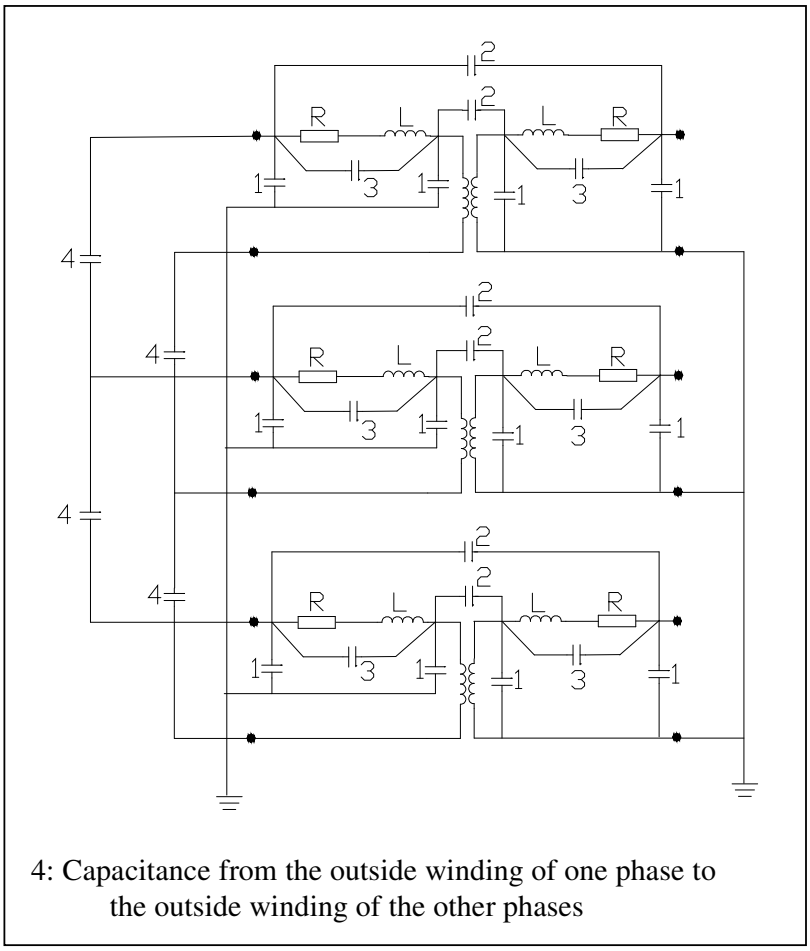


Fig. 2.17 Three-phase High Frequency Transformer

### 2.3.4 Source, main transformer, and switch models [8]

Since the aim of this study is the examination the reflections which are caused by system elements i.e. bus-bars, cables, transformers, etc., source side of the system will be modeled accordingly, in order to observe these reflections as clear as possible.

The main source is to be modeled as an ideal voltage source, which will be connected to the system through main transformer and circuit breaker. In the 3-phase systems, the sources will be wye (Y) - connected.

The main transformer will not be modeled as an ideal transformer, because ideal transformer connected to the ideal voltage source neglects whatever comes in with an opposite sign, therefore the voltage at the observation point is always the source voltage. On the other hand, inclusion of the stray capacitances to the main transformer distorts the reflected wave characteristics and complicates the resulted waveform. For these reasons, main transformer will be modeled by including only its winding inductance, so that incoming waves reflects with minimum distortion.

Two switches are used to simulate the source side circuit breaker (CB) and the fault making. Fault making is a time-controlled switch which is initially open and closed at the determined point of the voltage wave. On the other hand, the closure of the source side CB is simulated by a negative time which will reacts the system to be at steady state by the time the fault takes place. The opening of this CB is defined with operation time and an additional current criterion. The current criterion is predefined current margin i.e. if the absolute value of current becomes less than the defined current value; current through the switch is forced to zero at the next step. $t_{open}$ is the operation time of CB which clears fault. On the other hand, it must be kept larger than the simulation time for the fault switch in order to properly simulate the fault.

### 2.3.5 Earth model [2]

EMTP provides two different earth models, which are Carson's homogeneous earth model and Nakagawa's three layer stratified earth model.

Being homogeneous Carson's earth model is rather simpler. Substituting the resistivity of soil to the related routines is enough to simulate earth return in question. This simple model is usually enough to simulate the most practical applications, especially high frequency transients, since increasing frequency reduces the penetration depth. Nakagawa's three layer stratified earth model is relatively complicated compared to former model. As well as, resistivity of each layer, also depth, permittivity, and permeability of layers are required. In practice,

former model is preferred because usually needed data are not available for latter one.

Also EMTP introduce reasonable approximations to the Eqn 2.10 and Eqn 2.11 to simplify the calculations. As a result, related equations become as follows…

$$Z_{Earth} = \frac{\rho m^2}{2\pi}\left(-\ln\frac{\gamma m R}{2} + 0.5 - \frac{4}{3} m h\right) \qquad \text{Eqn. 2.83}$$

$$Z_{Mutual} = \frac{\rho m^2}{2\pi}\left(-\ln\frac{\gamma m d}{2} + 0.5 - \frac{2}{3} m \ell_2\right) \qquad \text{Eqn. 2.84}$$

where $\gamma$ = Euler's constant

$\ell_2$ = sum of depths of burial of the two conductors

# CHAPTER 3

# ANALYSIS OF TRAVELLING WAVES DUE TO FAULT

## 3.1 Introduction

Once a fault takes place, voltage that is equal to the pre-fault voltage at the faulted point with opposite sign starts to travel along the line, and eventually it reaches to the main sub-station. If some unique characteristics of such a wave can be found, they could be used to determine the fault location. Here the key ideas are wave propagation time, which gives fault distance when multiplied with propagation velocity, and the waveform which is distorted by the system elements i.e. bus-bar, transformer, etc.

Actually the wave characteristics are too complicated to be directly analyzed because of mutual couplings between phases. For this reason, studies will be first done on a simple single phase system which will then be carried on to the more complicated systems, and finally to the three phase practical systems.

## 3.1 Verification of simulation results by calculation

Reflections in the system take place according to reflection coefficient at the junction or discontinuity points. Once the general characteristics of reflection coefficient are determined, it will be easier to follow simulation and calculation

results. For the circuit in Fig. 3.1, there are mainly five such points. They can be examined as follows:

A: Right side of this point is cable, while the left side is connected to the transformer which has higher characteristic impedance than cable. Furthermore, transformer has inductive impedance which makes the impedance infinite at the impact instant. When the reflections under investigations are considered reflection coefficient could be assumed almost (+1) as shown if Fig. 3.2.

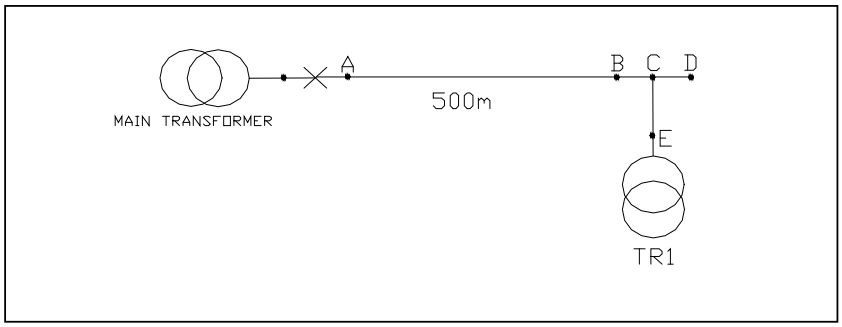


Fig. 3.1Simple Circuit That Contains All System Elements

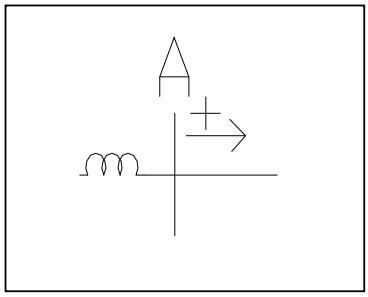

Fig. 3.2 Reflection Coefficient at Point A

B: Neighborhoods of this point are bus-bar on the right hand side, and cable on the left hand side. Since the characteristic impedance of bus-bar is higher, reflection coefficient for the wave coming from right is negative, and it is positive for the wave coming from the left (Fig. 3.3).

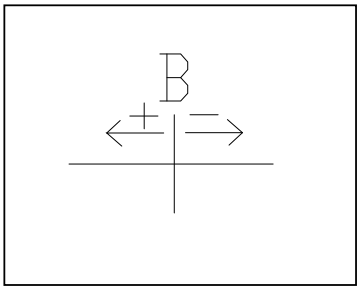


Fig 3.3 Reflection Coefficients at Point B

C: This is the midpoint of bus-bar. For the waves coming both from B and C reflection coefficient is negative, because related waves see parallel combination of other half of bus-bar and cable that is used for transformer connection. On the other hand, reflection coefficient for the wave coming from E depends on the number of connections at that point. If there is single connection at midpoint the characteristic impedance of cable is lower than the parallel connections of two bus-bar sections (this is the case assumed for simulations in this study), otherwise characteristic impedance of cable in question becomes higher than the parallel combination of other connections. Resultant cases are given in Fig. 3.4.

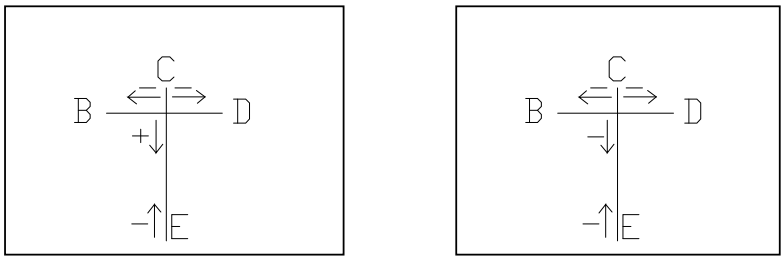


Fig. 3.4 Reflection Coefficients at Point C and E

D: Being the end-point of the bus-bar this point can either be connected to another cable or open-circuited. For the former case, it is mirror image of the reflection of point B, and for the latter case reflection coefficient sign for wave coming from c is positive as in Fig. 3.5.

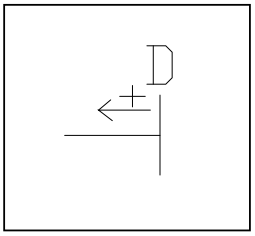


Fig 3.5 Reflection Coefficient at Point C

E: At this point, cable sees capacitive and inductive impedances in parallel which is the high frequency transformer model. Actually reflections are so fast that they cannot penetrate into the inductance, causing almost pure capacitive impedance. As a result, reflection coefficient at this point can be taken as negative for fast transients (Fig. 3.4).

Reflections characteristic of system in Fig 3.1 is as given or shown in Fig.3.6. Note that, fault introduce (-1) reflection coefficient to the related point no matter where the fault occurs.

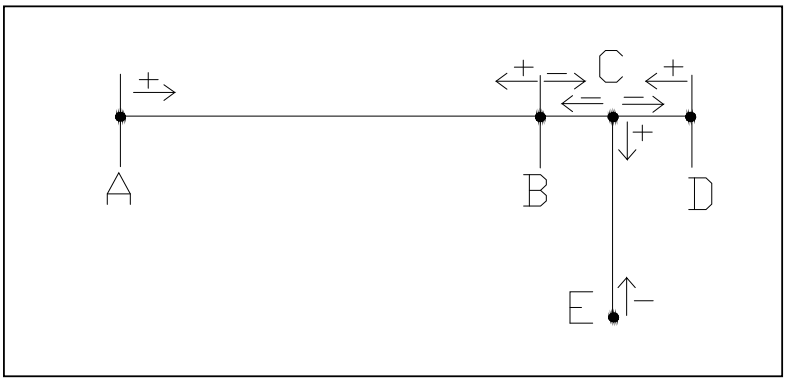


Fig. 3.6 Reflection Coefficients of Entire System

At this point, it is convenient to justify EMTP results by calculation for relatively simpler circuit. For this purpose, simple practical system will further be simplified to make hand calculations possible. System given in Fig. 3.7.a consists of practical models that are derived in the Chapter 2. Obviously, calculations for such circuit

are too complicated to be carried out by manually. For that reason, circuit should be simplified as in Fig. 3.7.b so that it can further be simplified (Fig. 3.7.c) to make calculations easy enough to be done manually. Detailed description of circuits in Fig. 3.7b and Fig.3.7c can be given as follows:

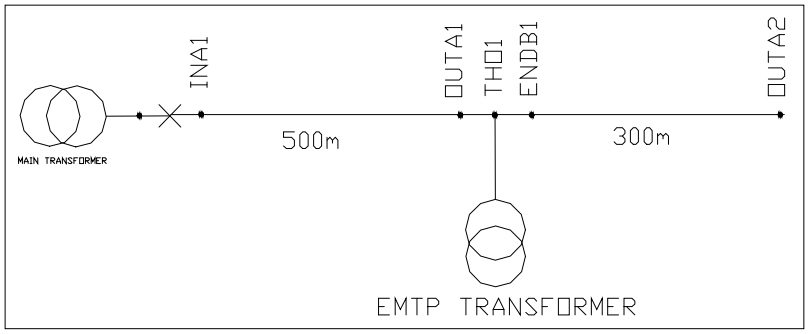


Fig. 3.7a A practical feeder branch

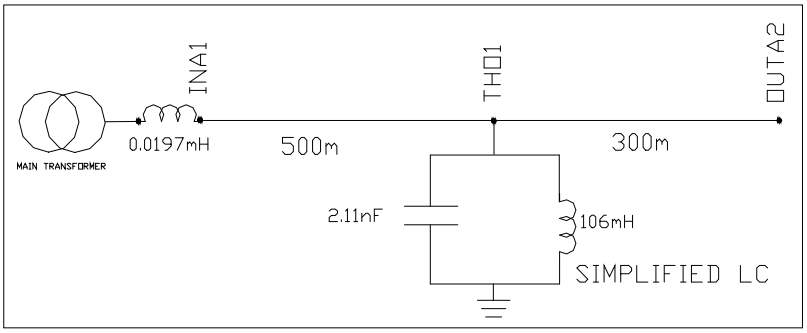


Fig. 3.7b Transformer replaced by its LC equivalent

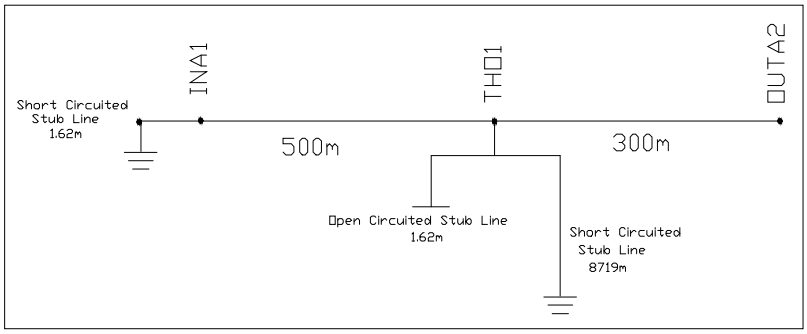


Fig. 3.7c L and C represented as stub lines

Fig. 3.7 Simplification Process for Manual Calculations

Fig. 3.7b is simplified circuit. Lines are assumed to be lossless. Bus-bars have been removed since they introduce reflections which increase exponentially in number and complicate the calculations enormously. Distribution transformer is represented by its LC equivalent, as given in section 2.2.3.5, to make it simple enough to be represented by the stub-lines. Finally, the main transformer is assumed to be ideal with small inductance. Without this inductance no reflection can be observed at the source side due to (-1) reflection constant. All capacitance and inductance values in the system are chosen so that their stub-lines lengths are equal or integer multiplicands of smallest line. This choice makes calculations easier by the coincident arrival of the successive reflections.

Fig. 3.7c is simple enough to carry out the manual calculations by replacement of capacitances and inductances with their stub-line equivalents. Note that, stub-line for the inductor at (THO1) is so long that reflections from the end of this line do not return to the junction point in the calculation period. Thus final form of Lattice Diagram that is used during calculation is quite simple as in Fig. 3.8

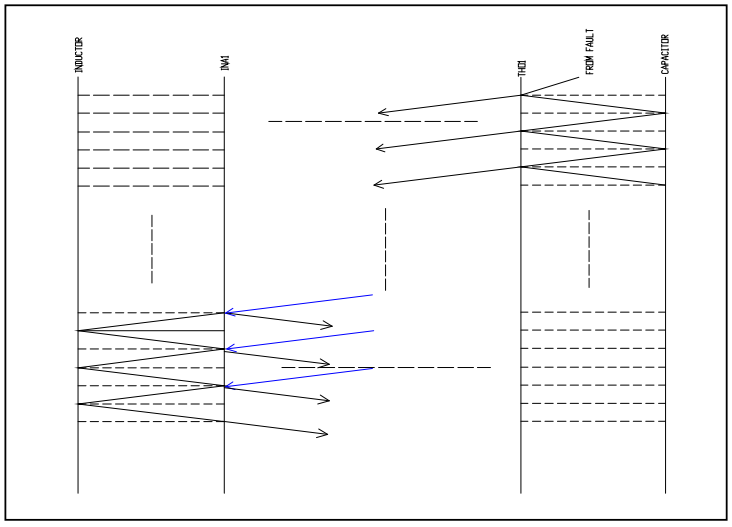


Fig.3.8 Lattice Diagram of First Few Reflections

When the final simplified circuit is run with EMTP, and it solved manually for the fault at the end of second line (OUTA2), results are the same as expected (Fig. 3.9).

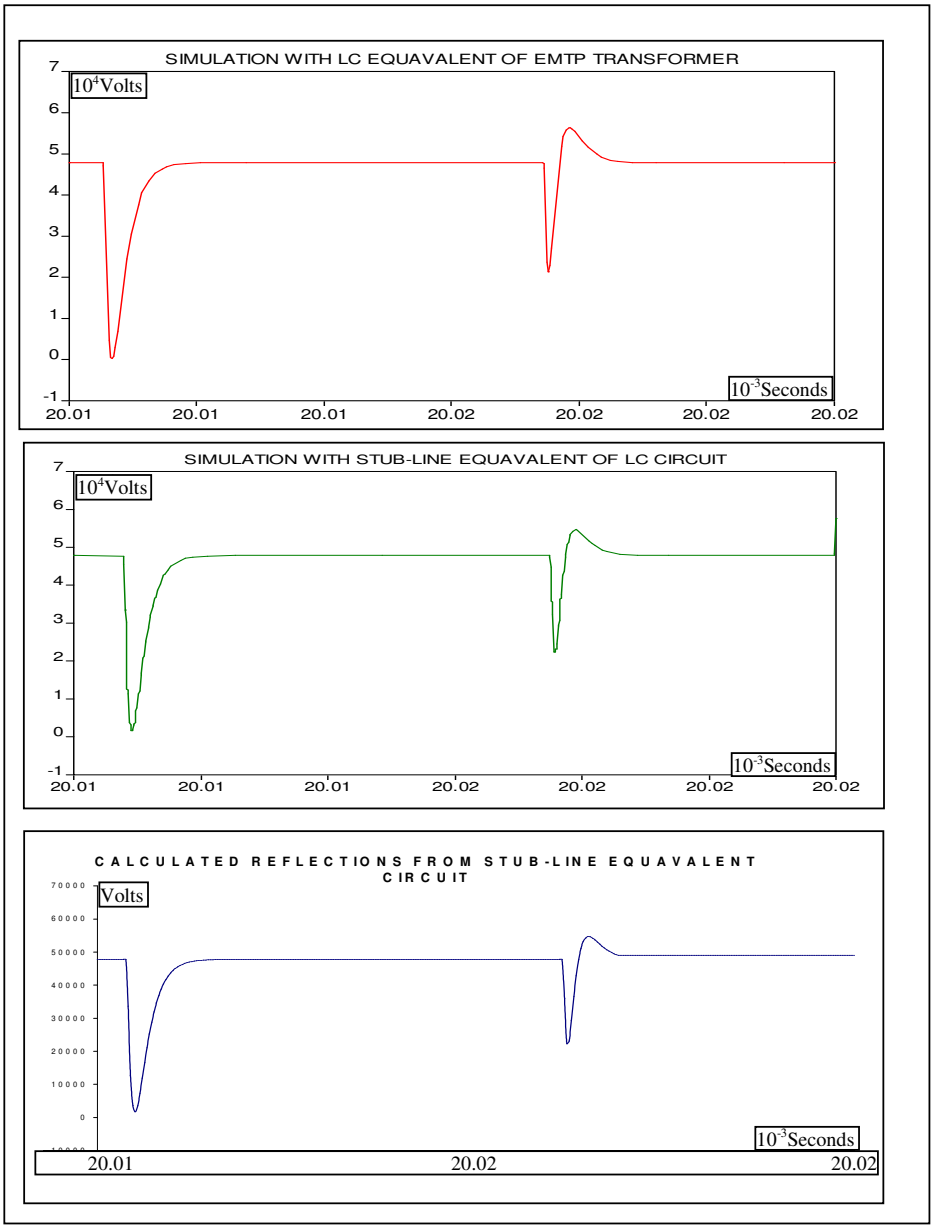


Fig. 3.9 Comparison of Simulation and Calculation Results

### 3.3 Effects of modeling of the elements of distribution system

Before starting to analyze practical systems, it is convenient to study each derived model given in Chapter 2, and observe their effects. Simulating faults at B, C, and D for the system in Fig. 3.1, will include cable, bus-bar, and transformer respectively into the system one by one. Effect of each element can be observed by simply comparing the related output with the previous one. Reflections will be observed from point A for all faults given below.

The output for the fault at point (B) (Fig.3.10) has the most basic characteristics. The negative wave originated due to fault at 6.25 $\mu$sec reaches to the observation point after a time delay. This time delay depends on cable length and propagation velocity. Since incoming wave is negative and it is reflected with a positive coefficient, sudden drop is observed. Change is not exactly twice of pre-fault voltage because of losses. Then wave travels back to the fault point and returns with the positive value due to (-1) reflection coefficient at the faulted point. This phenomena repeats itself until the magnitude of traveling waves becomes zero due to losses.

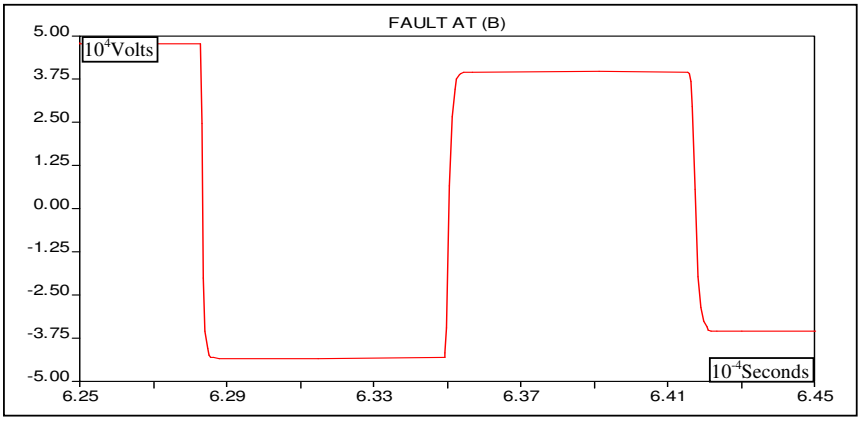


Fig. 3.10 Waveform for the Fault at Point B

When the fault occurs at in the middle of bus-bars where the transformer connection takes place, the situation slightly gets complicated, since bus-bar is

included into system. When voltage at the observation point (Fig. 3.11) compared with previous case, the first reflections give rise to the same response except for the smoother voltage drop in latter compared to former one. Major difference observed in second and further reflections. Note that, first reflected wave from the source is negative. When this wave reaches to the (B) it reflects with positive reflection coefficient before reaching the fault point where it is reflected with negative one. This occurrence introduces a peak at the end of characteristic as observed. Similar to the first case, reflections continue until they die out due to losses in the system.

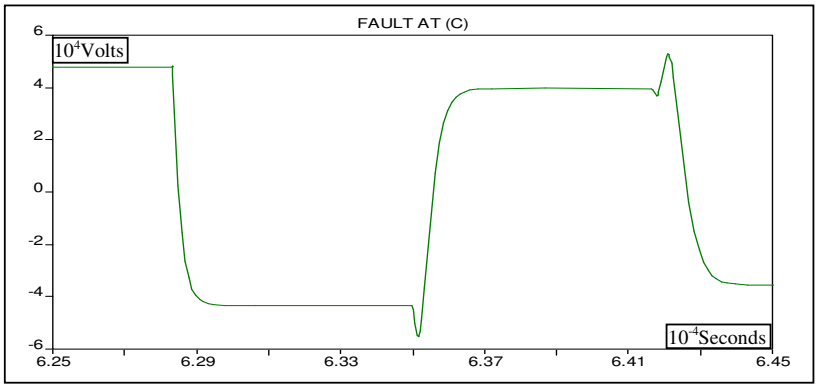


Fig.3.11 Waveform for the Fault at Point C

For the final case, where the fault takes place after the bus-bar (point D in Fig.3.1), the resulted waveform (Fig. 3.12) will be composed reflections from the transformer bus-bar junction, from the transformer, and cable bus-bar junction. On

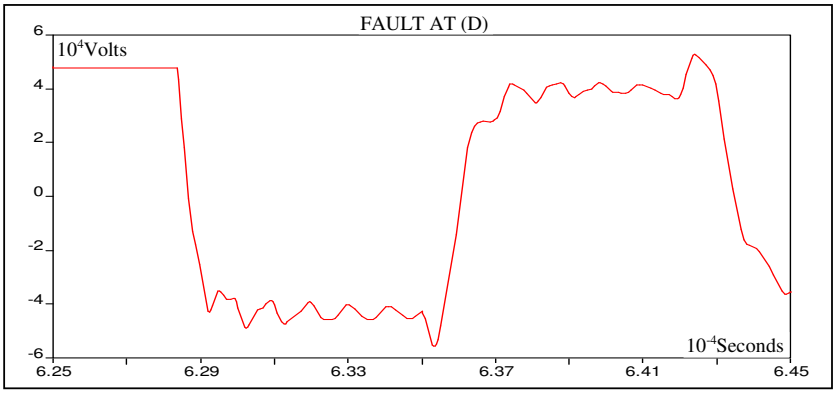


Fig. 3.12 Waveform for the Fault at Point D

the other hand, small oscillations at 1.2MHz are corresponding to the resonance frequency which is due to the transformer capacitance and the line inductance.

In this simple system, precise detection of fault location is possible by observing these characteristics. For example, since reflections from fault to observation point can clearly be observed, traveling time can easily be found, and fault location can be determined with small error for the faults before bus-bar as in first case. Alternatively, for the faults as in second and third case fault location can be deduced from related characteristics by observed oscillations and peaks in waveforms. As a result, by observing the traveling waves due to the faults, fault location can accurately be located for such simple systems.

### 3.4 Analyses with cable shield included

Single core cables with a shield wire are the most widely used type cable in practical distribution systems. For this reason, this type of cable will be used in simulations, in the studies carried out. Presence of shield wire can be handled in two different ways.

Case 1: Shield wire can be assumed continuously grounded for the low frequency changes. This case will be referred as “case 1” throughout this section.

Case 2: Presence of shield introduces an additional conductor to the system. This leads two separate propagation modes, one of which is through the conductor and the other one is through ground, giving rise to aerial and ground modes. This case will be referred as “case 2” throughout this section.

Having only one mode, Case 1 is considerably simpler than Case 2. For this reason analysis primarily will be carried on Case 1, and then they will be compared with Case 2 for the completeness of the case.

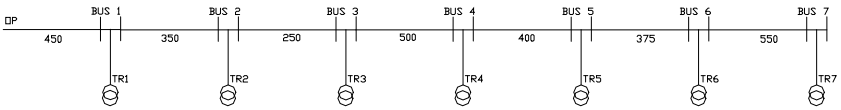


Fig. 3.13a Single-feeder System

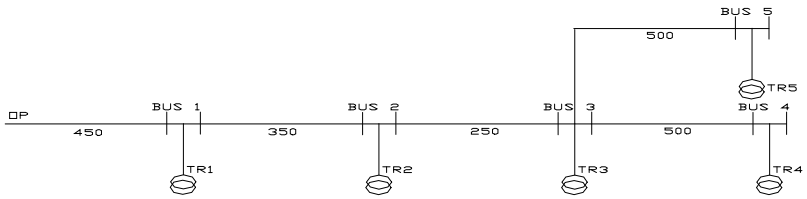


Fig. 3.13b Single-feeder two Branch System

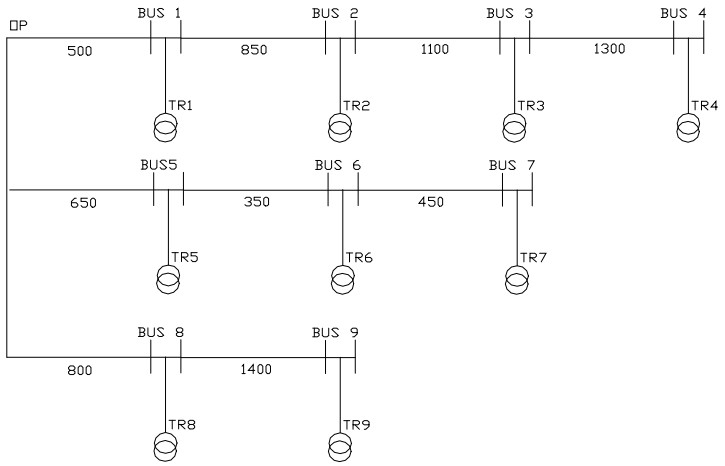


Fig. 3.13c Multi-feeder System

Fig. 3.13 Distribution Systems

Analyses will be carried for systems that contain, single branch (Fig. 3.13a), single branch at the main substation, and then multiple branches (Fig. 14b), finally multi-branches starting from main substation (Fig. 14c). Each system consists of enough number of distribution centers to observe necessary characteristics of traveling waves.

### 3.4.1 Single feeder system

This is the most basic system where will reveal the characteristics of multimode propagation. The line for continuous grounding has already been discussed for the fault at Bus 1. When the same simulation is run for Case 2, (i.e. the shield wire is not grounded continuously) the waveform obtained is given in Fig. 3.14. Comparison of these cases is given below by comparing Fig. 3.10 with Fig. 3.14.

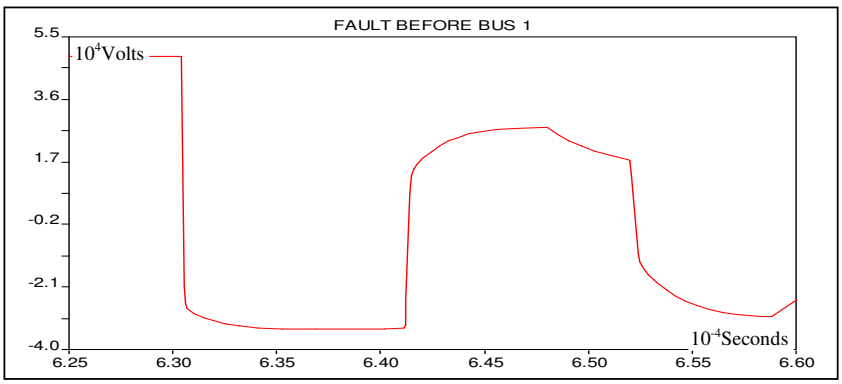


Fig. 3.14 Waveform for the Fault before Bus 1

Propagation velocity in Case 1 is higher than the one in Case 2. Because of the assumption made for Case 1 eliminates shield of conductor altogether, this introduces additional inductance to the system because of mutual couplings. Since the propagation velocity is proportional to $1/\sqrt{L}$, velocity in case 1 comes out to be higher. Since two results are not the same, it can be concluded that assumption of continuous grounding is not valid for this study, but the results that derived from that case can be used as a starting point for the more complicated practical cases.

Magnitude of traveling waves seems smaller in Case 2, although voltage magnitudes for the both case were identical just before the fault. In fact, injected negative voltage due to fault is the same for these cases. On the other hand, this negative injection travels as two parts namely 1$^{st}$ mode and 2$^{nd}$ mode components in the case 2. Note that, second reflection further attenuated because reflected wave from the fault again travels with two modes as just explained. As a result full

voltage reaches to the observation point as two parts with time delay between, and this cause the magnitude difference between the waveforms of the two cases.

In the particular example, velocity of 1st mode is about four times of the 2nd mode. For this reason, there is almost no shape difference between two waveforms up to the time 2nd mode reaches to the observation point. Once the 2nd mode arrives, the waveform is distorted accordingly. Note that, if this phenomenon can be observed that clearly for all cases, it can be used to determine the fault location by using velocity difference of two modes.

For the faults taking place at the Bus1 and at the end of the Bus 1, similar observation can be made by comparing Fig. 3.11 with Fig. 3.15 and Fig. 3.12 with Fig. 3. 16.

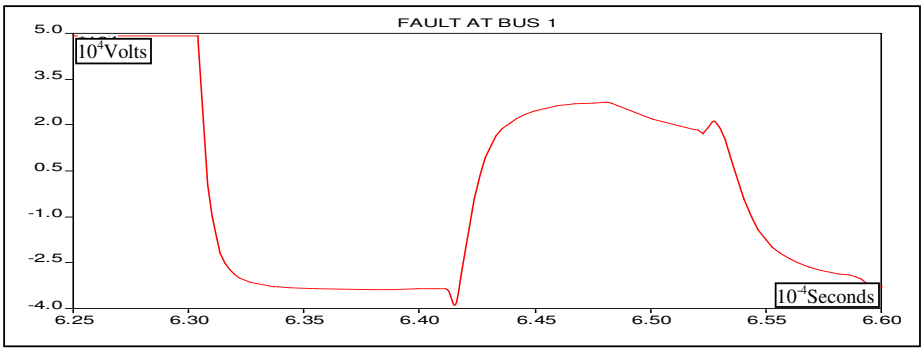


Fig. 3.15 Waveform for the Fault at Bus 1

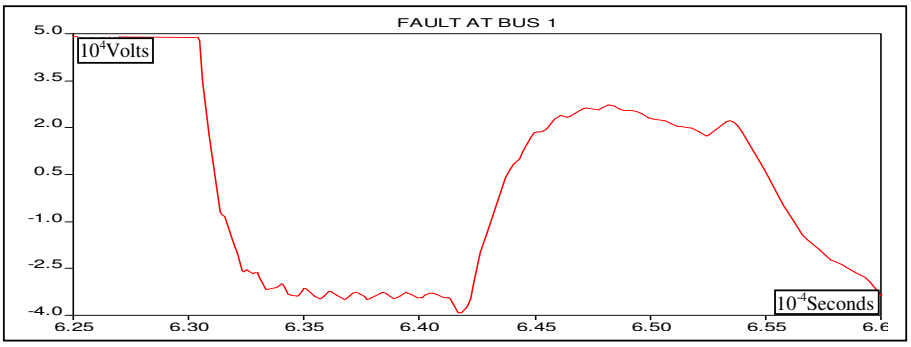


Fig.3.16 Waveform for the Fault after Bus 1

Despite of these differences, compared characteristics seem very similar only for the very first reflections. As the number of reflections increases due to the

appearance of different components the difference between waveform also increase accordingly, as given in Fig. 3.17. This is due to the fact that as the traveling wave reflects from discontinuity point, it further splits into two modes in Case 2. This occurrence increases the complexity of the case exponentially while there is only one wave reflecting back and forth in Case 1.

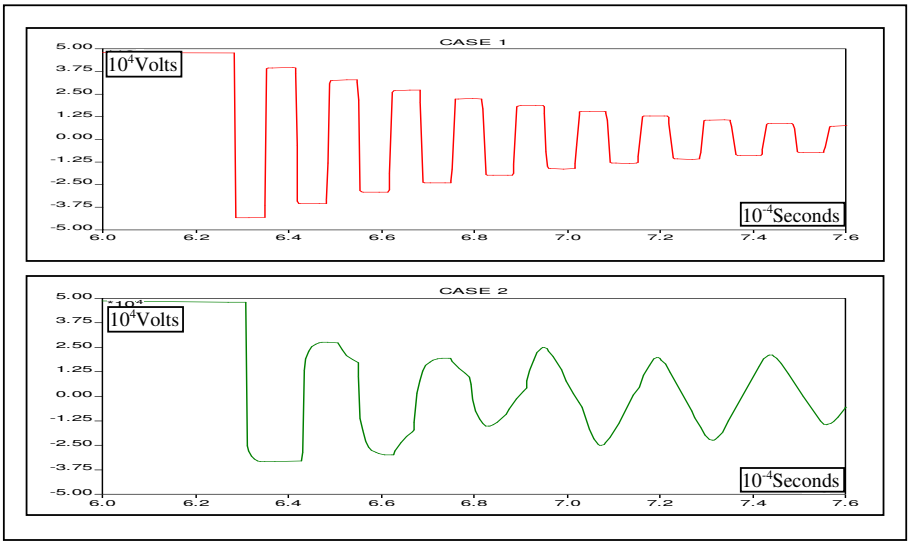


Fig. 3.17 Comparison of Single-mode and Two-mode Waveforms

When the fault occurs at Bus 2, the similarities between these cases further vanish. For Case 1 related output is as given in Fig.3.18.

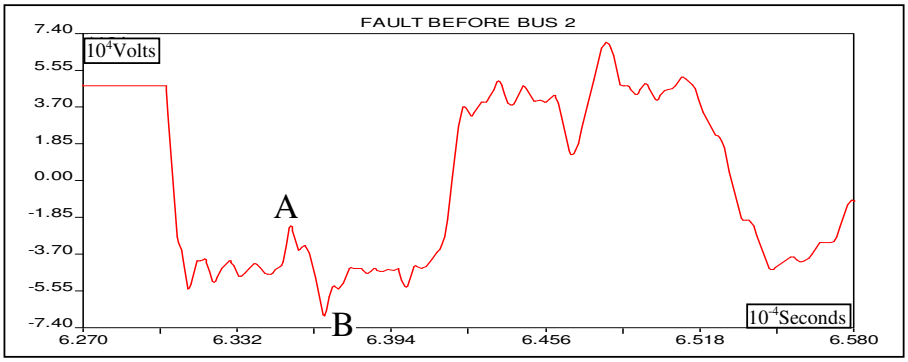


Fig. 3.18 Waveform for the Fault before Bus 2

Being very clear the main reflected waves can be observed easily. Fault distance can be calculated approximately by using the time difference between successive

reflections. Also there are intermediate reflections, due to Bus 1, between two main reflections. Positive peak (A) in Fig. 3.18 is caused by the wave that is first reflected from Bus 1 to the faulted point, and then to the observation point by gaining positive magnitude. Negative peak (B) is caused by the wave first reflecting from observation point, and then from Bus 1 by preserving its negative magnitude. Even though there are differences between the waveforms for the faults before and after Bus 2 (Fig.3.19), they are not clear as they were in the previous case. Since the fault distance is longer and there is Bus 1 between fault and observation point small differences are no longer observable.

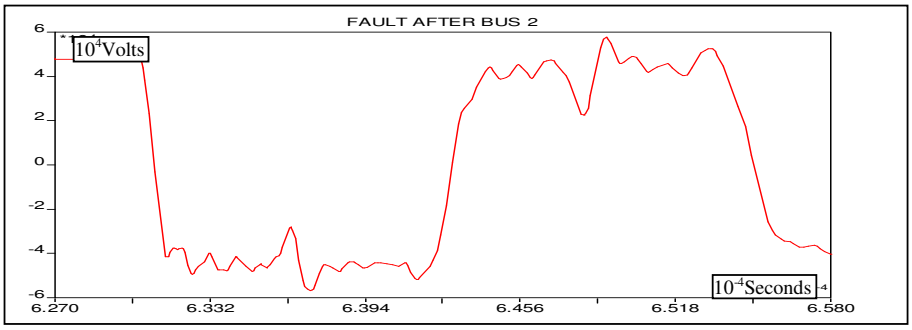


Fig. 3.19 Waveform for the Fault after Bus 2

The results due to a fault at Bus 4 can be examined in a similar manner. Fig. 3.20 is the output for the fault just before the Bus 4.

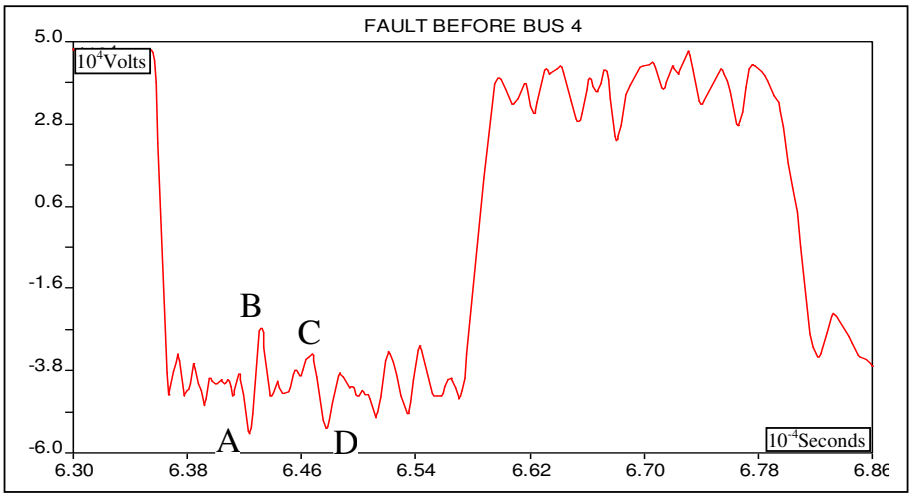


Fig. 3.20 Waveform for the Fault before Bus 4

As well as transformer oscillations, peaks between two main reflections can be explained as follows. (A) is caused by the wave first reflecting from the observation point, and then from Bus 1. The peaks (B) and (C) are due to reflections first from Bus 3 and Bus 2 respectively, then from the fault point by gaining positive magnitude. Similar to peak (A), peak (D) is as a result of reflections first from the observation point, then from Bus 2. Other peaks are composed by arbitrary reflections from bus-bars and fault point. Since the main reflections are observable, approximate location of fault can be determined. Differences between Fig. 3.20 and Fig. 3.21 are considerable, and it is felt like the exact location of fault can be determined, but it must be noted that this difference is not that clear in the case of a fault at Bus 2. In addition, it is still difficult to determine exact fault location by using just one of the waveforms, which is the case in practice.

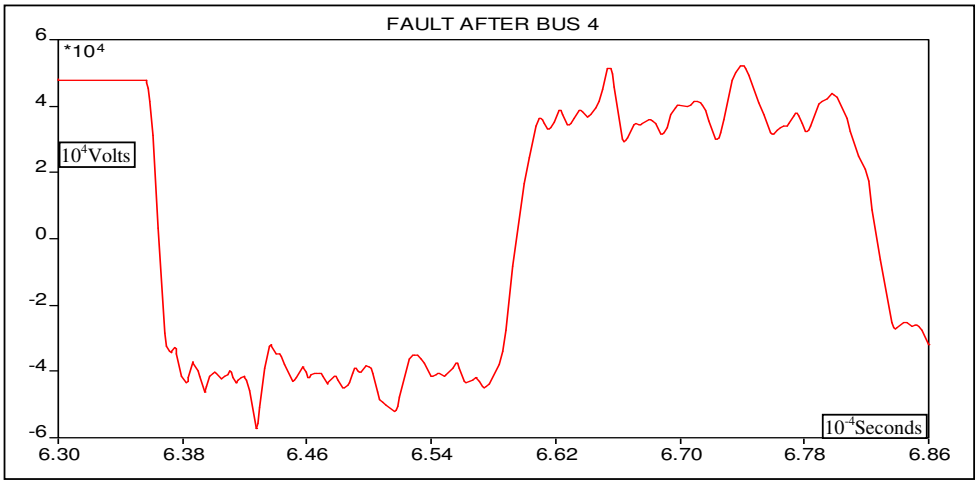


Fig. 3.21 Waveform for the Fault after Bus 4

Similar comments can be made for the faults before and after Bus 7 (Fig. 3.22), only differences being that the magnitudes of peaks become smaller and increase in number due to presence of more distribution transformer center between fault and observation point.

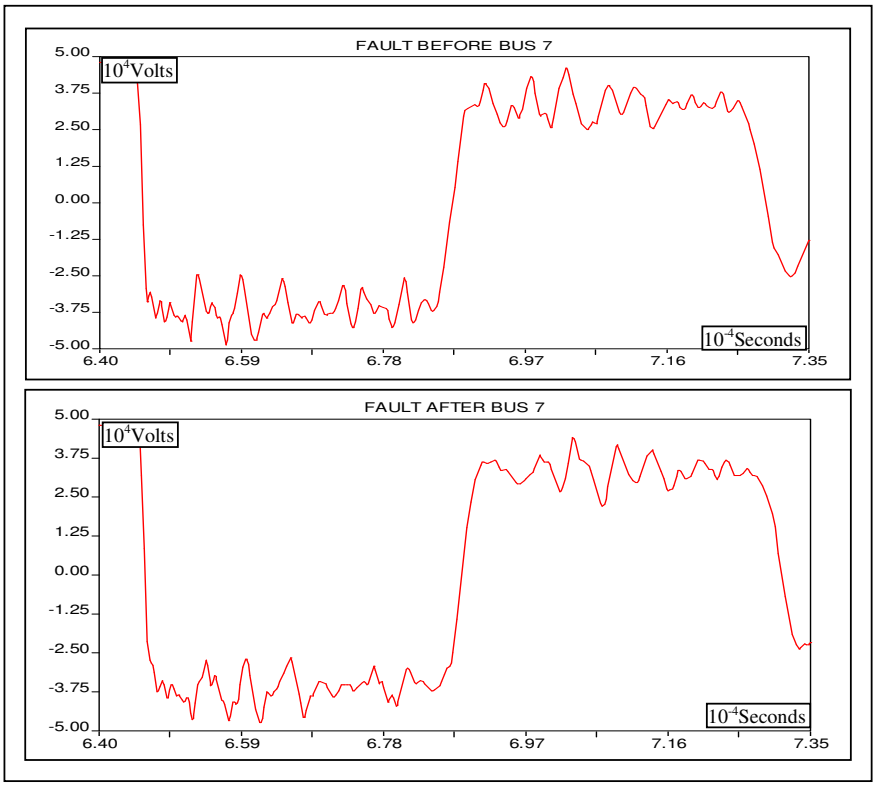


Fig. 3.22 Waveform for the Fault before and after Bus 7

This completes the analyses of single phase single feeder system with continuously grounded cable shield case i.e. case 1. As a result, fault point can be calculated by using time difference between two successive reflections. Once fault position is determined approximately, it can be pin-pointed on to whether it is before or after the distribution center by using line characteristic explained above. Indeed this is a difficult task, because of several reasons. First, there are errors in measurements. In this case, propagation velocity is so high that a small measurement error in time causes a large error in fault location. For example, largest error in Table 3.1 is caused by 0.8μs error. Second, the exact time delay between two successive reflections may not be determined due to complicated characteristics because of minor reflections. Checking figures from Fig. 3.18 through Fig. 3.22 gives an idea for that error. Note that, exact impact time of first wave is very clear while exact impact time of others is screened by minor reflections coming from the transformer distribution centers.

Table 3.1 Fault Distance that are Calculated from the Time Delay between Successive Reflections

| FAULTED BUS | EXACT LOCATION | ACTUAL LENGTH (m) | CALCULATED LENGTH (m) | ERROR (m) |
|---|---|---|---|---|
| BUS 1 | BEFORE | 450 | 450 | 0 |
| | AFTER | 456 | 450 | 6 |
| **BUS 2** | **BEFORE** | **806** | **750** | **56** |
| | **AFTER** | **812** | **825** | **-13** |
| BUS 3 | BEFORE | 1062 | 1050 | 12 |
| | AFTER | 1068 | 1125 | -57 |
| **BUS 4** | **BEFORE** | **1568** | **1650** | **-82** |
| | **AFTER** | **1574** | **1575** | **-1** |
| BUS 5 | BEFORE | 1974 | 2025 | -51 |
| | AFTER | 1980 | 2100 | -120 |
| **BUS 6** | **BEFORE** | **2355** | **2475** | **-120** |
| | **AFTER** | **2361** | **2475** | **-114** |
| BUS 7 | BEFORE | 2911 | 2925 | -14 |
| | AFTER | 2917 | 2925 | -8 |

For Case 2, characteristics are more complicated, even hardly understandable for most cases as given below because of the interference of the signals attached to the two modes. Since the system cannot be modeled as a continuously grounded system due to the high frequencies involved, the results obtained will be more realistic than those of Case 1.

For the faults at Bus 1, the simulation results were similar for both cases, especially for the first few reflections. This is not the case for the faults at Bus 2. Fig. 3.23 is the simulation output for the fault just before the Bus 2. Comparing this characteristic with Fig. 3.18, differences can be observed. (A) and (B) in the Fig. 3.23 are the same reflections as explained in case 1. The 1$^{st}$ mode component of main reflection returns at (C), and its 2$^{nd}$ mode component returns around (D).

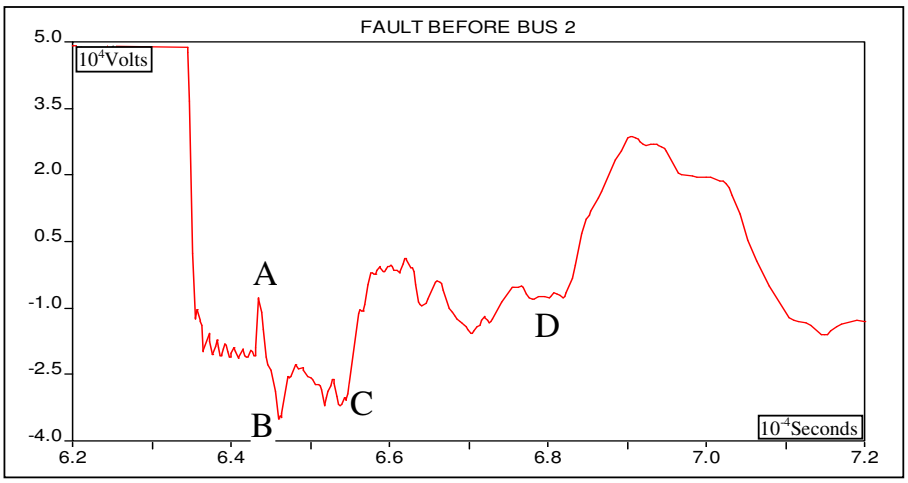


Fig. 3.23 Waveform for the Fault before Bus 2

The fault after Bus 2 (Fig.3.24), introduces similar waveforms shown. Major characteristics are almost the same with Fig. 3.23, but there are considerable differences so that the fault location may be determined exactly by careful inspection of waveform.

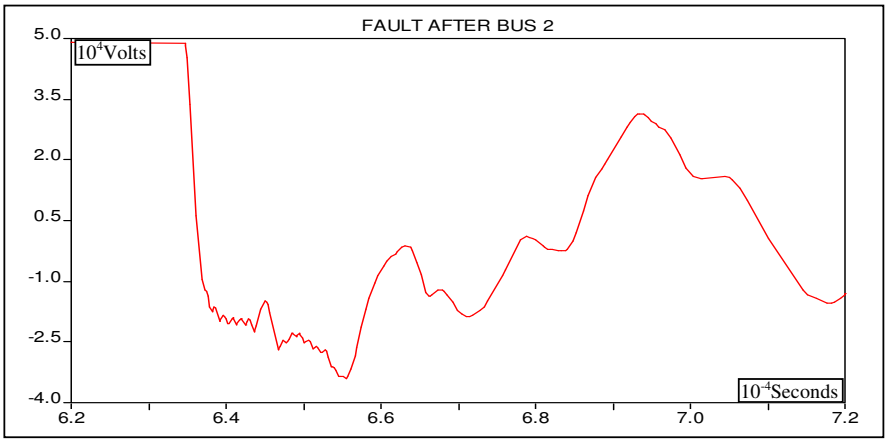


Fig. 3.24 Waveform for the Fault after Bus 2

The difference observed above decrease as the distance between fault and observation points increase. Although related waveforms for Bus 4 have minor

differences (Fig. 3.25), these differences further become negligible for the faults at the Bus 7 (Fig.3.26).

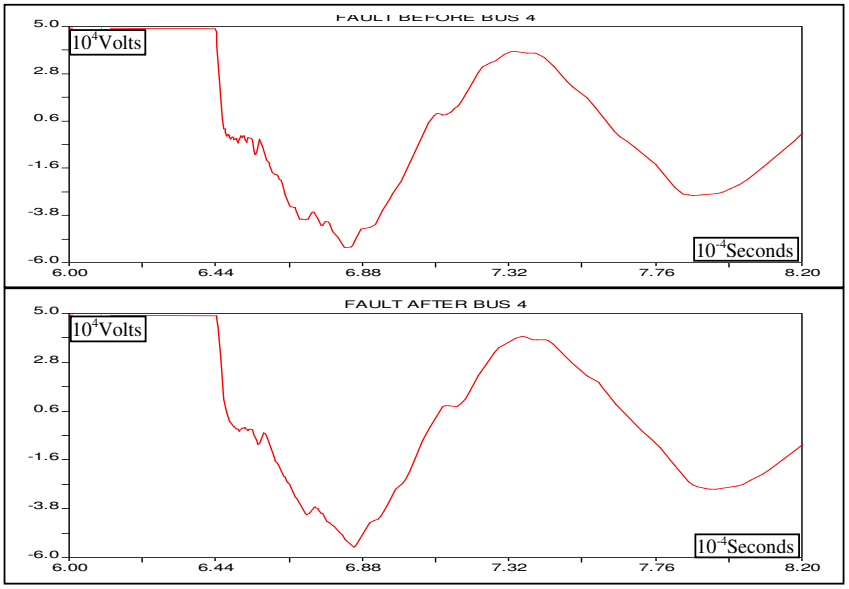


Fig. 3.25 Waveform for the Fault before and after Bus 4

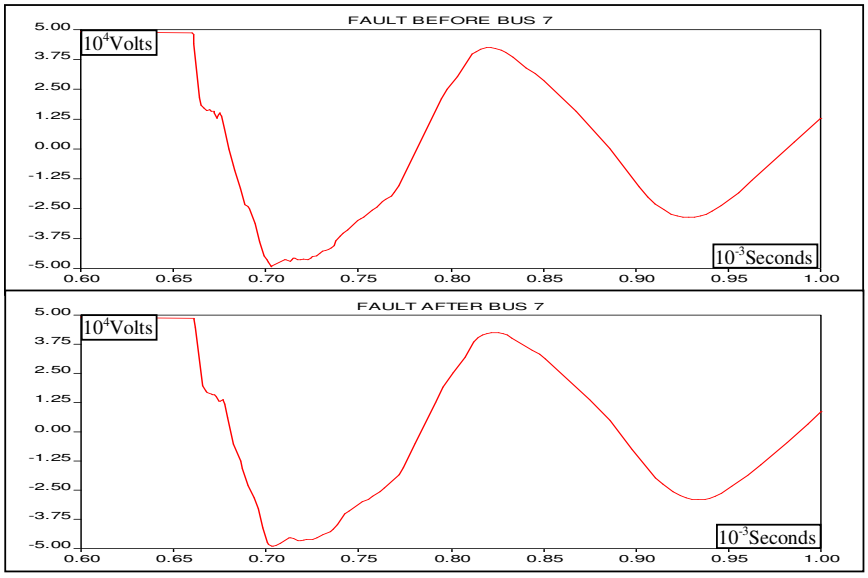


Fig.3.26 Waveform for the Fault before and after Bus 7

Unlike the Case 1, the resulted waveform is almost sinusoid starting from first reflections. For that reason, it is very difficult to determine fault location by observing particular time delay between two successive reflections. On the other hand frequency of sinusoid is related with the fault distance and it can be used to determine the fault location approximately. For the system in Fig. 3.13a fault calculation results from the waveform are given in Table 3.2.

Note that, for the faults at Bus 1 and Bus 2 errors are unacceptably high. These bus-bars are so close to the observation point that reflections quickly die out before getting sinusoidal shape. For that reason, it gets difficult to determine period or frequency of related characteristics. Alternatively, fault location for those points can be determined by using time delay between two successive reflections as in case 1. Because those points are close enough to the observation point, presence of two modes do not affect the wave characteristic as in other locations. Thus, related fault locations can be corrected as given in Table 3.3

Table 3.2 Fault Distance that are Calculated from the Sinusoidal Period of Related Waveforms

| FAULTED BUS | EXACT LOCATION | ACTUAL LENGTH (m) | CALCULATED LENGTH (m) | ERROR (m) |
|---|---|---|---|---|
| BUS 1 | BEFORE | 450 | 301 | 149 |
| | AFTER | 456 | 341 | 115 |
| **BUS 2** | **BEFORE** | **806** | **1044** | **-238** |
| | **AFTER** | **812** | **1027** | **-215** |
| BUS 3 | BEFORE | 1062 | 1055 | 7 |
| | AFTER | 1068 | 1136 | -68 |
| **BUS 4** | **BEFORE** | **1568** | **1568** | **0** |
| | **AFTER** | **1574** | **1617** | **-43** |
| BUS 5 | BEFORE | 1974 | 1948 | 26 |
| | AFTER | 1980 | 1990 | -10 |
| **BUS 6** | **BEFORE** | **2355** | **2381** | **-26** |
| | **AFTER** | **2361** | **2414** | **-53** |
| BUS 7 | BEFORE | 2911 | 2862 | 49 |
| | AFTER | 2917 | 2904 | 13 |

Table 3.3 Corrected Values for the Faults at Bus 1 and Bus 2

| FAULTED BUS | EXACT LOCATION | ACTUAL LENGTH (m) | CALCULATED LENGTH (m) | ERROR (m) |
|---|---|---|---|---|
| BUS 1 | BEFORE | 450 | 453 | 3 |
| | AFTER | 456 | 474 | 18 |
| **BUS 2** | **BEFORE** | **806** | **838** | **32** |
| | **AFTER** | **812** | **877** | **65** |

Note that, all fault locations are determined with an error. As a result, for this particular case, although it may be possible to locate the fault position exactly for the case 1, this is not the case for case 2, even though the fault location can be located exactly for the nearest the distribution centers to the observation point.

### 3.4.2 Single observation point and feeder with several branches

The system in Fig.3.13b is one of the simplest cases that can occur in practical situation. Since the system that contains single observation point is already analyzed extensively, this case will be examined just the case which includes parallel braches with the same cables lengths to the junction point. Actually, this is not necessary, because fault at the same length of two parallel cables can happen even though they have different lengths.

The main difference that parallel branch introduces into the system is an additional reflection point. For the faults at Bus 4, Bus 5 is an additional reflection point or vice versa. For this reason, relatively simple waveform of previous system (Fig. 3.21) changes into more complex one for case 1, as in Fig. 3.27. Furthermore, the faults that take place Bus 4 and Bus 5 have identical reflection pattern. For that reason, it is impossible to determine faulted branch by just monitoring the system from observation point.

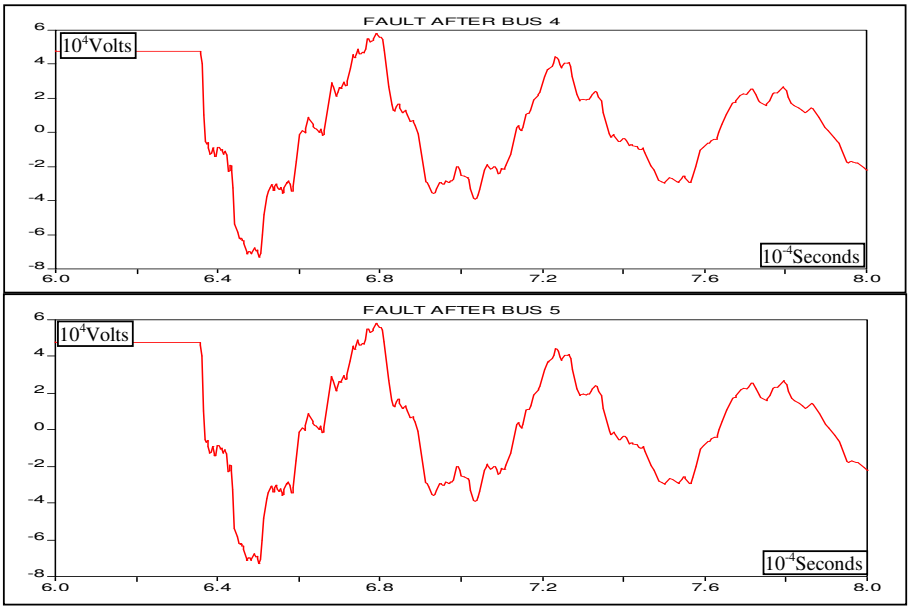


Fig. 3.27 Waveform for the Fault after Bus 4 and Bus 5

Determination of the fault location becomes also problematic. It is difficult to determine successive reflections even though there is one propagation mode. Also, period of oscillations depends on both the fault location and the length of healthy parallel system. For those reasons, fault distance may not be obtained by employing both methods.

Similar observation can be maid also for case 2. Only difference is that, waveform becomes sinusoidal (Fig. 3.28) due to two propagation mode and presence of parallel branch.

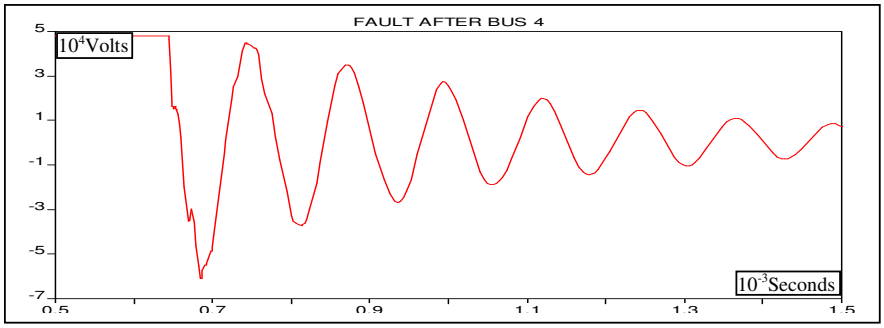


Fig. 3.28 Waveform for the Fault after Bus 4

### 3.4.3 Single phase multi-branch system

The complexity of Fig. 3.13a can be increased by adding parallel feeder to the system as in Fig. 3.13c. Unlike the previous system, these parallel branches can be observed separately, so that faulted branch can easily be determined. Main difference of this system is that, incoming waves to the observation point are not reflected backward only but also they are transmitted to the other branches and they reflect from the end of those branches. As it can be seen from Fig. 3.29, waveforms are so complicated even for the Case 1 that it is impossible to determine necessary successive reflections to locate fault point. For this reason, it will be better to move Case 2, and examine the more realistic system.

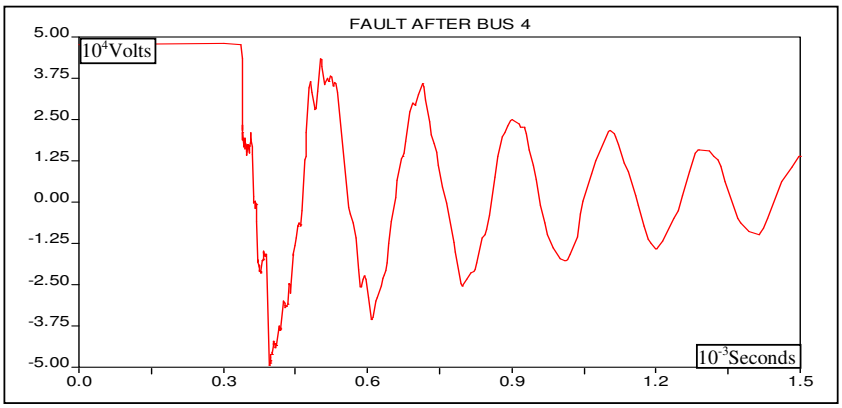


Fig. 3.29 Waveform for the Fault after Bus 4

Since the lengths of parallel branches are known, it is possible to determine fault distance by checking oscillation periods. On the other hand, since one of the reflection points shifts from observation point to the end points of parallel branches, situation becomes little bit tricky. Oscillation period will be affected by each parallel line in the system. Difference can be seen by changing the number of parallel feeders. When there is single branch and the fault occurs at Bus 4, oscillation period is 259μsec, which occurs between observation point and fault point. After the addition of the second branch, oscillation period becomes 347μs, which occurs between Bus 7 and fault point. Things get more complicated after the addition of the third branch. Oscillation period increases to 464μs which neither

corresponds to second branch nor third one only but combination of them. Sample output related with three feeder case is given in Fig. 3.30.

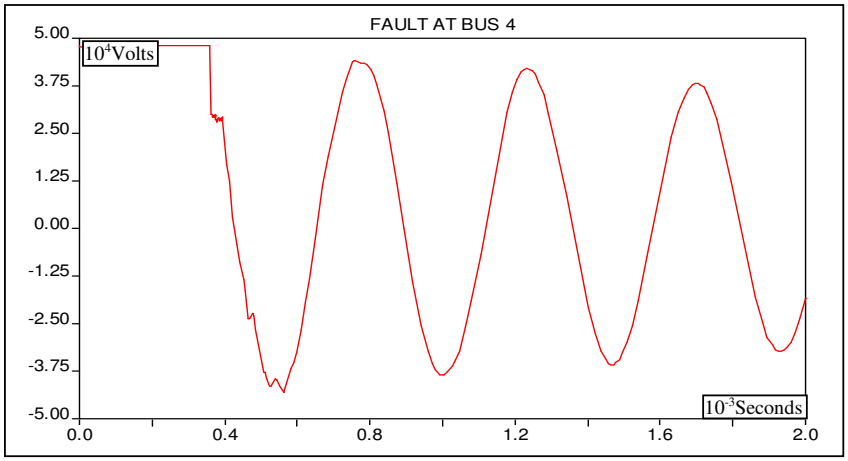


Fig. 3.30 Waveform for the Fault at Bus 4

Another issue is that precision in locating fault tend to decrease as the complexity i.e. number of feeders in the system increases, as in Table 3.4.

Table 3.4 Error due to Increase in Feeder Number

| FAULTED BUS | ACTUAL LENGTH | CALCULATED LENGTH FOR 1- FEEDER | ERROR | CALCULATED LENGTH FOR 2- FEEDERS | ERROR | CALCULATED LENGTH FOR 3- FEEDERS | ERROR |
|---|---|---|---|---|---|---|---|
| BUS 3 | 2486 | 2541 | 55 | 2563 | 77 | 2717 | 231 |
| BUS 2 | 1374 | 1275 | -99 | 1495 | 121 | 1644 | 270 |

### 3.5 Analyses on 3-phase systems

So far, simple single phase systems that are useful to understand main characteristics of reflections are examined. The practical distribution systems on the other hand are more complicated in nature, since they have mutually coupled three phases. The 3-phase system the single line diagram of which is given in Fig. 3.31 will be analyzed throughout this section.

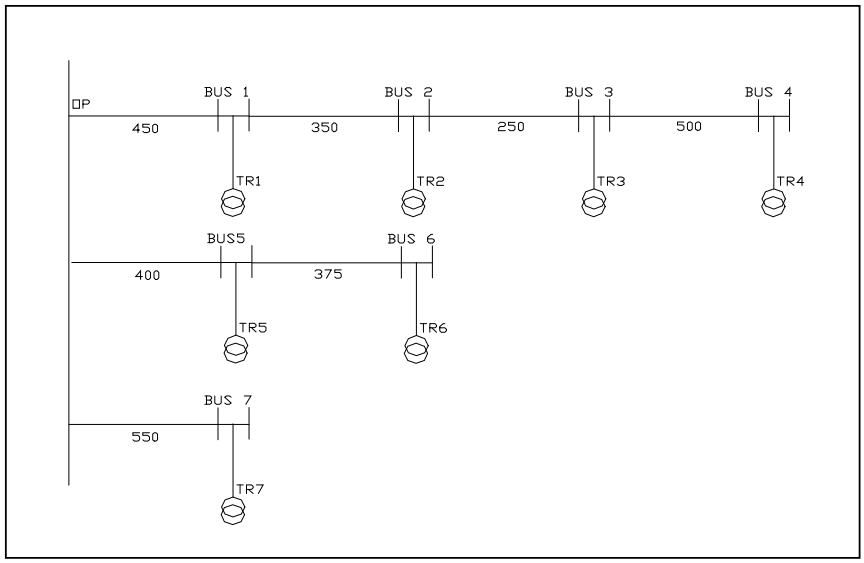


Fig. 3.31 Three-phase Multi-feeder System

This system includes three feeders, and the grounding of the cable sheaths is discrete as in practice. System does not have any sub-branches as in section 3.5.2, because fault location for such systems could not be determined successfully as explained in related section. Primarily analyses will be carried for one phase to ground fault and then they will be extended to 2-phase and 3-phase faults.

Fig. 3.32 shows the voltage waveform for the ground fault before Bus 1. This is the most complicated characteristics up to this point. Although the fault takes place very close to the observation point, characteristics are very complicated, when compared to the previous cases because of mainly three reasons. First of all, reflection coefficient at the observation point becomes so small that incoming wave is mainly transmitted to the other branches instead of being fully reflected to the fault point as in one feeder case. Secondly, presence of six modes increase reflection factor complexity, and finally, having different lengths, the healthy branches introduce more complex wave characteristics, since transmitted waves fully reflects back from the end points of them.

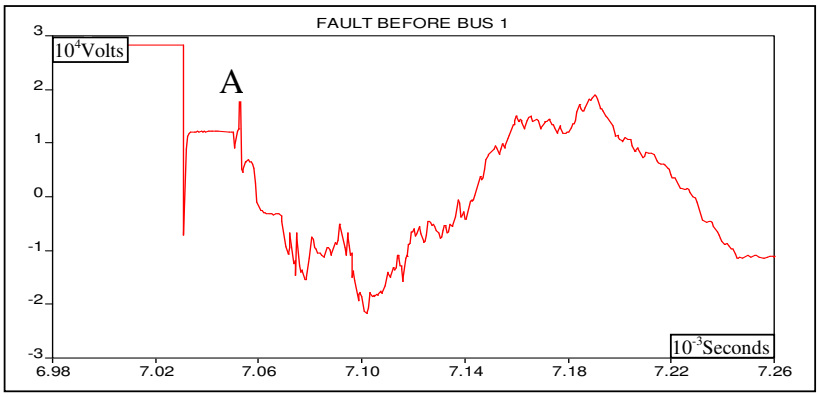


Fig.3.32 Waveform for the Fault before Bus 1

As a result, only the first reflection (A) from the fault point can clearly be identified. Then waveform quickly tends to a sinusoid, and such identification becomes impossible. Increase in fault distance and presence of distribution transformer centers also suppress such characteristics. Even for the fault just after the Bus 1 (Fig. 3.33) first reflection (B) from the fault point is hardly observable compared to previous case.

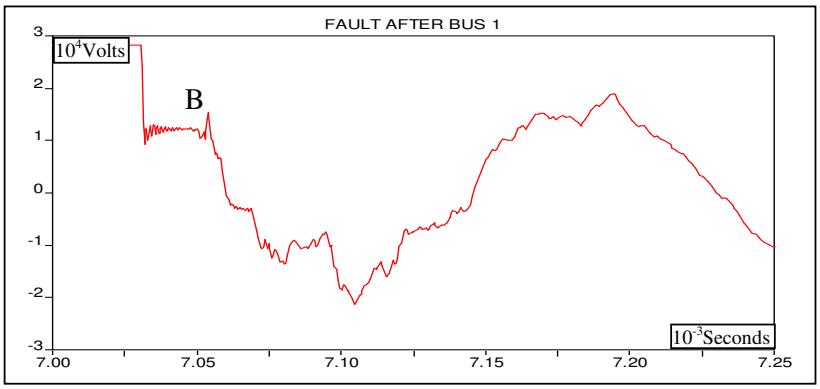


Fig.3.33 Waveform for the Fault after Bus 1

Thus, the fault distance can be calculated by using time difference between two successive waves, and by comparing last two figures the fault may be located as before or after Bus 1. On the other hand, as the fault point moves away from the observation point characteristics get more and more complex (Fig. 3.34) such that successive reflections cannot be determined. In that case, the fault location determined approximately by using period of sinusoids. Although there are minor differences between characteristics of the faults before and after bus-bars when they

are compared, it is again difficult to determine exact fault location by using just one of them. Calculation results for faults both side of bus-bars are in Table 3.5

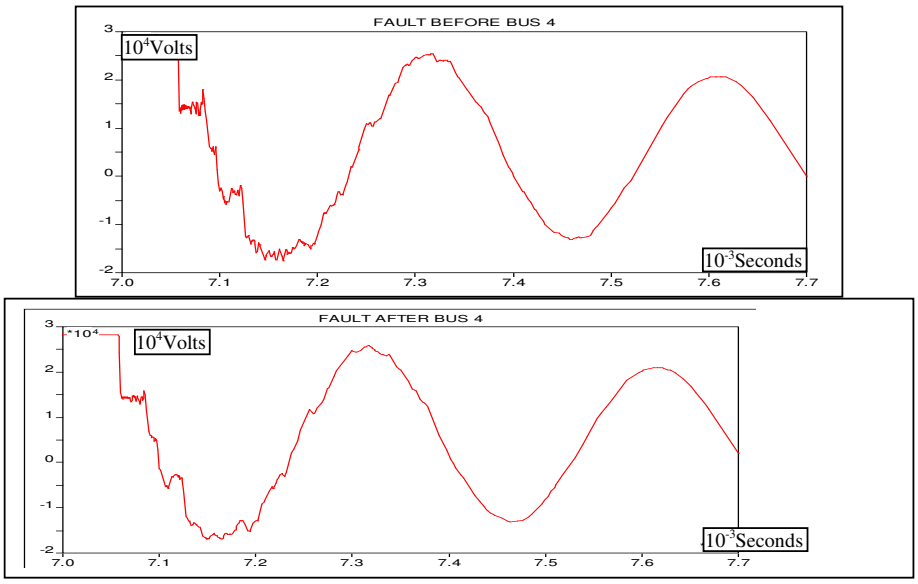


Fig.3.34 Waveform for the Fault before and after Bus 4

Table 3.5 Fault Distance that are Calculated from the Sinusoidal Period of Related Waveforms

| FAULTED BUS | EXACT LOCATION | ACTUAL LENGTH (m) | CALCULATED LENGTH (m) | ERROR (m) |
|---|---|---|---|---|
| BUS 1 | BEFORE | 450 | 569 | 119 |
| | AFTER | 456 | 565 | 109 |
| **BUS 2** | **BEFORE** | **806** | **955** | **149** |
| | **AFTER** | **812** | **978** | **166** |
| BUS 3 | BEFORE | 1062 | 1167 | 105 |
| | AFTER | 1068 | 1194 | 126 |
| **BUS 4** | **BEFORE** | **1568** | **1537** | **-32** |
| | **AFTER** | **1574** | **1565** | **-9** |

Alternatively, faulted phase current can be analyzed to retrieve further information. Fault current rapidly increase after the fault as in Fig. 3.35. Although it has relatively sharp reflections at the beginning, they are retarded and shifted by the inductance in the system so that they do not provide more useful information than voltage reflections. The period of current wave sinusoids is the same with the period of sinusoids in voltage wave.

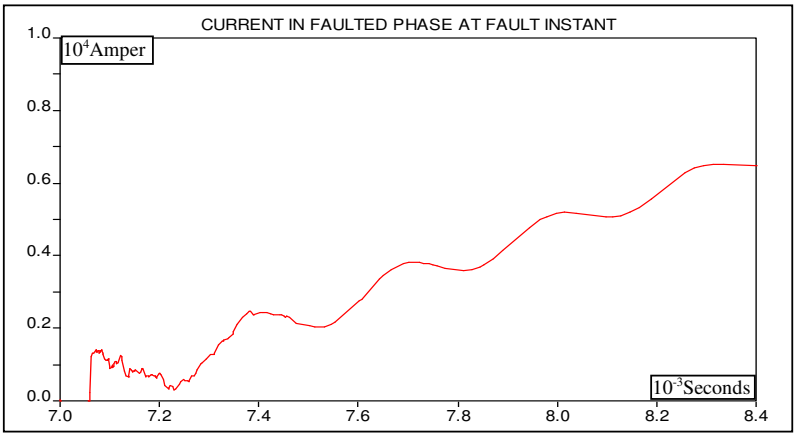


Fig. 3.35 Current in the Faulted-phase at the Fault Instant

Since three phases are mutually coupled, there are changes also in the healthy phases. As in Fig. 3.36, current in healthy phase changes sharply at the beginning of the fault, but again it is difficult to retrieve additional information because of the explained reasons above.

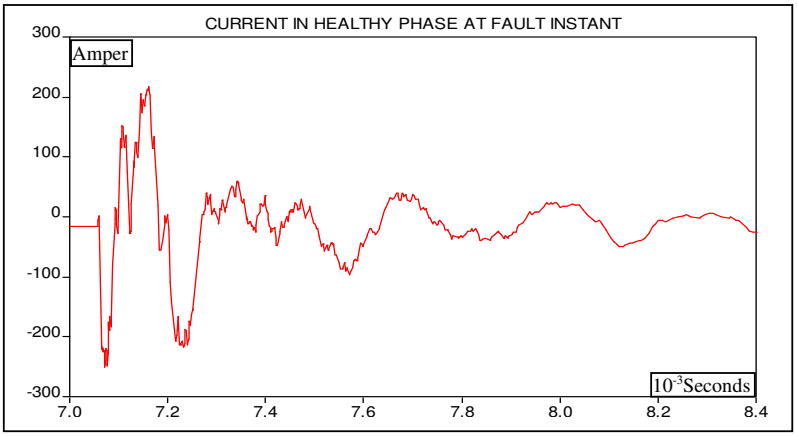


Fig. 3.36 Current in the Healthy-phase at the Fault Instant

Voltage on the healthy phases also changes accordingly during the fault (Fig.3.37). Similar to the current waveform no additional information can be derived from it. Actually, analysis of healthy phase is more difficult. Since it is affected by source resultant waveform is distorted as given in Fig. 3.37.

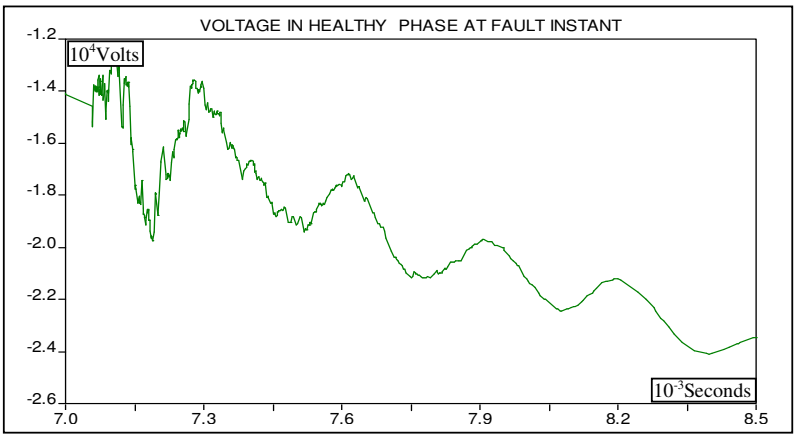


Fig. 3.37 Voltage in the Healthy-phase at the Fault Instant

The most common type of faults in cable distribution systems is the phase to ground fault, which is analyzed so far. Even though they are rare, 2-phase, 2-phase to ground, 3-phase, and 3-phase to ground faults could occur. For this reason, they also should be examined for completeness of the case. First of all, 2-phase and 3-phase faults can only take place at the bus-bars, because cables have shields that prevent direct conduction between phases.

General difference between the phase to ground fault and the rest are; a decrease in period of sinusoids in waveform and an increase in the fast oscillations in the latter cases because of increased number of reflections. With Fig. 3.38 compared with Fig. 3.34, the above differences can be observed easily. It should be noted that both figures are given in the same time scale.

Although all latter cases have similar wave pattern (Fig. 3.38) they may differ in magnitude according to fault type and relative magnitude of pre-fault voltages. Difference among periods of latter cases' waveforms is relatively small compared to the former case, but this difference also should be accounted during calculations in order to find fault locations as precise as possible. For example, for the phase to ground fault at Bus 1, the sinusoidal period of the waveform is $166\,\mu\text{sec}$, while the periods for 2-phase and 3-phase faults are 141.2 and 141.6 $\mu\text{sec}$ respectively. Note that these values also include measurement errors and periods of latter cases could

be assumed the same. After these adjustments calculated fault distance and corresponding errors are given in Table 3.6.

Table 3.6 Calculated Fault Distances for Different Fault Types

| **PHASE TO PHASE FAULT** | | | |
|---|---|---|---|
| Faulted Bus | Actual Length | Calculated Distance | Error |
| BUS 4 | 1568 | 1574 | 6 |
| BUS 3 | 1062 | 1189 | 127 |
| BUS2 | 806 | 856 | 50 |
| BUS1 | 450 | 541 | 91 |
| | | | |
| **TWO PHASE GROUND FAULT** | | | |
| Faulted Bus | Actual Length | Calculated Distance | Error |
| BUS 4 | 1568 | 1574 | 6 |
| BUS 3 | 1062 | 1114 | 52 |
| BUS2 | 806 | 897 | 91 |
| BUS1 | 450 | 505 | 55 |
| | | | |
| **3-PHASE & 3-PHASE TO GROUND FAULT** | | | |
| Faulted Bus | Actual Length | Calculated Distance | Error |
| BUS 4 | 1568 | 1573 | 5 |
| BUS 3 | 1062 | 1166 | 104 |
| BUS2 | 806 | 905 | 99 |
| BUS1 | 450 | 529 | 79 |

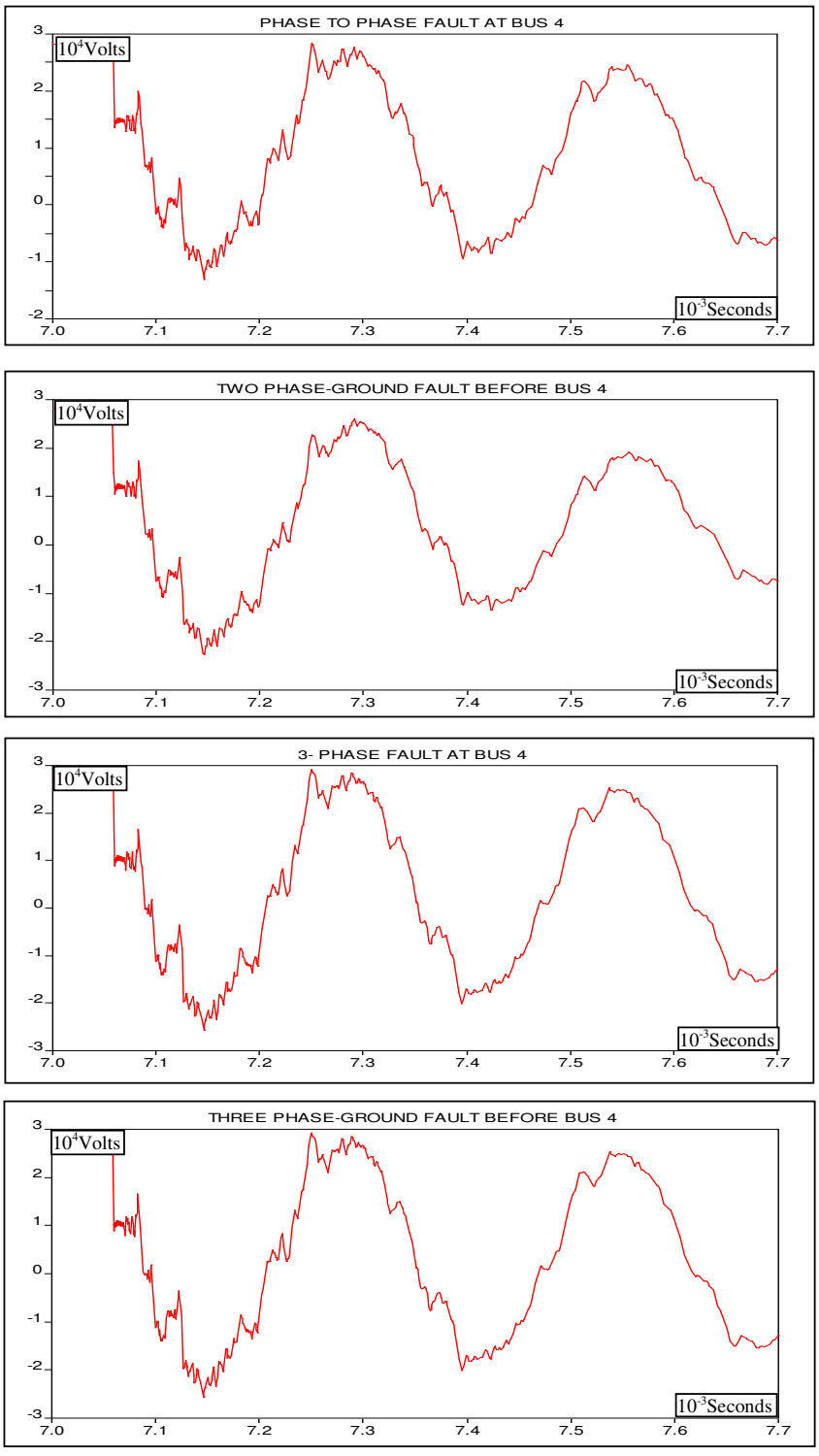


Fig.3.38 Waveforms for Different Types of Faults

Considering that, there could be distribution transformer center even 150m apart errors given in the Table 3.6 and Table 3.7 are considerably high. During the calculations Bus 4 is chosen as a reference, and other locations were found based on its period. Not surprisingly, error corresponding to Bus 4 is relatively low. On the other hand, these results could be used to locate the fault position more precisely.

Once the fault point approximated above, two distribution centers, before and after found location can be chosen as reference for better approximation. Corrected results are as given in Table 3.7.

Table 3.7 Corrected Fault Distances for Different Fault Types

| **PHASE TO GROUND FAULT** | | | |
|---|---|---|---|
| Faulted Bus | Actual Length | Calculated Distance | Error |
| BUS 3 | 1062 | 1098 | 36 |
| BUS2 | 806 | 829 | 23 |
| | | | |
| **PHASE TO PHASE FAULT** | | | |
| Faulted Bus | Actual Length | Calculated Distance | Error |
| BUS 3 | 1062 | 1156 | 94 |
| BUS2 | 806 | 746 | -60 |
| | | | |
| **TWO PHASE GROUND FAULT** | | | |
| Faulted Bus | Actual Length | Calculated Distance | Error |
| BUS 3 | 1062 | 1060 | -2 |
| BUS2 | 806 | 837 | 31 |
| | | | |
| **THREE PHASE FAULT** | | | |
| Faulted Bus | Actual Length | Calculated Distance | Error |
| BUS 3 | 1062 | 1106 | 44 |
| BUS2 | 806 | 809 | 3 |

# CHAPTER 4

# ANALYSIS OF TRAVELLING WAVES DUE TO CIRCUIT BREAKER OPERATION

## 4.1 Introduction

As every switching action, circuit breaker (CB) operation also causes traveling waves in the system. Unlike the fault case, traveling waves originates from observation point. The magnitude of traveling waves corresponds to the current that flows through CB at the operation instant, the impedance seen from operation point, and the fault distance.

Operation of CB isolates the parallel branches from the faulted sections. Furthermore, the effect of mutual coupling is negligible. For this reason, three phase multi-branch systems can directly be studied without an initial analysis on single phase systems.

## 4.2 Wave characteristics

Primarily being triangular, the waveform due to fault clearing is quite different than that resulted waveform due to fault. The injected negative voltage to simulate fault was a step voltage, and the resulted waveform was in rectangular form as in Fig. 3.10. In this case, to simulate CB operation current that is opposite direction to the

fault current is injected to the system. The injected current is a ramp current which increases as time.

$$i = I \sin \omega t \cong I \omega t \quad where \;\; t \approx 0 \qquad \text{Eqn. 4.1}$$

Then the resulted voltage is directly proportional with the impedance seen from the injection point.

$$v = Z_0 i = Z_0 I \omega t \qquad \text{Eqn. 4.2}$$

where $Z_0$ is the characteristic impedance of cable. The resulted voltage waveform is primarily triangular as in Fig. 4.1

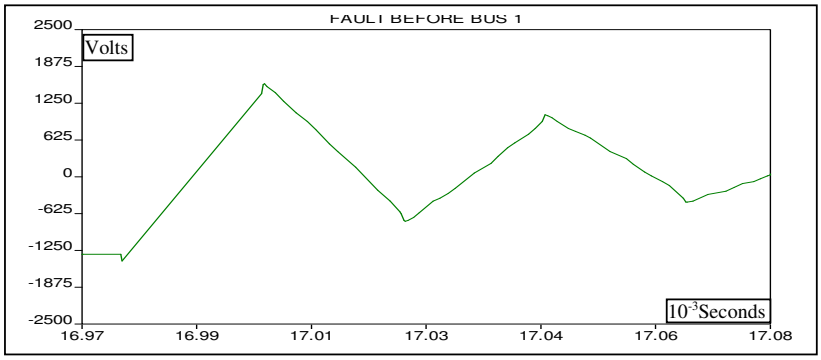


Fig. 4.1 Waveform for the Fault before Bus 1

Magnitude of voltage depends on the fault distance, as well as current and equivalent impedance seen from the injection point. Since there is ramp voltage it tends to increase until the arrival of the negative ramp that comes from fault point. Being open circuited reflection coefficient is (+1) at the observation point. For this reason, while the incoming wave canceling the increasing ramp reflected wave reverses the polarity, and the voltage starts to decrease by gaining negative slope, as in Fig. 4.1. This phenomenon continues until the reflected waves die out due to losses explained in Chapter 3. Meanwhile, the shape of waveform is distorted by the system elements and it looses its triangular shape by tending to a sinusoidal waveform (Fig. 4.2).

Distortion effects of each system element can be examined in a similar manner to the fault case. For example, in Fig. 4.1, only element between fault and observation point is a cable. On the other hand, the jump that is caused by CB current chopping around zero is important in the view point of the distortion caused. From then onwards there is almost no distortion in the waveform up to first peak. A distortion at the peak is mainly related with the jump mentioned above. After that point waveform starts to deviate from ramp characteristics.

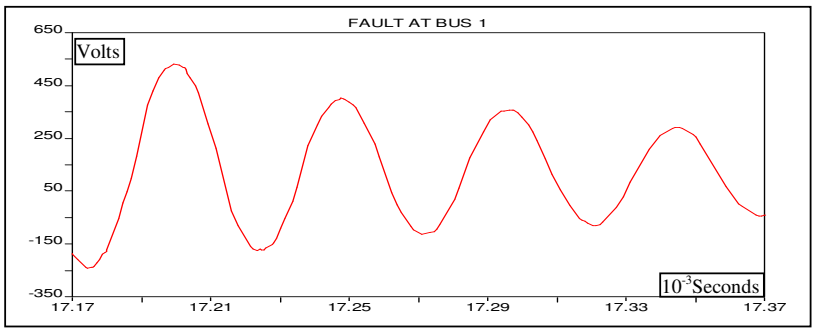


Fig. 4.2 Waveform for the Fault at Bus 1

The distortion in the waveform increases, after including the bus-bars into the system (Fig.4.3). Small jump at the near of the peak is reflection of the jump due to CB operation from the bus-bars with positive coefficient. Then reflection from the fault point comes, and the same jump comes as positive and larger in magnitude. Moreover, increase in voltage continues until the negative reflections from the fault overcome to the positive reflections from the bus-bars. This occurrence causes a smooth curve at the peak instead of sharp ramp decrease.

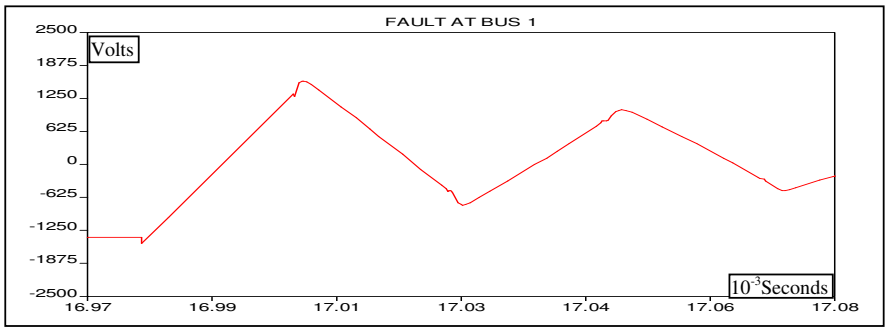


Fig.4.3 Waveform for the Fault at Bus 1

Finally, presence of whole distribution center between fault and observation point further increase the distortion in the waveform (Fig. 4.4). Except for that, the reflections take place as the previous case.

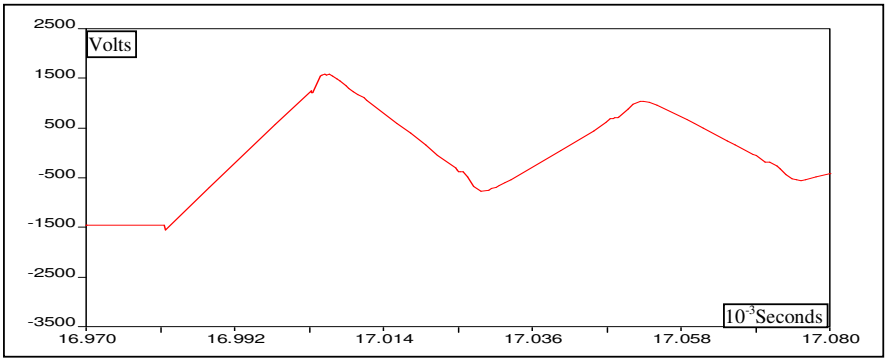


Fig. 4.4 Waveform for the Fault after Bus 1

### 4.3 Analyses of the systems

By using the voltage waveform, fault can be located either from the time between CB operation and first incoming reflection or from the period of triangular of sinusoidal waves.

The former method gives more accurate results if the first incoming wave instant can be detected exactly. Because the first reflected wave is aerial which enables accurate calculation and the distortion due to distribution transformer centers is minimum. On the other hand, exact instant of impact may not be determined because of distortions explained previous section. Especially, for faults away from observation point, this procedure becomes considerably difficult.

The latter method is simpler, since waveform preserves its average period even though distortions. On the other hand, distribution centers between fault and observation point affect the period of waveform so that change in period is not linear with respect to the fault distance. Also the effect of ground modes increases

with increasing fault distance. Thus, some kind of a correction factor or procedure should be used to overcome these disadvantages.

Therefore the presence of ground modes and the distribution transformer centers reduce the certainty in locating the fault location by disturbing both the waveform and linearity.

### 4.3.1 Three-phase single branch systems

Actually this case also covers the multi-feeder systems as mentioned in the introduction. Following system will be examined throughout this section in order to observe voltage waveform variations due to fault clearing actions.

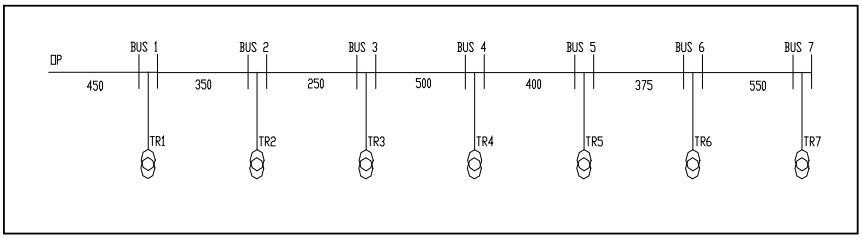


Fig. 4.5 Three-phase Single-feeder System

As mentioned, detection of first incoming wave is difficult for the faults away from observation point. For such cases, detection can be aided by analyzing the slope (derivative) of the waveform of the transients. However, change in slope may not be sufficient to detect the impact instant of first wave. For example, for the fault after Bus 7, the waveform continues to increase almost with the same slope after the impact reflected wave (Fig. 4.6). This is about 6 to 8 μsec which corresponds 120m to 240m error depending on propagation velocity for different types of cables. Propagation velocity may change according to physical layout of cables i.e. velocity is higher in the single 3-phase cables because of low inductance. Comparing Fig. 4.6 with Fig. 4.3 the effect of distribution transformer centers can also be observed. Having similar patterns other faults i.e. phase to phase, 2-phase-ground, 3-phase-ground, etc. can be examined in a similar manner.

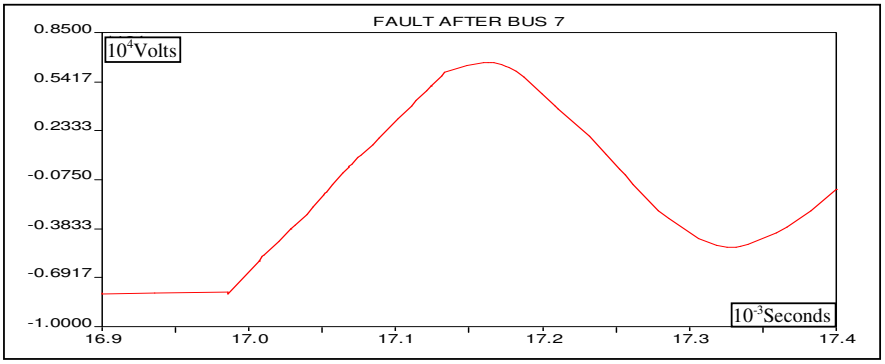


Fig. 4.6 Waveform for the Fault after Bus 7

Measured traveling times obtained by taking time difference between CB operation and slope change before first peak are in Table 4.1

Table 4.1 Measured Traveling Times (msec) (from CB operation to Slope Change)

| FAULT POINT | | FOR (1x3ph) CABLE | FOR (3x1ph) CABLE |
|---|---|---|---|
| BUS 1 | **BEFORE** | **0,007** | **0,011** |
| | AFTER | 0,007 | 0,011 |
| BUS 2 | **BEFORE** | **0,013** | **0,019** |
| | AFTER | 0,015 | 0,020 |
| BUS 3 | **BEFORE** | **0,017** | **0,026** |
| | AFTER | 0,019 | 0,026 |
| BUS 4 | **BEFORE** | **0,027** | **0,038** |
| | AFTER | 0,028 | 0,040 |
| BUS 5 | **BEFORE** | **0,034** | **0,049** |
| | AFTER | 0,035 | 0,050 |
| BUS 6 | **BEFORE** | **0,040** | **0,059** |
| | AFTER | 0,042 | 0,059 |
| BUS 7 | **BEFORE** | **0,049** | **0,072** |
| | AFTER | 0,051 | 0,074 |

The line length or fault distance is equal to multiplication of highest observable velocity with travel time $(\ell = V.t)$, and calculated values for the faults at different locations and different type of cables are given Tables 4.2 and 4.3 as indicated.

Table 4.2 Phase to Ground Fault (for "3x1ph" Cable System)

| FAULT POINT | | LENGTH (m) | | ERROR(m) |
|---|---|---|---|---|
| | | ACTUAL | CALCULATED | |
| BUS 1 | **BEFORE** | **450** | **464** | **14** |
| | AFTER | 456 | 463 | 8 |
| BUS 2 | **BEFORE** | **806** | **823** | **17** |
| | AFTER | 812 | 844 | 32 |
| BUS 3 | **BEFORE** | **1062** | **1098** | **36** |
| | AFTER | 1068 | 1098 | 30 |
| BUS 4 | **BEFORE** | **1568** | **1604** | **36** |
| | AFTER | 1574 | 1668 | 94 |
| BUS 5 | **BEFORE** | **1974** | **2048** | **74** |
| | AFTER | 1980 | 2111 | 131 |
| BUS 6 | **BEFORE** | **2355** | **2470** | **115** |
| | AFTER | 2361 | 2470 | 109 |
| BUS 7 | **BEFORE** | **2911** | **3040** | **129** |
| | AFTER | 2917 | 3103 | 186 |

Table 4.3 Phase to Ground Fault (for "1x3ph" Cable System)

| FAULT POINT | | LENGTH (m) | | ERROR(m) |
|---|---|---|---|---|
| | | ACTUAL | CALCULATED | |
| BUS 1 | **BEFORE** | **450** | **434** | **-16** |
| | AFTER | 456 | 434 | -22 |
| BUS 2 | **BEFORE** | **806** | **806** | **0** |
| | AFTER | 812 | 899 | 87 |
| BUS 3 | **BEFORE** | **1062** | **1085** | **23** |
| | AFTER | 1068 | 1178 | 110 |
| BUS 4 | **BEFORE** | **1568** | **1644** | **76** |
| | AFTER | 1574 | 1737 | 163 |
| BUS 5 | **BEFORE** | **1974** | **2109** | **135** |
| | AFTER | 1980 | 2171 | 191 |
| BUS 6 | **BEFORE** | **2355** | **2481** | **126** |
| | AFTER | 2361 | 2574 | 213 |
| BUS 7 | **BEFORE** | **2911** | **3039** | **128** |
| | AFTER | 2917 | 3287 | 370 |

As seen from the Table 4.2 and Table 4.3, error is unacceptably high especially beyond Bus 4. Note that, travel times in Table 4.1 are found based on change of

slope, and time delay between CB operation and this slope change instant is assumed as travel time. Actually this is not the case in practice due to presence of DTC's between the fault and observation point. As mentioned in Section 3.1, the reflection coefficient from DTC's (bus-bars) to cables is positive, and resultant reflection coefficient configuration for a system that contains seven DTC's is given in Fig. 4.7.

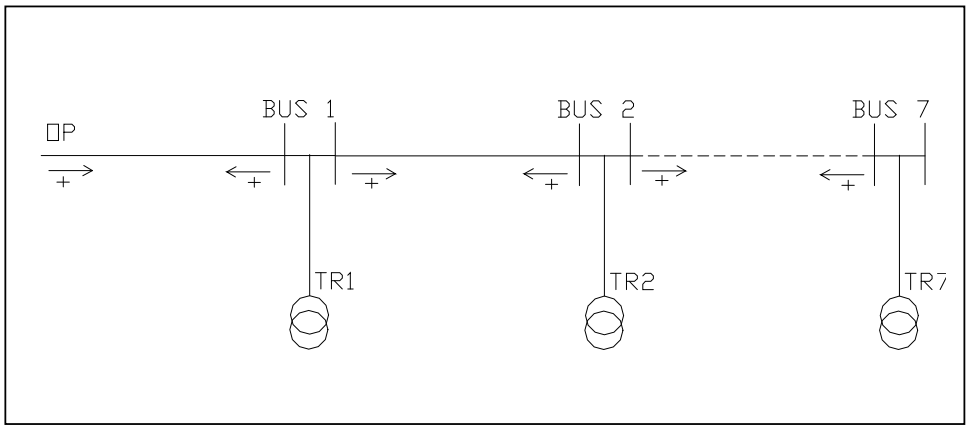


Fig.4.7 Reflection coefficient configuration

The effect of DTC's can be explained by assuming a fault after Bus 2. CB operation isolates the feeder and injects the ramp-wave from observation point (OP). Before reaching to the fault and reflecting with (-1), this wave first reflects from Bus 1 to OP, and this reflected wave continues its travel in a similar manner by reflecting from OP with (+1). Similarly, the main wave reflects from Bus 2 to Bus 1, it is partially reflected with positive coefficient and partially transmitted towards to OP, and these reflections continue by giving rise to positive reflections in the system. Finally the main wave reaches to the fault point, and reflects back to the OP by gaining negative magnitude or slope. When this wave reaches to the OP it reflects with (+1) and reverses the slope, but this change in the slope cannot be realized instantaneously, because as well as original positive wave, also positive reflections explained above should be nullified in order to reverse the slope. For this reason, change in slope which should be instantaneous, is retarded a certain time delay depending on the number of DTC's present between fault and observation point. Furthermore, even the slope of the first ramp portion of waveform not constant, and

there are small changes because of reflections from DTC's. In order to assure the correct slope change instant, change in slope should be larger than these small changes. As a result of these factors, determination of travel time from slope changes turn out to be greater than actual travel time.

The effect of DTC's can be observed in Fig. 4.8 by comparing the waveforms for the faults before Bus 1, Bus 4 and Bus 7.

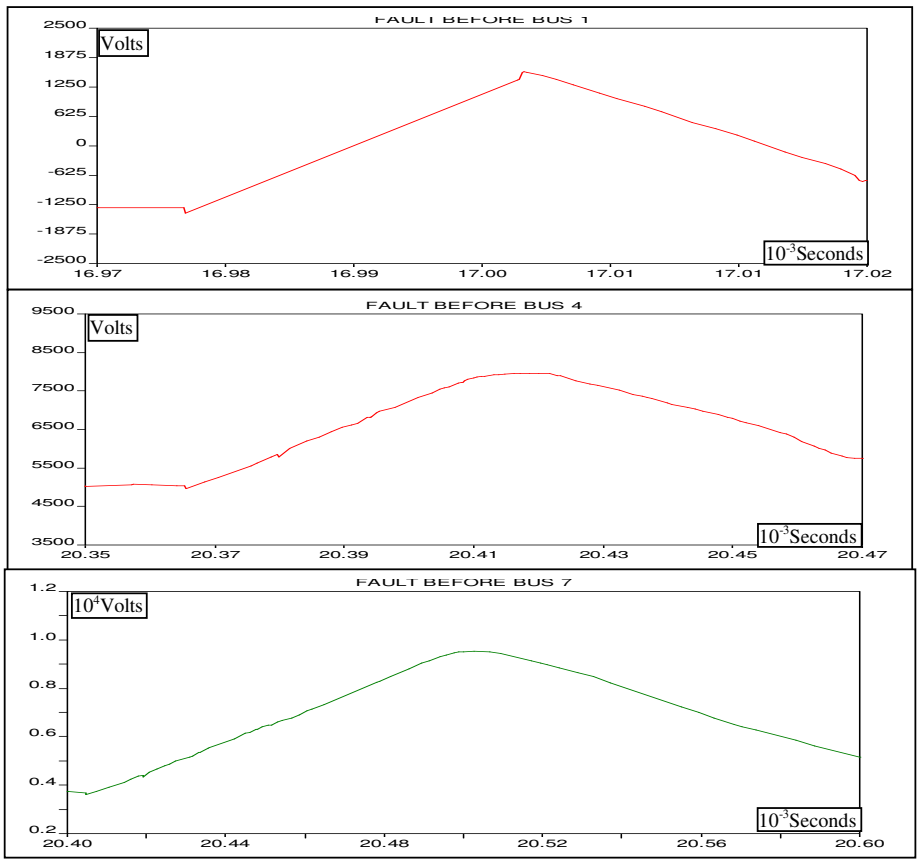


Fig. 4.8 Comparison of Waveforms for the faults at different DTC's

Note that, both time and voltage scales of the waveforms in Fig. 4.8 are different. It is obvious that, the waveform for the fault at Bus 1 has the steepest peak, and it gets smoother as the number of DTC's increase between fault and OP.

In view of these observations, more accurate fault location calculations can be obtained by improving this method. This will be illustrated only for (3x1ph) cable but the same procedures can be applied also to the (1x3ph) cables.

When the actual fault distances divided to corresponding traveling times which are equal to velocity (Table 4.4), not surprisingly results are not the same because of the errors just explained above. All calculated velocities are lower than the actual velocity since the change in slope takes place later than the actual impact. This phenomenon is the main reason of the high errors in fault locations given in Tables 4.2 and 4.3, because during the calculation, actual constant velocity is used as a multiplicand.

Table 4.4 Velocity Found from Direct Travel Time Measurement Corresponding to Change in Slope

| FAULT POINT | | VELOCITY (km/s) | |
|---|---|---|---|
| | | ACTUAL | CALCULATED |
| BUS 1 | **BEFORE** | **42189** | **40909** |
| | AFTER | | 40900 |
| BUS 2 | **BEFORE** | | **41333** |
| | AFTER | | 40600 |
| BUS 3 | **BEFORE** | | **40846** |
| | AFTER | | 41077 |
| BUS 4 | **BEFORE** | | **41263** |
| | AFTER | | 39848 |
| BUS 5 | **BEFORE** | | **40701** |
| | AFTER | | 39600 |
| BUS 6 | **BEFORE** | | **40256** |
| | AFTER | | 40359 |
| BUS 7 | **BEFORE** | | **40431** |
| | AFTER | | 39687 |

Instead of taking the actual velocity, average of all velocities of travel (40739 km/s) in Table 4.4 can be taken as multiplicand. This simple approximation yields considerable decrease in error. Calculated fault distance for the fault at Bus 6 becomes,

$\ell = 40739\ x\ 0.059 = 2383\ m$

so that corresponding error is greatly reduced. The result of calculations and corresponding errors change as given in Table 4.5.

Table 4.5 Calculations from Slope Change Assuming Average Multiplicand

| FAULT POINT | | LENGTH (m) | | ERROR(m) |
|---|---|---|---|---|
| | | ACTUAL | CALCULATED | |
| BUS 1 | **BEFORE** | **450** | **448** | **-2** |
| | AFTER | 456 | 460 | 4 |
| BUS 2 | **BEFORE** | **806** | **794** | **-12** |
| | AFTER | 812 | 815 | 3 |
| BUS 3 | **BEFORE** | **1062** | **1059** | **-3** |
| | AFTER | 1068 | 1059 | -9 |
| BUS 4 | **BEFORE** | **1568** | **1548** | **-20** |
| | AFTER | 1574 | 1609 | 35 |
| BUS 5 | **BEFORE** | **1974** | **1976** | **2** |
| | AFTER | 1980 | 2037 | 57 |
| BUS 6 | **BEFORE** | **2355** | **2383** | **28** |
| | AFTER | 2361 | 2383 | 22 |
| BUS 7 | **BEFORE** | **2911** | **2933** | **22** |
| | AFTER | 2917 | 2994 | 77 |

In a similar approach, once the approximate position of fault determined by one of the previous methods, multiplicand can be found by taking nearest two buses at the fault as reference. For example, for the fault around Bus 6, Bus 5 and Bus 7 can be taken as reference. Then calculated velocity for Bus 6 becomes the average velocity of Bus 5 and Bus 7.

From Table 4.4

$V_{Bus\ 5}$ = 39600 km/s, and $V_{Bus\ 7}$ = 40431km/s ➔ $V_{average}$ = 40016 km/s

$\ell = 40016\ x\ 0.059 = 2360\ m$

Although, this process leads very small error for this calculation, this is just a coincidence, but generally the errors are reduced. Rest of calculation results are in Table 4.7. Note that, highest error in Table 4.2 is 186m, decreases to 77m in Table 4.5, and finally it is 47m in the Table 4.6.

Table 4.6 Calculations from Slope Change Assuming Nearest Two Busses to the Fault as Reference

| FAULT POINT | | LENGTH (m) | | ERROR(m) |
|---|---|---|---|---|
| | | ACTUAL | CALCULATED | |
| BUS 1 | **BEFORE** | **450** | **464** | **14** |
| | AFTER | 456 | 432 | **-24** |
| BUS 2 | **BEFORE** | **806** | **819** | **13** |
| | AFTER | 812 | 822 | **10** |
| BUS 3 | **BEFORE** | **1062** | **1062** | **0** |
| | AFTER | 1068 | 1067 | **-1** |
| BUS 4 | **BEFORE** | **1568** | **1538** | **-30** |
| | AFTER | 1574 | 1619 | **45** |
| BUS 5 | **BEFORE** | **1974** | **1927** | **-47** |
| | AFTER | 1980 | 2024 | **44** |
| BUS 6 | **BEFORE** | **2355** | **2339** | **-16** |
| | AFTER | 2361 | 2360 | **-1** |
| BUS 7 | **BEFORE** | **2911** | **2882** | **-29** |
| | AFTER | 2917 | 2944 | **27** |

Alternatively, first peak of the waveform after CB operation can be used in similar way. Detecting peak is easier than detecting slope change as in the previous method. However, this method gives rise to unacceptably high errors in some cases (Table 4.7) due to positive reflections from the bus-bars. Furthermore, these results cannot be improved, because peak points are due to random oscillations depending on fault point and positions and number of DTC's between fault and observation point.

Table 4.7 Calculation from First Peak

| FAULT POINT | | LENGTH (m) | | ERROR(m) |
|---|---|---|---|---|
| | | ACTUAL | CALCULATED | |
| BUS 1 | **BEFORE** | **450** | **381** | **-69** |
| | AFTER | 456 | **462** | 6 |
| BUS 2 | **BEFORE** | **806** | **761** | **-45** |
| | AFTER | 812 | **897** | 85 |
| BUS 3 | **BEFORE** | **1062** | **1006** | **-56** |
| | AFTER | 1068 | **1087** | 19 |
| BUS 4 | **BEFORE** | **1568** | **1522** | **-46** |
| | AFTER | 1574 | **1604** | 30 |
| BUS 5 | **BEFORE** | **1974** | **1930** | **-44** |
| | AFTER | 1980 | **2039** | 59 |
| BUS 6 | **BEFORE** | **2355** | **2283** | **-72** |
| | AFTER | 2361 | **2419** | 58 |
| BUS 7 | **BEFORE** | **2911** | **3044** | **133** |
| | AFTER | 2917 | **3398** | 481 |

The other similar method would be the determination of the period of the sinusoids as in the fault case, but there is a limitation for this procedure. Since reflections have low magnitudes, especially for the faults close to the observation point, reflected wave characteristic can be disturbed by minor reflected waves due to presence of distribution transformer centers. In spite of this drawback this method gives acceptable results as given in Table 4.8.

Table 4.8 Calculation from the Sinusoidal Period

| FAULT POINT | | LENGTH (m) | | ERROR(m) |
|---|---|---|---|---|
| | | ACTUAL | CALCULATED | |
| BUS 1 | **BEFORE** | **450** | **361** | **-89** |
| | AFTER | 456 | 398 | -58 |
| BUS 2 | **BEFORE** | **806** | **834** | **28** |
| | AFTER | 812 | 847 | 35 |
| BUS 3 | **BEFORE** | **1062** | **1028** | **-34** |
| | AFTER | 1068 | 1047 | -21 |
| BUS 4 | **BEFORE** | **1568** | **1517** | **-51** |
| | AFTER | 1574 | 1627 | 53 |
| BUS 5 | **BEFORE** | **1974** | **2017** | **43** |
| | AFTER | 1980 | 2033 | 53 |
| BUS 6 | **BEFORE** | **2355** | **2343** | **-12** |
| | AFTER | 2361 | 2369 | 8 |
| BUS 7 | **BEFORE** | **2911** | **2815** | **-96** |
| | AFTER | 2917 | 2856 | -61 |

### 4.3.2 Single observation point and feeder with three braches

For completely symmetric circuits, which is examined in 3.4.2, it is impossible to determine faulted branch, since corresponding fault and fault clearing characteristics are identical. Even if the branch lengths are slightly different i.e. around 100-200m, it is again very difficult to locate fault considering errors in the previous section. On the other hand, for systems like in Fig.4.9, corresponding waveforms are different at the each branch even though fault is the same distance relative to observation point, because traveling waves also reflects from the unsymmetrical healthy branches. For this reason, although Bus 3 and Bus 5 are at

the same distance from observation point, faults occurring at each one of the buses result in different waveforms, as given in Fig.4.10.

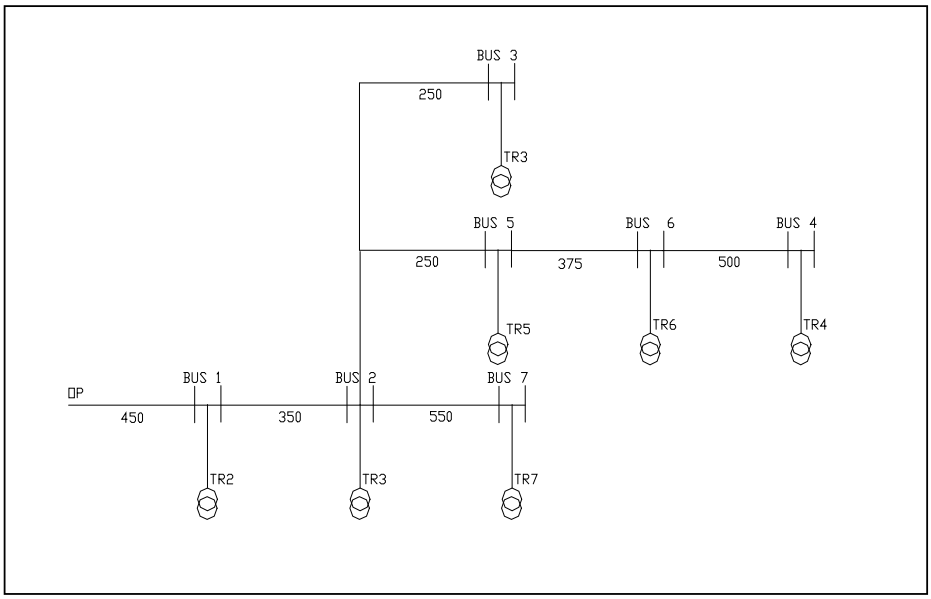


Fig. 4.9 Single-feeder Three-branch System

It can be seen that, it is very difficult to determine any unique characteristic which helps to determine faulted branch. Differences between two waveforms are caused by the asymmetry of system. Attenuation in the waveform for the fault at Bus 5 is higher, because traveling path for these waves is shorter, and therefore, reflections take place very quickly, and magnitude of reflected waves decrease considerably after few reflections. On the other hand, as well as having a different pattern, waveform for the fault at Bus 3 has lower attenuation. Only these types of differences could be the key points for the determination of faulted branch around junction point, and obviously it needs detailed inspection of waveforms.

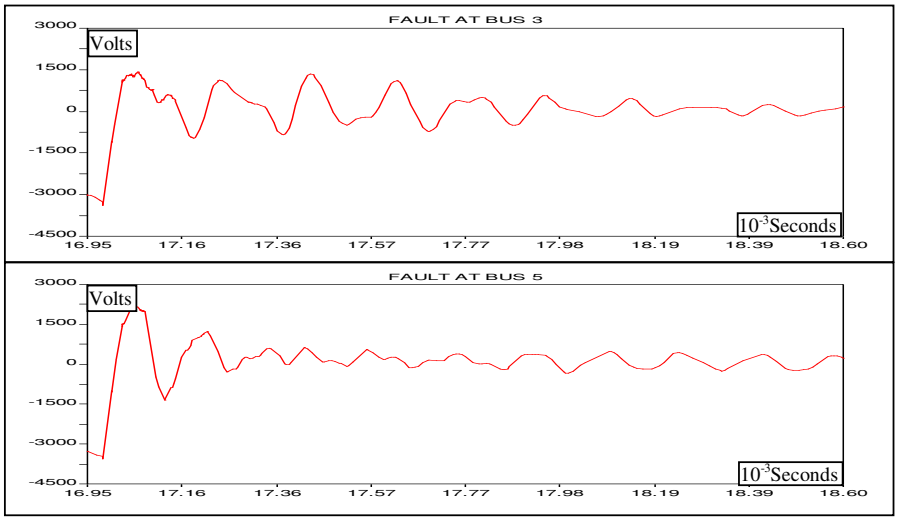


Fig. 4.10 Comparison of faults at Bus 3 and Bus 5

Although faulted branch can possibly be determined, this is not the case for fault distance around junction point. First of all change in the slope of waveform before first peak occurs at the same time for the faults at Bus 3, Bus 5, and even Bus 7 (Fig.4.11), since the first negative reflection comes from the junction point at Bus 2 instead of the fault. For this particular case, traveling time obtained from slope changes for these buses are $20\,\mu\text{sec}$. This phenomenon makes impossible to determine the fault location from change of slope for the faults around junction point.

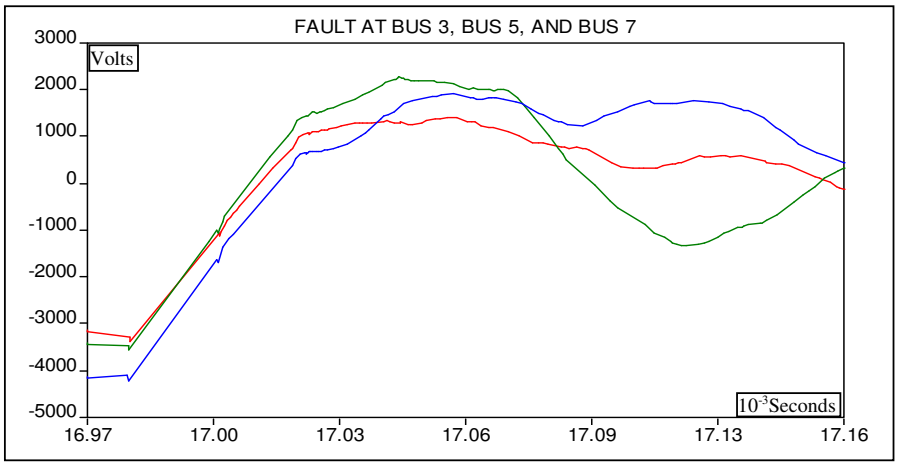


Fig. 4.11 Comparison of faults at Bus 3, Bus 4, and Bus 5

In the previous section it was determined that, fault location from the first peaks are quite erroneous, and this method cannot also be used here. Finally, sinusoidal period method is hardly useful for the faults occur near the junction point, because waveform cannot gain sinusoidal form before its attenuation due to successive reflections from discontinuity points (Fig. 4.10). Consequently, all fault detection algorithms introduced so far fail for the faults near to junction point.

As the fault point moves away from junction point, both the slope change before first peak and sinusoidal period of waveform are detectible (Fig.4.12). Travel time determined from slope change gives approximate uniquely determined fault distance, but the branch corresponding to the fault cannot be determined. Unlikely, the same sinusoidal period could take place for different fault distance corresponding to different branches of unsymmetrical systems. As a result, once fault distance is determined from slope of the change, faulted branch can be deduced from sinusoidal period, necessary condition being that the fault occurs away from junction point and the system under investigation is asymmetric.

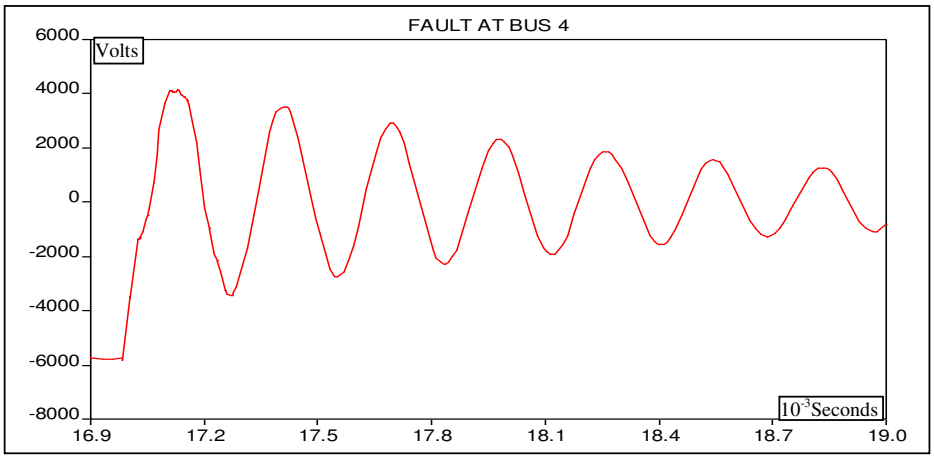


Fig. 4.12 Waveform for the fault at Bus 4

# CHAPTER 5

# CONCLUSIONS

The aim of this thesis was to analyze the system behavior during the times of fault initiation and fault clearing with the operation of CB by modeling the high frequency characteristics of system elements, and develop alternative algorithms for determination of fault location using traveling waves.

There is also a third alternative which has been used by the industry, i.e., the determination of the impedance to the fault by the division of steady-state voltage to the steady-state current as in impedance relay assuming that the fault current reaches a steady-state value just before the CB operation to clear the fault current

Although some components of calculated impedance are well known, such as core and shield wire resistances, some components i.e. arc (fault) resistance are variable according to fault conditions. Furthermore, unlike the transient cases, the low frequency current at steady-state can penetrate into earth which introduces another variable impedance. Even for the homogeneous earth resistivity, current through earth is changing according to number of DTC's because of grounding of shields wire at each station. As a result, current decrease is not linear as the fault distance increase, and such assumptions leads quite erroneous results even though solid fault between core and shield wire is assumed. For example, for the system in Fig. 4.5, error in calculated fault distance increase as shown Table 5.1, when linear relation between fault distance and calculated impedance is assumed.

Table 5.1 Calculations from Steady-state Impedance Assuming Homogeneous Earth and Solid Fault

| FAULT POINT | LENGTH (m) | | ERROR(m) |
|---|---|---|---|
| | ACTUAL | CALCULATED | |
| BUS 1 | 450 | 436 | -14 |
| **BUS 2** | **800** | **832** | **32** |
| BUS 3 | 1050 | 1094 | 44 |
| **BUS 4** | **1550** | **1625** | **75** |
| BUS 5 | 1950 | 2110 | 160 |
| **BUS 6** | **2325** | **2558** | **233** |
| BUS 7 | 2875 | 3193 | 318 |

This drawback may be eliminated by assuming non-linear change in impedance according to fault distance and the number of DTC's present between fault and observation point. On the other hand, fault resistance is still variable and it is sometimes comparable with cable impedance. Comparison of fault location and corresponding errors with changing fault impedance are given in Table 5.2. Low fault impedances do not affect the results while slightly high impedances increase the error especially for short fault distances. As a result, determination of fault distance is quite erroneous especially for the cases that include fault resistance comparable with cable impedance.

**TABLE 5.2 COMPARISON OF CALCULATED FAULT DISTANCE FOR DIFFERENT FAULT IMPEDANCES**

| FAULT POINT | LENGTH (m) | CALCULATED FOR SOLID FAULT | ERROR(m) | CALCULATED FOR FAULT THROUGH 0.01 OHM | ERROR(m) | CALCULATED FOR FAULT THROUGH 0.1 OHM | ERROR(m) |
|---|---|---|---|---|---|---|---|
| **BUS 1** | 450 | 435 | **-15** | 436 | **-14** | 727 | **277** |
| **BUS 2** | 800 | 829 | **29** | 828 | **28** | 1000 | **200** |
| **BUS 3** | 1050 | 1047 | **-3** | 1046 | **-4** | 1173 | **123** |
| **BUS 4** | 1550 | 1531 | **-19** | 1529 | **-21** | 1606 | **56** |
| **BUS 5** | 1950 | 1965 | **15** | 1957 | **7** | 2013 | **63** |
| **BUS 6** | 2325 | 2334 | **9** | 2332 | **7** | 2378 | **53** |
| **BUS 7** | 2875 | 2889 | **14** | 2964 | **12** | 2923 | **48** |

In this thesis, more accurate fault detection algorithms which make use of traveling waves are discussed. In order to develop such algorithm using the traveling waves due to fault initiation several systems starting from single-phase single-feeder systems to three-phase multi-feeder systems are analyzed. Finally, for the practical systems like in Fig. 3.31, it is concluded that, because of complexity due to presence of several feeders in the system during the fault initiation, only meaningful fault distance calculations can be done by using the period difference of resultant waveforms. Calculation results given in Section 3.5 are quite acceptable values, and they are independent from the change in fault resistance, since they depend on waveform period, which is not affected by the change in fault resistance (Fig. 5.1).

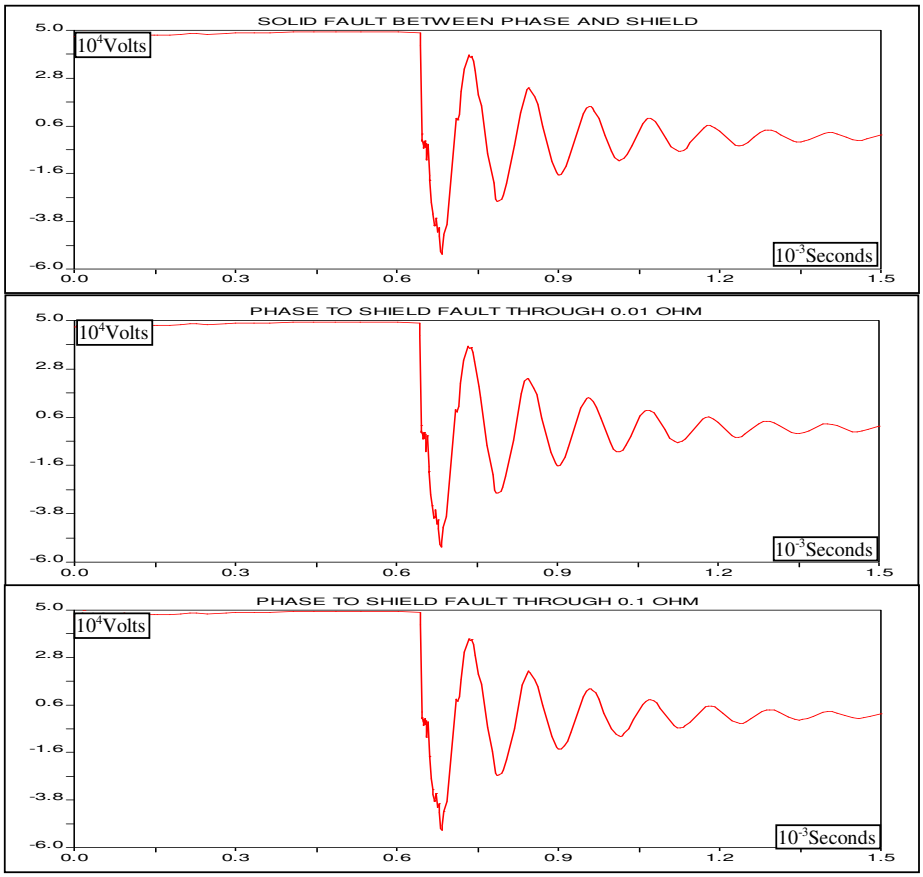


Fig. 5.1 Waveforms for Fault Initiation for Different Fault Resistance

CB operation also initiates traveling waves which results in more consistent information. In the fault initiation case, since the waveform period is directly related with all system, any opened feeder or line section in healthy feeders directly affects the resultant waveform period, and leads erroneous results. On the other hand, since the faulted feeder is isolated by the CB operation so that the condition of other feeders does not affect resultant waveform. Furthermore, waveform contains more unique characteristics, because the waves travel only in the feeder under investigation. Using these properties, fault location can be determined by the time delay between CB operation and first returned wave from the fault or time delay between CB operation and first peak in the waveform, and finally by using the period of resultant waveform as in the case of fault initiation. As discussed in Section 4.3.1, fault location can be calculated more easily and more precisely by using the time delay between CB operation and first returned wave with described algorithm. In all cases studied, these algorithms also are independent from fault resistance, since resulted waveform is not affected by fault resistance, as given in Fig. 5.2.

Only limitation of newly introduced algorithms is the inability of determination of faulted branch for symmetric or nearly symmetric networks, because wave characteristics of such networks turn to be identical for either one of the symmetric branch. Such determination is only possible for the asymmetric network by using series of algorithms as explained in Section 4.3.2.

As a result, fault location can be determined in the vicinity of at most two transformers and fault can be isolated by de-energizing only the related transformers and maintaining service to other consumers. Furthermore, faulted section can easily be pin-pointed by checking only corresponding sections, instead of whole distribution feeder.

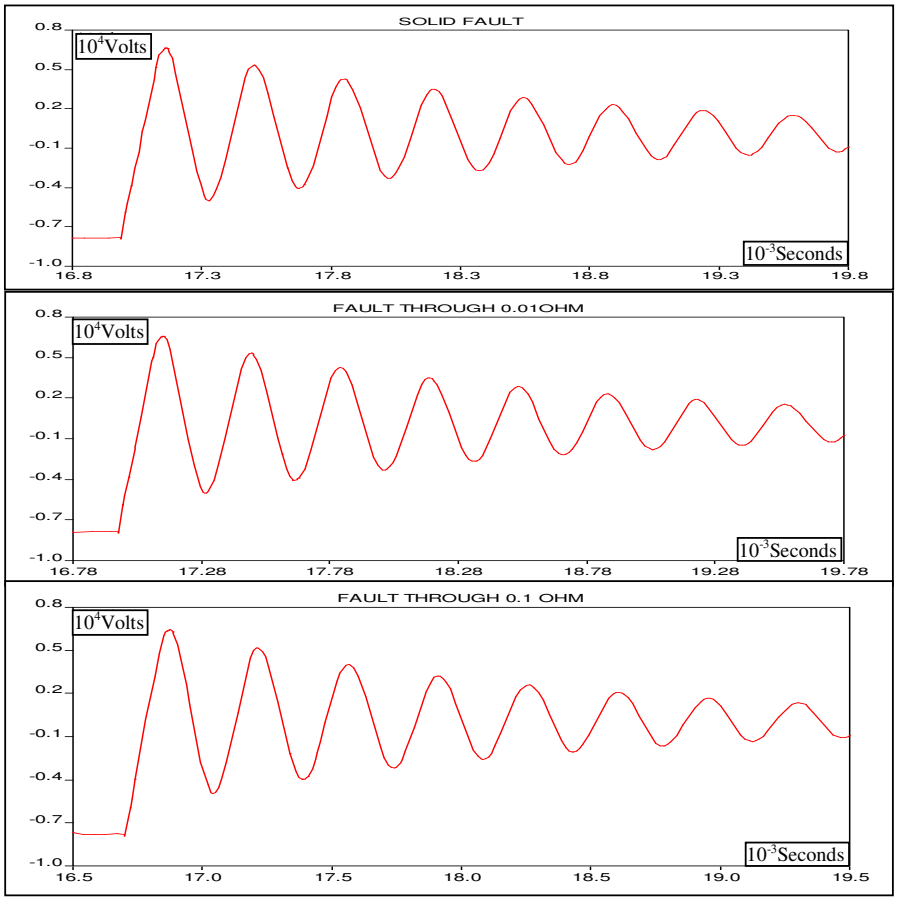


Fig. 5.2 Waveforms for Fault Initiation for Different Fault Resistance

All introduced algorithms are based upon the computer simulation and also should be verified by the site measurement for further verification. This could be the topic of further studies about determination of fault location using traveling waves.

## REFERENCES


[1] L. M. Wedepohl, and D.J. Wilcox, "Transient analysis of underground power-transmission systems" Proc. IEE, Vol. 120, No. 2, pp 253-260, February 1973.

[2] EMTP Theory Book, Chapter 5, "Underground Cables".

[3] S. Bojic and I. Uglesic, "Researching the Efficiency of Measures for Decreasing the Transient Enclosure Voltage Rise of the Gas Insulated Swicthgears", International Conference on Power System Transients, July 2001

[4] L.V. Bewley, "Traveling Waves on Transmission Systems", New York, Dover Publications Inc., 1963.

[5] EMTP User Manual.

[6] J. A. Martinez, "ATP Modeling of Power Transformer", EEUG News, pp 63-76, Aug-Nov 1998.

[7] S. Chimklai and J. R. Marti, "Simplified Three-Phase Transformer Model for Electromagnetic Transient Studies", IEEE Transactions on Power Delivery, Vol.10, No. 3, pp 1316-1323, July 1995.

[8] EMTP Theory Book, Chapter 10, "Switches".

[9] H. INAN, " Thesis on Design Limitation in Distribution Systems due to Selectivity in Protection", Turkey, Middle East Technical University, September 2002.

[10] L. M. Wedepohl “Application of matrix methods to the solution of Traveling wave phenomena in Polyphase systems” Proc, IEE, 110, pp 253-260, December 1963.

[11] S. A. SHELKUNOFF “The Electreomagnetic Theory of Coaxial Transmission Lines and Cylindrical Shields”, Bell Syst. Tech. J., 1934, 13, pp. 532-579.

[12] M.D. Amore and M. Salerno, “Simplified Model for Simulating Transformer Windings Subject to Impulse Voltage”, paper A 79431-8, presented in IEEE PES Summer Meeting, Vancouver, British Columbia, Canada, July 15-20 1979,

[13] J. R. MARTI, “Accurate Modeling of frequency Dependent Transmission Lines in Electromagnetic Transient Simulations”, IEEE Trans, Vol. PAS-101, 1982

[14] P. T. M. VAESSEN, “Transformer Model for High Frequencies”, IEEE Trans. On Power Delivery, Vol3, No.4,pp 1761-1768, October 1988,

[15] R. J. GALARZA, J.H. CHOW and R.C. DEGENEFF, “Transformer Model Reduction Using Time and Frequency Domain Sensitivity Techniques”, IEEE Trans. On Power Delivery, Vol. 10, No. 2

[16] N. MULLINEUX and J.R. REED, “Calculation of Electrical Parameters for Short and Long Polyphase Transmission Lines”, Proc. IEE. 1965, 112 (4), pp 741-742